Universidade do Minho
Escola de Ciências

Pedro Alexandre Ferreira Passos

The hydrodynamic approach for plasmonics in graphene

October 2022

The hydrodynamic approach for plasmonics in graphene
Pedro Passos
UMinho | 2022

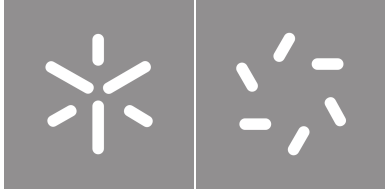

Universidade do Minho
Escola de Ciências

Pedro Alexandre Ferreira Passos

The hydrodynamic approach for plasmonics in graphene

Master Thesis
Master in Physics

Work developed under the supervision of:
Dr. Nuno Miguel Machado Reis Peres

October 2022

Acknowledgements

The development of this thesis was a regarding and fulfilling experience. It is the culmination of all the hard work and the effort that i put in my degree and master's in physics taken in University of Minho. The five years that i spend on this institution allowed me to have personal growth and became more aware of how exciting and stimulating science can be. The memories and experiences that i retrieve along the way, were only possible due to the numerous people who offer their unconditional support and that i would not be able to overcome the challenges that were imposed on me. To all these people it is my wish to leave a mention here. Firstly, i would like to thank my supervisor Dr Nuno Peres for giving me the tools necessary to accomplish this thesis, for its availability and readiness to answer my questions, helping me to overcome the difficulties. Also for showing me how research in science is done, and at this point i must mention FCT for granting me with a research grant on graphene, whose project lead to this thesis. Next, i must thank all my friend and colleagues from outside and inside my course for their support and for always be there for me. In particular, to my fellow course friends: Patricia, Mélina, Pinheiro, Mónica and Rui, with whom i spend many days studying. Without you this would not have half the fun. Finally, my biggest thanks goes to my family, whom i dedicate this thesis to. To my cousin Claudia for the english revision and to my brother Tiago for helping me with the design for some figures in this thesis. Not forgetting the rest of my family, you were the inspiration and my strength to overcome many obstacles that came in my way during these years. To all of you i am forever grateful.

STATEMENT OF INTEGRITY

I hereby declare having conducted this academic work with integrity. I confirm that I have not used plagiarism or any form of undue use of information or falsification of results along the process leading to its elaboration.

I further declare that I have fully acknowledged the Code of Ethical Conduct of the Universidade do Minho.

Abstract

The hydrodynamic approach for plasmonics in graphene

The hydrodynamic model approach to plasmonics is based on the simultaneous solution of Euler's equation, Poisson's equation, and the continuity equation. The quantum mechanical effects enter the model via the statistical pressure induced by the gas of electrons. It is also a form of including the effect of nonlocality. The aim of this thesis is to study the dispersion relation of the surface plasmon-polaritons and the plasmonic wakes created by an external potential, when a graphene sheet is in the vicinity of a metal. It is known they disperse linearly with the wave vector, therefore are of acoustic nature. This problem has been studied for normal plasmons, but the study for acoustic plasmons is missing. In the first part of this thesis, the hydrodynamic model will be used to solve some electrostatic boundary-value problems in planar geometry, that will give the linear dispersion of the SPPs in graphene near a semi-infinite and finite nonlocal metal. The study for the metals, gold and titanium, showed that the nonlocal effects are more visible in titanium, due to its intrinsic proprieties, such as plasmon frequency and background permittivity. The dielectric separation between graphene and metal also enhances the nonlocal effects. The decrease of the dielectric thickness increases the nonlocality. Regarding the finite metal, the results show that the increase of the metal thickness results in a higher energy of the surface plasmon-polaritons in graphene. In this case, the dispersion is also linear in the wavenumber k. The second part encompasses the study of the induced potential in graphene, due to an external charge moving parallel to graphene in the y-direction at an height z_0. When graphene is in the vicinity of a dielectric an oscillatory V-shaped pattern was perceived, and the dependence of the angle on the Froude number (or dependence on the velocity of the external charge) provided two different regions, a constant angle region for low Froude numbers where the wake angle takes the value of $21°$. This is similar to the Kelvin region, where the angle takes the constant value of $19.47°$. A transition for a Mach region occurs for a plasmonic Froude number of 2.2, where the decrease of the angle happens for higher velocities following the law $1/v$. When a local metal is added to the system, the oscillatory behavior vanishes and a more continuous V-shaped wake appears in graphene. In this case, the angles follow a quadratic polynomial law, where these decrease with the increasing Froude number. Studying the phase velocity and the dispersion for the classical water wakes and the plasmonic wakes it is possible to see two limiting cases for $\kappa = -1$ and $\kappa = 0$, which correspond to pure gravity waves in deep water and gravity waves in shallow water, respectively. In such manner, it is possible to make an analogy between gravity waves and the plasmonic waves in graphene.

Keywords: Nonlocality, SPPs, Graphene, Plasmonic wakes, Kelvin region, Mach region

Resumo

A abordagem do modelo hidrodinâmico à plasmônica é baseada na solução simultânea da equação de Euler, da equação de Poisson e da equação de continuidade. Os efeitos da mecânica quântica entram no modelo através da pressão estatística induzida pelo gás de eletrões. É também uma forma de incluir o efeito da não-localidade. O objetivo desta tese é estudar a relação de dispersão e as perturbações plasmônicas criadas por um potencial externo, quando o grafeno está nas proximidades de um metal. É sabido que os plasmões dispersam linearmente com o vetor de onda, portanto possuem uma natureza acústica. Este problema foi estudado para plasmões normais, no entanto falta o estudo para plasmões acústicos. Na primeira parte desta tese, o modelo hidrodinâmico será usado para resolver alguns problemas eletrostáticos de valor de fronteira, que darão a dispersão linear dos SPPs quando o grafeno está próximo a um metal não local semi-finito e finito. O estudo para os metais ouro e titânio mostraram que os efeitos não locais são mais visíveis no titânio, devido às suas propriedades intrínsecas, como frequência plasmônica e permissividade de fundo. A separação dielétrica entre o grafeno e o metal, também potencializa os efeitos não locais. A diminuição da espessura do dielétrico, aumenta a não-localidade. Em relação ao metal finito, os resultados mostram que o aumento da espessura do metal leva ao aumento da energia dos plasmões-polaritões de superfície no grafeno. Neste caso, a dispersão também é linear no vetor de onda k. A segunda parte abrange o estudo do potencial induzido no grafeno, devido a uma carga externa movendo-se paralelamente ao grafeno na direção dos y's, a uma altura z_0. Quando o grafeno está na vizinhança de um dielétrico, foi visto um padrão oscilatório em forma de "V", e a dependência do ângulo no número de Froude (ou dependência da velocidade da carga externa) mostra duas regiões diferentes, a primeira de ângulo constante para números de Froude baixos onde o ângulo do cone é constante e de valor 21°. Sendo semelhante à região de Kelvin, onde o ângulo constante toma o valor de 19.47°. Observa-se uma transição para a região de Mach ocorre para um número de Froude plasmónico de 2.2, onde a diminuição do ângulo ocorre para velocidades mais altas seguindo a lei $1/v$. Quando um metal local é adicionado ao sistema, o comportamento oscilatório é quebrado e uma onda em forma de "V"contínua aparece no grafeno. Neste caso, os ângulos seguem uma lei polinomial quadrática, onde os ângulos diminuem com o aumento do número de Froude. Estudando a velocidade de fase e a dispersão para as ondas clássicas na água e as ondas plasmônicas é possível ver dois casos limites para $\kappa = -1$ e $\kappa = 0$, que correspondem a ondas gravíticas puras em águas profundas e ondas gravíticas em águas rasas, respectivamente. Desta forma, é possível fazer uma analogia entre as ondas gravitacionais e as ondas plasmônicas no grafeno.

Palavras-chave: Não-localidade, SPPs, Grafeno, Ondas plasmónicas, Região de Kelvin, Região de Mach

Contents

List of Figures

List of Tables

Acronyms

2D 2-Dimensional
3D 3-Dimensional

BVPs Boundary Value Problems

GHz Gigahertz

HDM Hydrodynamic Model

LED Light Emitting Diode
LRA Local Response Approximation

SPPs Surface Plasmon-Polaritons

THz Terahertz

Chapter 1

Introduction

The study of plasmonic and nanoplasmonic in noble metals and semiconductors has become of the uttermost importance in the latest years. Because of its remarkable electromagnetic, optical, and thermodynamic proprieties, the study of Surface Plasmon-Polaritons (SPPs) and bulk plasmons have led to the discovery of groundbreaking technology in many areas of science, overcoming many problems and limitations of non-plasmonic devices in use. Smaller sizes and higher response speeds will characterize these new plasmonic technologies. Graphene and plasmonics comes together to develop a new field of physics known as graphene plasmonics, due to the important proprieties of graphene, such as its 2-Dimensional (2D) nature, graphene is an excellent material to study the plasmonic effects in tighter regions. This means that, in graphene, the surface plasmon-polaritons are confined to atomic-size structures where the nonlocal effects cannot be ignored. The Hydrodynamic Model (HDM) came to life as a new way to study electron gases and graphene in the light of the nonlocal effects. In this thesis, we will analyze the hydrodynamic model and its application to graphene by perceiving it as a nearly perfect fluid, in order to have a hydrodynamic approach to plasmonics in graphene. The thesis will be structured in the following way: in chapter 1 we will introduce the basics of plasmonic and graphene plasmonic, as well as the instances of importance of nonlocal effects which play an important role in the optical and electromagnetic proprieties of plasmons, with the usage of the hydrodynamic model. In chapter 2, we will perform a mathematical derivation of the HDM for 3-Dimensional (3D) and 2D electron gases in the electrostatic regime. In chapter 3, we will use the hydrodynamic model as a tool to derive the dispersion relation of some electrostatic problems in planar geometry. In chapter 4 we will derive the expressions for the induced potential in graphene when an external particle is moving parallel to it. The study will cover two cases: graphene in the vicinity of a dielectric and graphene in the vicinity of a nonlocal metal. Finally, in chapter 5, we will discuss about classical Kelvin and Mach waves and provide an analogy between water wakes and graphene potential wakes created by the moving external particle, in order to recognize

the differences and similarities between the two different phenomena.

1.1 General Topics in Plasmonics

In the latest years, plasmonics and nanoplasmonics have been interesting and sovereign fields of research in physics and nanophotonics. This field of research allows us to see how electromagnetic fields can be confined to scales no greater than their wavelength dimensions. These light-matter interactions lead to optical proprieties, giving rise to the main fields of investigation, known as nanophotonics. In recent years, the emergence of faster, smaller, and more efficient electronic devices brought a new perspective and interest in plasmonics and nanophotonics. This has led to the investigation and building of groundbreaking technology, such as electronic devices, terahertz detectors [1, 2], signal processing devices, plasmonic integrated circuits [3] and some technological applications in other areas of science [4]. Although the scientific enthusiasm for plasmonics is relatively new, the unknown discovery of plasma effects can be attributed to Wood in 1902, due to an effect, which later became known as Wood anomalies [5]. At the time, these anomalies were considered to be one of the most fascinating phenomena in optics. Wood anomalies are essential rapid variations in the intensity of the light diffracted spectrum. We can observe this abnormal phenomenon through the spectrum of visible light diffracted by a metal grating. Even though it was a remarkable observation at the time, Wood could not find an explanation for the phenomena. Further work was developed with the aim of explaining these anomalies. Lord Rayleigh, who stated that the existence of anomalies occurs at a wavelength that corresponds to the transition to a higher order spectrum, conducted the first experiments on Wood's anomalies. Rayleigh's study was of limited interpretation and the first reappraisal to his study was made by Strong showing that the metal influences the position of the anomalies [6]. Since the location of the transition is a consequence of the geometry of the grating, the metal does not influence it. So Rayleigh study was in need of a revision.

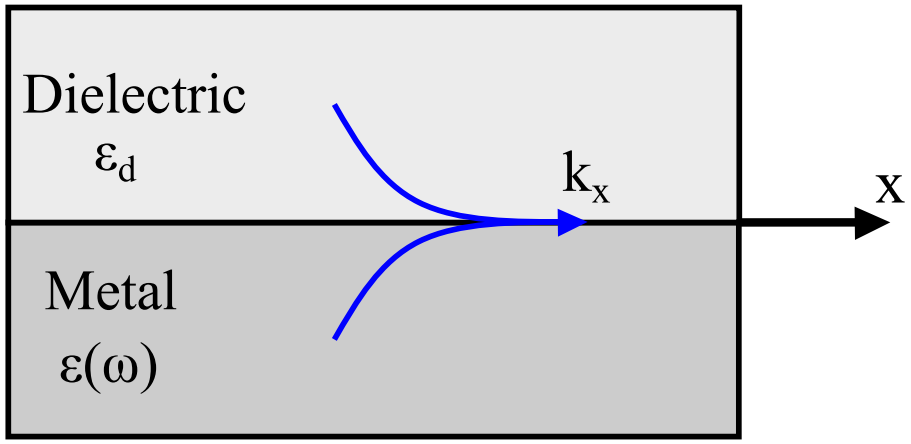

Figure 1.1: Representation of an evanescent surface plasmon wave at an interface between a metal and a dielectric. The wave propagates along the x-axis, without loss of generality.

Only a few years later, with the subsequent work of Fano, was a theoretical breakthrough on Wood anomalies provided. Fano observed that the origin of the anomalies was due to the excitation of evanescent surface waves propagating along the metal grating, meaning along the surface of the material [6]. This was the first step towards a plasmonic description of the phenomena, although further research (see [6, 7] for more details) was necessary in order to relate these anomalous excitations with the surface plasmons.

Surface plasmons are localized excitations of an electron gas that propagates as waves along an interface of two materials (usually a metal and a dielectric), decaying exponentially away from the interface (see figure 1.1). It can also be seen as polarization oscillations of metallic nanoparticles. In a way as plasmons are collective excitation of electrons, metals are the perfect materials to observe these phenomena. From a solid-state physics point of view, metals are known as good conductors. Thus, once we apply an external field to a metallic system, the electrons with energies near the Fermi level can move freely in the material. In such case, we can conclude that the metal is a free electron gas bounded to a certain geometry. Of course, the electrons are moving in a charge ion background where the only interactions are the instantaneous electron-ion collisions. To get the most basic electromagnetic and optical responses for a metal, Drude came up with a simple model, having in mind the particularity of considering the metal as a free electron gas. This model later became known as the Drude model and is stated in the following way

$$\epsilon(\omega) = 1 - \frac{\omega_p^2}{\omega^2 + i\Gamma\omega} \tag{1.1}$$

where $\omega_p = \sqrt{ne^2/m\epsilon_0}$ is the plasma frequency of the electron gas and Γ is a phenomenological parameter that counts for the scattering rate of electrons with the ionic background. The plasma frequency comes from applying an electric field to a thin metallic film that embodies n free electrons per unit volume. This will exert a force on the film, which can be quantified using Newton's second law of motion for a single electron with mass m and an electric charge e. Recalling that surface plasmons are visible in the interface between two materials, classically they are possible if one of the two materials has a real and negative permittivity ϵ, such as the Drude model provides. The other material is usually taken to be a dielectric, the most simple being vacuum with real and positive permittivity. For an ideal electron gas, this is, for $\Gamma = 0$, the Drude permittivity is negative for frequencies smaller than the plasma frequency ω_p. As such, one characteristic of the surface plasmons is that the frequency for surface waves to exist within the interface of the material is taken to be at $\omega < \omega_p$. To find these surface modes, one must find a solution to Maxwell's equations, which give rise to longitudinal waves that propagate along the interface between the two media but are exponentially damped away from the surface. However, the plasmons do not exist alone, and that is a very interesting point. We know that the usual study of metallic structures is accompanied by a dielectric, which forms a certain interface. The electrons in the metal are excited to form plasmons while simultaneously in the dielectric an electromagnetic wave couples to a polarization excitation in the material, which are known as polaritons. In that case, there is a more general description of the plasma phenomena, of the evanescent waves that occur in the interface between the two materials. It is common to describe them as surface plasmon-polaritons (SPPs). The dispersion for the plasmons in

an air interface, coming from Maxwell's equations, is seen in figure 1.2.

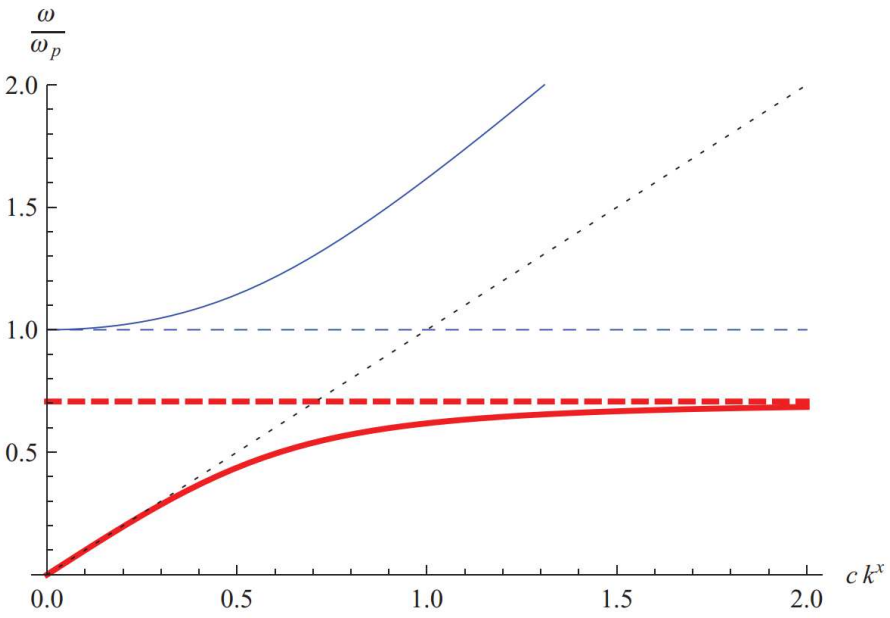

Figure 1.2: Dispersion relation for the surface plasmon-polaritons (red line) and the volume plasmons (blue line) for an air and ideal Drude metal ($\Gamma = 0$) interface. The red dashed line corresponds to the asymptotic SPP limit $\omega/\sqrt{2}$, the dotted black line is given by $\omega = ck_x$ and the black dashed line shows $\omega = \omega_p$. This figure was retrieved from [8].

The solution describes two types of behavior: the surface plasmon-polaritons for the frequency interval of $0 < \omega < \omega_p/\sqrt{2}$ (red line) and the volume plasmons for $\omega > \omega_p$. Note that there is no solution for region $\omega_p/\sqrt{2} < \omega < \omega_p$ (blue line) and the light line is represented by $\omega = ck_x$, where it is considered the propagation of waves to be the x direction. The nonexistence of solutions in this region happens due to the purely imaginary value of the SPPs wavevector [7]. The volume plasmons represent a propagating bulk wave in the Drude type metal, where contrary to the surface plasmons, the dielectric function for the metal $\epsilon(\omega)$ is positive. The volume plasmons are collective oscillations within the bulk of the metal, and the SPPs correspond to electron gas excitations confined at the interface between the two media. Turning now to the SPPs curve, it lies to the right of the light line ($\omega = ck_x$), so this type of plasmons cannot be excited by direct light, which means there are quite a few methods to couple light to surface plasmons. Just to name a few, let's talk about grating coupling [1, 4, 7] and prism coupling [4, 7, 9, 10].

- **Grating coupling:** in this type of device, the grating array period takes a major part in the increasing of the free surface radiation momentum. The excitation of SPPs occurs from an optical point of view. That is, when a beam of incident light hits the grating structure, it gives rise to different diffraction orders that carry increasing momentum contributions. When the momentum of the diffracted light coincides with the momentum of the surface plasmon-polaritons, the phase-matching condition is achieved and the SPP excitation takes place.

- **Prism coupling:** the base method for this type of coupling is the totally attenuated reflection method. Here, an optical wave is observed, reflecting at the interface between a prism and a thin metal layer. This light excites the plasmons in the metal's surface, and consequently registers a drop in the intensity of the reflected light. There are two important configurations for this system: the Otto configuration, which consists of a prism separated from the metal by a thin air gap and the SPPs, which are found in the interface metal/dielectric. Another is the Kretschmann configuration, which closes the gap, making the prism come into contact with the metal, where the surface plasmons propagate on the far side of the metal.

Although plasma oscillations happen in many metals and semiconductors, in this thesis we are interested in the study of plasmonics in graphene. In the latest years, this 2D material has been subject of many studies and remarkable discoveries, due to its electronic, optical, and mechanical properties, pursued both by academics and industries. The plasmonics in graphene came with the study of graphene surface plasmon-polaritons in periodic arrays of graphene ribbons, experimentally discovered by Ju [11] in 2011. From this study onwards, graphene plasmonics have become the starting point for research in nanoplasmonics, so it is of considerable importance to understand and talk about the origins of graphene and its importance to plasmonics.

1.2 Graphene Plasmonics

Graphene is a 2-dimensional material with a thickness of a carbon atom, in a way that comprises a layer of carbon atoms arranged in a honeycomb lattice (see fig. 1.3). It was discovered by Andre Geim and Konstantin Novoselov in 2004. Geim and Nosovelov won the Nobel prize in 2010 for experiments carried out in this two-dimensional material [12]. Their discovery of this material demonstrates how interesting and adventurous science can be. With only tape, their goal was to exfoliate graffiti in order to reach an atom layer of carbon. This discovery sparked a whole new interest in 2D materials, but especially in graphene due to its remarkable proprieties. Stronger than steel and harder than diamond, but still very flexible, graphene is understood as having an extremely large thermal conductivity, which sustains high current densities. Therefore, it is a great material to conduct electricity. Its charge carriers are massless Dirac fermions that obey the Dirac equation [7]

In terms of electronic and optical properties, graphene is a half-filled system. Meaning that the valence band is filled while the conduction band is empty. Furthermore, from a thigh-binding Hamiltonian analysis, the energy spectrum for graphene shows to be particle-hole symmetric. The energy spectrum shows us it is in the Dirac points K and K' where the valence and conduction band touch each other. This makes graphene a semiconductor, where the Fermi energy is localised in the Dirac points. These are also the points of high-symmetry of the system that carry momentum values given by **K** and **K'**. The energy bands of graphene are cone shaped-like and around these symmetry points, it is usual to make a low energy approximation up to first order of the energy, which leads to a spectrum of the form

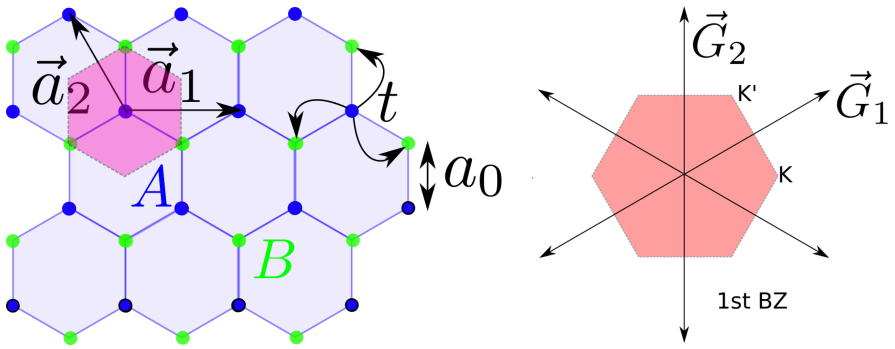

Figure 1.3: Left: Representation of the real space hexagonal lattice of graphene, with the Wigner-Seitz cell in pink. The distance between carbon atoms is given by $a_0 \simeq 1.42$ Å and the hopping integral $t \simeq -2.7$ eV. The primitive lattice vectors are $\mathbf{a}_1$ and $\mathbf{a}_2$. Right: First Brillouin zone of graphene, where $\mathbf{G}_1$ and $\mathbf{G}_2$ are the reciprocal lattice vectors. Two special points, the Dirac points, are represented in the figure by K' and K. This figure was retrieved from [7].

$$E_{\pm}(\mathbf{k}) = \pm\hbar v_F k \tag{1.2}$$

where the Fermi velocity is $v_F = c/300$. With c the velocity of light in vacuum and k the momentum measured regarding the Dirac points. Equation (1.2) also shows that the electrons in graphene behave as massless Dirac fermions, and that these particles disperse linearly with the momentum near the Dirac points [13, 14]. From equation (1.2) it is possible to get the Fermi energy simply by finding the energy for Fermi momentum k_F, which takes $E_F = \hbar v_F k_F$.

Another important physical properties of graphene is its optical conductivity, and together with the linear dispersion, these relate important proprieties of plasmonics and electromagnetic interactions between external fields and graphene. The conductivity of graphene must be divided into two contributions in order to study all the potential effects that can occur regarding the band structure of graphene. The contribution from the intraband transition happens within the same band (the conduction or valence band) and the momentum is not conserved, whereas the interband transitions occur between distinct bands and the conservation of momentum is verified (see figure 1.4). Further linear analysis of the conductivity shows us that in the Terahertz (THz) and mid-IR (infrared) frequencies, the Drude model can describe the optical effects in graphene, which is a local model; therefore, one must promptly ignore the nonlocal effects. Within this spectral region, and under the usual doping level of graphene ($E_F \sim 0.2 - 0.5$ eV), the optical intraband conductivity dominates the electronic processes, while the interband transition can be neglected. To study effects away from the THz and the mid-IR range, the low energy approximation around the Dirac points no longer holds, and it becomes necessary to study nonlinear effects as stated in [14]. This research also points out that the low optical absorption of light in graphene and the low sheet resistance elevates graphene to a high position for modern technologies that need transparent and conductive layers of material, such as touch screens, solar cells, organic Light Emitting Diode (LED) displays, just to name a few.

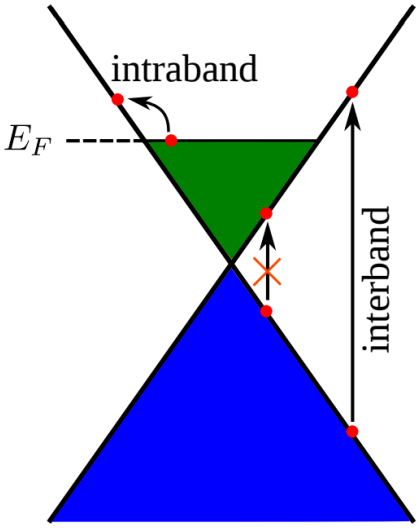

Figure 1.4: Schematic representation of the transitions in the energy bands of graphene. The intraband transitions happen in the same band (conduction or valence band). The interband transitions occur between bands. The cross arrow is an example of a transition prohibited by Pauli blocking. This figure was retrieved from [7].

Plasmonics and graphene physics are two fields of research that have been growing separately, however, in the last couple of years, the combination of plasmonic effects and graphene has seen a surge of interest due to the peculiar proprieties of graphene and the range of plasmonic technologies that can be developed. Since graphene is a 2D material, the intrinsic graphene plasmons are confined to tighter regions, which will be important when considering nonlocal effects, and can be tuned by gating or doping of the material, which differs from plasmons in noble metals. Graphene plasmons are encountered between frequencies of THz and mid-IR, which makes them a great candidate to the construction of photodetectors of Terahertz radiation [14]. Regarding the dispersion of plasmons in graphene, an equation that describes this optical property can be easily uncovered by finding a solution of Maxwell's equations that describes the motion of an electromagnetic wave in graphene. In that order, it becomes necessary to apply the following boundary conditions to a single monolayer of graphene: the continuity of the tangential component of the electric field and the discontinuity of the tangential component of the magnetic field in the interface. Of course, the same analysis has been done for other geometries, such as a double layer of graphene, plasmonic in graphene ribbons, and plasmons in graphene nanostructures. All this plasmon research and further mathematical descriptions of this subject are found detailed in [7]. Moreover, all the electromagnetic properties of graphene are comprehended in its conductivity. If this property is fully imaginary and the real part vanishes, then the SPPs dispersion in graphene has real solutions, while for a non-vanishing real part for the conductivity, the dispersion solution has complex values. The dispersion of graphene SPPs is displayed in figure 1.5 for different values of damping parameters Γ that account for absorption effects in graphene. From a first analysis, the plasmons in graphene disperse as $\sqrt{q}$, with q

being the plasmon momentum. It is also understood that the spectrum curves lie on the right side of the light lines, and although for the low momentum vector the curve lies on the right, it is still not possible to excite plasmons with direct light onto graphene as the plasmons cannot be sustained in this region due to the overdamped regime that is characterized by $\hbar\omega_{SPP}/\Gamma < 1$.

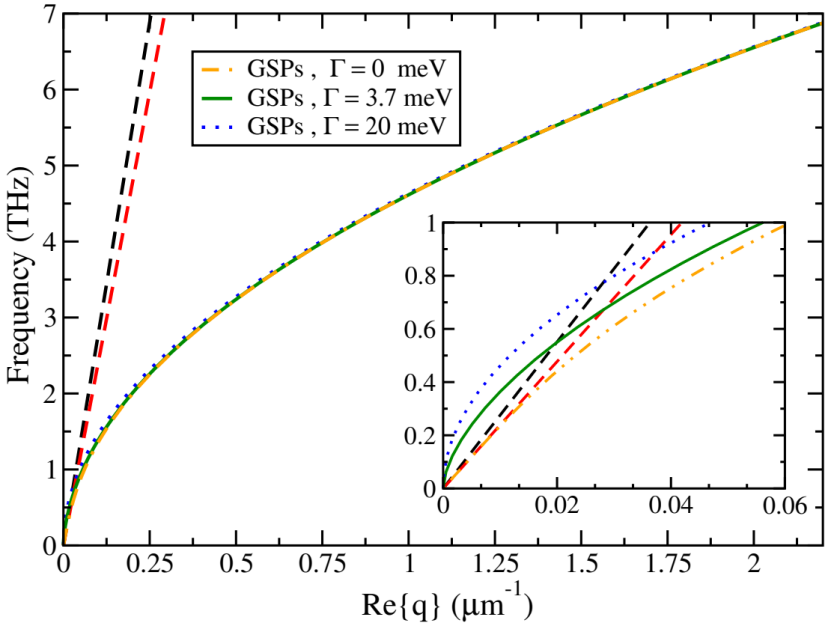

Figure 1.5: Dispersion relation of SPPs for a monolayer of graphene, with different values of the damping parameter. The dashed lines correspond to the light dispersion for the dielectrics surrounding graphene. The black dashed line corresponds to the light dispersion in air and the red dashed line corresponds to the light dispersion in SiO_2. The parameters are: $E_F = 0.45\,\text{eV}$, $\epsilon_{air} = 1$ and $\epsilon_{SiO_2} = 3.9$. This figure was retrieved from [7].

In terms of electronic density n_e, for graphene the Fermi energy is given by $E_F = \hbar v_F k_F$, where $k_F \propto n_e^{1/2}$ and so the behavior $\omega_{SPP} \propto n_e^{1/4}$ is an exclusive result for graphene. The excitations of SPPs in graphene can also be achieved through grating coupling and prism coupling [1, 7], like the plasmons in metals and semiconductors. This will allow us to study electronic devices at the scale of nanoparticles and manipulate light at the nanoscale. The last years have seen an increase in plasmonic electronic structures that are steadily approaching the nanometer scale. The field of research of nanoplasmonics analyze the ultra-confined plasmonic modes in some materials. Graphene is a great candidate for nanoplasmonics, not only because of its remarkable optical, thermodynamic, and electromagnetic proprieties, but also because it shows SPPs confined to its nanoscale surface. The search for nanoplasmonic devices is important since they can overcome some existing obstacles in current electronic systems; the most obvious being the size of these systems. Plasmonics will then be able to create technology with fast operating speed but with just a few nanometers in size. Nonetheless, the structures at these sizes may experience effects that local models cannot describe, such as the Drude model and the local description of graphene's conductivity up until now. Thus, it is necessary to introduce the moment where the nonlocal effects will play an important

role in graphene and metals. Also, finding a suitable nonlocal theory to apply to graphene/metal structures is of extreme importance to study such effects that go beyond the plasmonic locality.

1.3 Nonlocal theory: a hydrodynamic approach

In the latter sections of this chapter, it was assumed that the Drude model could describe the electromagnetic response of metals and semiconductors. Drude came up with a simple model that explains the motion of an electron in a conductor and the response of an applied electric field and responding current densities. Furthermore, the Drude model assumes a law of proportionality between the current density at a given point and the applied electric fields at that exact point. In other words, the Drude model assumes locality. The same happens to the conductivity of graphene, where it is considered that this conductivity is a function only of the frequency ω, which gives rise to a Drude-type local conductivity [7]. However, the Drude model has its limitations: this model accounts for the contribution of the free electrons in the conduction band, but at higher frequencies, the Drude model cannot describe the interband transitions that could occur in conductors. Nevertheless, for lower frequencies, the approximation provided by the model describes with great accuracy the electromagnetic response of noble metals. Another limitation, and the most important in our case, has to do with the locality. The Drude model is a local model, so does not account for nonlocal effects or, in the same manner, spatial dispersion [6]. This means that the dielectric function in equation (1.1), must also depend on the wavevector k to figure out the nonlocality. In real space, this means that the polarization of the medium at a given point not only depends on the electric field at that specific point but also within its vicinity, which is why it is necessary a nonlocal theory. The Local Response Approximation (LRA) neglects the dependence of the wavevector in the dielectric function by taking the long-wavelength limit, this means $\mathbf{k} \rightarrow 0$. However, the local model fails to describe some experimental results for thin metallic films, such as the position and the width of the plasmon resonance and field enhancement. In that order, the nonlocal effects become important due to the following reasons:

- The system configuration in the study approaches the characteristics of length scales in the range of nanometers. The field at a given point gains a contribution from the fields in the neighboring points. In that case, the dielectric function becomes dependent on the wavevector and that affects the spectrum of plasmonic resonances.

- The LRA does not provide an appropriate description of the systems when the size of the metallic nanostructures and nanoparticles or the separation between two materials in the study fall between a few nanometers. This happens, for example, when we have a graphene sheet parallel and in proximity to a metallic surface [15].

- If the ratio between the wavenumber of the plasmons, k, and the Fermi wavenumber, k_F is smaller than one ($k/k_F \ll 1$) the local model gives an accurate description of the results. However, for acoustic graphene plasmons and small metallic structures the wavenumber is large compared to

the wavelength of the radiation of the free space, and the condition $k/k_F > 1$, tells that the nonlocal effects have an important place in the electromagnetic response of the system, which can change the results predicted by the local model [15, 16].

In [17] it is shown that graphene-metal plasmons (graphene in the vicinity of a metal) have energies in the mid-IR range of the electromagnetic spectrum with a wavenumber of $200\,\mu\text{m}^{-1}$, which puts graphene in the strong nonlocal regime because the nonlocal condition is $kc/k_F v_F \sim 100$. This means that the conductivity of graphene must depend on the wavenumber ω and on the wavevector $\mathbf{k}$ to build up the proper nonlocal effects. However, plasmonic structures, even when small, possess a large number of atoms to consider. In that order, it was necessary to find an alternative calculation to the nonlocal Drude dielectric and graphene conductivity functions because of their time-consuming and computational burden. With a need for an alternative approach to these calculations, a nonlocal model, also known as the hydrodynamic model it came to light.

To explain the experimental results, Bloch and Jensen introduced a theory that explains the behavior of an electron gas when in the presence of external fields [15]. The hydrodynamic model allows the inclusion of nonlocal effects by considering a term that corresponds to the statistical pressure (where quantum effects are contained) on the position of a particle. The Coulomb interactions arise by coupling Euler's equation with Maxwell equations of electromagnetism. The hydrodynamic model can be applied to a 2D electron gas, which is considered a perfect fluid. However, nonlocal plasmonic effects in the THz and mid-IR spectral range are not possible for noble metals due to the poor spatial confinement at these frequencies. In that order, graphene emerges as a new material to study these effects in this specific spectral range. The massless Dirac electrons in graphene behave as a nearly perfect fluid, whose electronic motion is given by the Navier-Stokes equation, from which Euler's equation follows. This nonlocal model can characterize the conductivity of graphene and its plasmonic properties. In the following sections, we will give the mathematical details of the hydrodynamic model and equations that describes this model. In the lastest years, the hydrodynamic model has become the reference to study the nonlocal effects of metallic interfaces and metallic nanostructures.

Chapter 2

An Hydrodynamic Model

The Hydrodynamic model came about as a quantum nonlocal theory to describe the plasmonic properties of thin metallic structures, whereas the local-response theory failed to provide a coherent description of plasmonics in metals [1]. This nonlocal theory allows treating the electrons in a metal as a degenerate electron gas. The hydrodynamic model is built on three principal equations: Euler's equation (or equation of drift motion), the Poisson equation, and the continuity equation. In this chapter, we will see that the Boltzmann equation is the starting point to derive the hydrodynamic equations and, with the proper boundary conditions for a specific system, these equations will stand useful in providing the plasmonic properties of metallic nanostructures and nanoparticles. Moreover, it is provided the hydrodynamic information for 2-dimensional systems such as the degenerate 2D electron gas and a graphene layer.

2.1 Boltzman and Euler Equations

The Hydrodynamic Model has its foundations in Boltzmann and Euler's equations of fluid dynamics. The study of these equations will provide us with some insight and knowledge into how this model works and will allow us to reach a set of hydrodynamic equations for an electron gas in the electrostatic regime. This electron gas can be characterized by a distribution function $f(\mathbf{r}, \mathbf{v})d\mathbf{r}d\mathbf{v}$, which gives us the number of electrons in the gas having position and velocity centered at $\mathbf{r}$ and $\mathbf{v}$ when we take into account, respectively, the small volume $d\mathbf{r}$ and the small velocity range $d\mathbf{v}$. Considering the case for conservative forces $\mathbf{F} = -\nabla\Phi$, where Φ is the potential energy, the time evolution of the distribution function $f(\mathbf{r}, \mathbf{v})$ is given by the Boltzmann equation

$$\frac{\partial f}{\partial t} + \mathbf{v} \cdot \frac{\partial f}{\partial \mathbf{r}} + \mathbf{g} \cdot \frac{\partial f}{\partial \mathbf{v}} = 0 \tag{2.1}$$

where $\mathbf{g}$ represents the external forces per unit mass. Equation (2.1) is also called the collisionless Boltzmann equation. To account for collisions of the electrons in the gas, it is necessary to add a term of the form $\Gamma(t)$ to the right-hand side of this equation. However for our purposes, the collision term can be neglected. The position of the particles as a function of time can be obtained, simply by integrating (2.1) on the coordinate $\mathbf{v}$. In that order let us take the zero moment of the Boltzmann equation.

$$\int d\mathbf{v}\left[\frac{\partial f(\mathbf{r},\mathbf{v})}{\partial t}+\mathbf{v}\cdot\frac{\partial f(\mathbf{r},\mathbf{v})}{\partial \mathbf{r}}+\mathbf{g}\cdot\frac{\partial f(\mathbf{r},\mathbf{v})}{\partial \mathbf{v}}=0\right] \tag{2.2}$$

By introducing the mass density (assuming the same mass m for all particles in the gas) and the velocity moment, respectively, using the relations

$$\rho(\mathbf{r})=\int d\mathbf{v} f(\mathbf{r},\mathbf{v})m \tag{2.3}$$

$$\langle v_i\rangle=\frac{1}{\rho(\mathbf{r})}\int d\mathbf{v} f(\mathbf{r},\mathbf{v})mv_i \tag{2.4}$$

then equation (2.2) can be expressed in the form

$$\frac{\rho(\mathbf{r})}{\partial t}+\frac{\partial}{\partial \mathbf{r}}\cdot[\rho(\mathbf{r})\langle\mathbf{v}\rangle]=0 \tag{2.5}$$

which is the continuity equation that amounts to the conservation of mass. Note that we have used the divergence theorem in the last term of equation (2.2), which provides the identity

$$\int_V d\mathbf{v}\frac{\partial f(\mathbf{r},\mathbf{v})}{\partial \mathbf{v}}=\int_{S_\infty} f(\mathbf{r},\mathbf{v})d\mathbf{S}_\mathbf{V}=0 \tag{2.6}$$

where $f(\mathbf{r},\mathbf{v})$=0 over a surface at infinity, S_∞.
Let us now consider the first moment of Boltzman equation

$$\int d\mathbf{v}\mathbf{v}\left[\frac{\partial f(\mathbf{r},\mathbf{v})}{\partial t}+\mathbf{v}\cdot\frac{\partial f(\mathbf{r},\mathbf{v})}{\partial \mathbf{r}}+\mathbf{g}\cdot\frac{\partial f(\mathbf{r},\mathbf{v})}{\partial \mathbf{v}}=0\right] \tag{2.7}$$

This last equation can be simplified by recalling the expressions of mass density (eq. 2.3) and velocity moment (eq. 2.4) as

$$\frac{\partial}{\partial t}[\rho(\mathbf{r})\langle\mathbf{v}\rangle]+\sum_i\frac{\partial}{\partial x_i}[\rho(\mathbf{r})\langle\mathbf{v}v_i\rangle]-\mathbf{g}\rho(\mathbf{r})=0 \tag{2.8}$$

where the third term was obtained with integration by parts. This last equation is called the momentum equation and, together with the continuity equation, the Euler equation naturally appears, as we will show. First, it is necessary to introduce the tensor $\tau_{ij}^2=\langle v_iv_j\rangle-\langle v_i\rangle\langle v_j\rangle$. The term $\langle v_iv_j\rangle$ is the second moment of the velocity and can be written in an integral form as.

$$\langle v_iv_j\rangle=\frac{1}{\rho(\mathbf{r})}\int d\mathbf{v} f(\mathbf{r},\mathbf{v})mv_iv_j \tag{2.9}$$

by defining the tensor in this way, it will be possible to write the term with the second momentum in equation (2.8) in terms of products of first moments. Subtracting from the momentum equation [eq. (2.8)] the continuity equation we obtain, for each component

$$\rho(\mathbf{r})\frac{\partial\langle v_j\rangle}{\partial t}+\rho(\mathbf{r})\sum_i\langle v_i\rangle\frac{\partial\langle v_j\rangle}{\partial x_i}=g_j\rho(\mathbf{r})-\sum_i\frac{\partial[\rho(\mathbf{r})\tau_{ij}^2]}{\partial x_i} \tag{2.10}$$

or in vectorial terms

$$\rho(\mathbf{r})\frac{\partial\langle\mathbf{v}\rangle}{\partial t}+\rho(\mathbf{r})(\langle\mathbf{v}\rangle\cdot\nabla)\langle\mathbf{v}\rangle=\mathbf{g}\rho(\mathbf{r})-\nabla P \tag{2.11}$$

This last equation is Euler's equation of fluid dynamics and it is the starting point for the hydrodynamic model of plasmons in metals and graphene. Quantum mechanical effects enter this model via the statistical pressure P induced by the electron gas. In addition this pressure is a function of position due to charge inhomogeneity. Since the statistical pressure depends on the position-dependent charge density, this model is a good approach to describing nonlocal plasmonic effects in metals and graphene.

2.2 Hydrodynamic Model of a 3D electron gas in the electrostatic regime

The Hydrodynamic model is a nonlocal theory described by three equations: Euler's equation (the equation of motion), the continuity equation, and the Poisson equation. Since this model describes the behavior of an electron gas when in the presence of external fields, it is natural to think that the hydrodynamic model combines Euler's equation of motion [eq. (2.11)] with Maxwell's equations of electromagnetism. These equations, when properly linearized, will be capable of providing a nonlocal description of plasmonics, such as the dispersion of the surface plasmon-polaritons and the potentials created in these structures. The validity of the hydrodynamic model holds for different nanostructure geometries when provided with specific boundary conditions for each case. For that, Euler's equation can be written in terms of the density of particles in the gas $n(\mathbf{r})$ where the mass density is $\rho(\mathbf{r})=mn(\mathbf{r})$

$$mn(\mathbf{r})\frac{\partial\mathbf{v}}{\partial t}+mn(\mathbf{r})(\mathbf{v}\cdot\nabla)\mathbf{v}=\mathbf{g}mn(\mathbf{r})-\nabla P \tag{2.12}$$

Other physical phenomena, such as electron-phonon and electron-electron interactions, can be introduced to the study, but only if we consider scattering effects. Then we add the term $mn(\mathbf{r})\mathbf{v}/\tau$ in the left-hand side of the previous equation, where τ is the relaxation time that takes into consideration the momentum nonconservation of the electrons in the gas. Let us consider now that this gas is being perturbed by an external electric field $\mathbf{E}$. Since $\mathbf{g}$ represents the external forces per unit mass, we have $\mathbf{g}=-e\mathbf{E}/m$, where $-e$ is the electron charge. In the electrostatic regime we write $\mathbf{E}=-\nabla\phi(\mathbf{r})$, so that the external force can be expressed in terms of the electrostatic potential ϕ, which leads to

$$mn(\mathbf{r})\frac{\partial \mathbf{v}}{\partial t} + mn(\mathbf{r})(\mathbf{v}\cdot\nabla)\mathbf{v} = en(\mathbf{r})\nabla\phi(\mathbf{r}) - \nabla P \tag{2.13}$$

The statistical pressure stored in the kinetic energy of the electron gas gives the simplest estimate for the pressure. In that case, for a 3D Fermi gas, the determination of the pressure requires the calculation of the kinetic energy.

$$K_g = 2V\int \frac{d\mathbf{k}}{(2\pi)^3}\frac{\hbar^2k^2}{2m}\theta(k_F-k) = \frac{V}{5\pi^2}\frac{\hbar^2k_F^5}{2m} \tag{2.14}$$

where V is the volume of the system and k_F the Fermi wavenumber. The integral can be done in spherical coordinates, $d\mathbf{k} = k\sin\theta dk d\theta d\varphi$, with the azimutal angle integrated into $0 \leq \varphi \leq 2\pi$ and the polar angle with integration limits in $0 \leq \theta \leq \pi$. The Heaviside function states that the upper limit in the integral in dk must be k_F, so the wavenumber of the particles in the electron gas can never be greater than the Fermi wavenumber. On the other hand, the total number of particles reads

$$N_e = 2V\int \frac{d\mathbf{k}}{(2\pi)^3}\theta(k_F-k) = \frac{V}{3\pi^2}k_F^3 \tag{2.15}$$

we solved this last integral in the same way as the integral in equation (2.14). For an electron gas, we can write the Fermi wavenumber in terms of N_e and V as

$$k_F = \left(\frac{3\pi^2N_e}{V}\right)^{1/3} \tag{2.16}$$

Then, the kinetic energy is rewritten as

$$K_g = \frac{1}{5\pi^2}\frac{\hbar^2}{2m}\left(3\pi^2N_e\right)^{5/3}V^{-2/3} \tag{2.17}$$

from where it follows the statistical pressure as

$$P = -\frac{\partial K_g}{\partial V} = \gamma n^{5/3} \tag{2.18}$$

where $n(\mathbf{r})$ is the electron density which is defined as the number of particles per unit volume in the electron gas, and it is related to this last equation of state with $\gamma = (1/5)(3\pi^2)^{2/3}(\hbar^2/m)$. The gradient of the pressure is given by

$$\nabla P = \frac{5}{3}\gamma n^{2/3}\nabla n(\mathbf{r}) \tag{2.19}$$

Finally its possible to describe the hydrodynamic model in the electrostatic limit with the Euler's equation [eq. (2.20a)], the Poisson's equation [eq. (2.20b)] and the continuity equation [eq. (2.20c)] as

$$\frac{\partial \mathbf{v}}{\partial t} + (\mathbf{v}\cdot\nabla)\mathbf{v} = \frac{e}{m}\nabla\phi(\mathbf{r}) - \frac{5}{3}\gamma\frac{1}{mn^{1/3}}\nabla n(\mathbf{r}) \tag{2.20a}$$

$$\nabla^2\phi = -\frac{e}{\epsilon_0}[n_+ - n(\mathbf{r})] \tag{2.20b}$$

$$0 = \frac{\partial n(\mathbf{r})}{\partial t} + \nabla\cdot[n(\mathbf{r})\mathbf{v}] \tag{2.20c}$$

we have n_+ as the ionic background charge density neutralizing the electron gas and ϵ_0 as the vacuum permittivity. To find a solution to these hydrodynamic equations, it becomes necessary to proceed to their linearization since equation (2.20a) in its form includes nonlinear effects that are unnecessary to the case in study, in which the applied electric field is a weak perturbation, and linear terms are enough to describe the potentials and the electronic densities of the electron gas. By the usual linearization method, we get: $n(\mathbf{r},t) = n_0 + n_1(\mathbf{r},t) + n_2(\mathbf{r},t) + ...$, and $\phi(\mathbf{r},t) = \phi_0(\mathbf{r}) + \phi_1(\mathbf{r},t) + \phi_2(\mathbf{r},t) + ...$, the zeroth-order elements correspond to the electronic density and the static potential in the equilibrium state (static), where the n_0 is assumed to be constant throughout the homogeneous and infinite electron gas. The linear case is implicit in the first-order perturbation terms and, assuming $n_0 \gg n_1 \gg n_2$, we can argue that the linear order is enough to describe the system. Note the velocity $\mathbf{v}$ is intrinsic of first order (linear), there is no current flowing in the static system so $v_0 = 0$. Which explains the nonlinear character of the hydrodynamic equations and the necessity to carry out a linearization of the same. With this in mind, we write the linear hydrodynamic model as:

$$\frac{\partial \mathbf{v}}{\partial t} = \frac{e}{m}\nabla\phi_1(\mathbf{r}) - \frac{5}{3}\gamma\frac{1}{mn_0^{1/3}}\nabla n_1(\mathbf{r}) \tag{2.21}$$

$$\nabla^2\phi_1(\mathbf{r}) = \frac{e}{\epsilon_0}n_1(\mathbf{r}) \tag{2.22}$$

$$0 = \frac{\partial n_1(\mathbf{r})}{\partial t} + n_0\nabla\cdot\mathbf{v} \tag{2.23}$$

Taking the divergence of the linearized Euler's equation multiplied by n_0, it becomes more intuitive to use the Poisson's equation and the continuity equation to write Euler's equation as

$$\left(\beta^2\nabla^2 - \frac{\partial^2}{\partial t^2} - \omega_p^2\right)n_1(\mathbf{r}) = 0 \tag{2.24}$$

where β is a parameter that characterizes the nonlocality of the theory and is defined as $\beta^2 = \hbar^2k_F^2/3m^2 = v_F^2/3$ in our model. However, we can consider other sources of nonlocality that take our hydrodynamic model more realistic, and in that case, the value of the nonlocal parameter will slightly change ([17],[18],[19]). In the electrostatic regime, the value of β obtained in equation (2.24) is considered for low frequencies. To obtain the local response of the system, nothing is easier than taking $\beta \longrightarrow 0$. Physically, the nonlocal parameter tells us the speed of propagation of density disturbances in the electron gas. The wave equation (2.24) also gives the bulk plasmon frequency $\omega_p = \sqrt{e^2n_0/m\epsilon_0}$ (see chapter 1.1) and is independent of

the velocity of light c, but rather depends on the Fermi velocity v_F of the electron gas. For an infinite and homogeneous medium the electronic density is given as a plane wave solution $n_1(\mathbf{r},t) = Ae^{i(\mathbf{k}\cdot\mathbf{r}-\omega t)}$. With equation (2.24) the dispersion admits solutions of the form

$$\omega_{bulk} = \sqrt{\omega_p^2 + \beta^2 k^2} \tag{2.25}$$

Once $n_1(\mathbf{r})$ is determined, the potential follows from equation (2.22), and the velocity from equation (2.23).

2.2.1 2D electron gas and graphene

In the latter section, we derived the linearized hydrodynamic equations for a 3-dimensional electron gas. However, it is possible to reproduce the same equations but for 2-dimensional configurations. This will be important because we want to study some structures where graphene will play an important role. For 2D structures, the position vector is $\mathbf{r} = (\mathbf{r}_\parallel, z)$, with $\mathbf{r}_\parallel$ being the 2D position vector in the plane of the 2D electron gas or in graphene, this is for $z = 0$, while the configurations are chosen to be perpendicular to the z-direction. The starting point is once again Euler's equation

$$mn(\mathbf{r}_\parallel)\frac{\partial \mathbf{v}}{\partial t} + mn(\mathbf{r}_\parallel)(\mathbf{v}\cdot\nabla)\mathbf{v} = en(\mathbf{r}_\parallel)\nabla\phi(\mathbf{r}_\parallel, z=0) - \delta(z)\nabla P \tag{2.26}$$

There are some differences between the electron gas and the layer of graphene, so let us calculate the gradient of the pressure for each case. Note that the calculations are similar to the 3-dimensional electron gas.

2D electron gas

For a 2D electron gas the kinetic energy reads

$$K_g = 2A\int \frac{kdkd\theta}{(2\pi)^2}\frac{\hbar^2k^2}{2m}\theta(k_F-k) = \frac{A}{\pi}\frac{\hbar^2k_F^4}{8m} \tag{2.27}$$

where A is the area of the system. The total number of electrons in the gas is given by

$$N_e = 2A\int \frac{kdkd\theta}{(2\pi)^2}\theta(k_F-k) = \frac{A}{2\pi}k_F^2 \tag{2.28}$$

we can then write the Fermi momentum in terms of the 2D homogeneous electronic density $n_0 = N_e/A$ as

$$k_F = \sqrt{2\pi n_0} \tag{2.29}$$

It follows that the statistical pressure is given by

$$P = -\frac{\partial K_g}{\partial A} = \gamma_{2D}n_0^2 \tag{2.30}$$

where $\gamma_{2D} = \hbar^2\pi/2m$. The calculations were made to a homogeneous 2D electron gas, however; we are interested in the pressure of the inhomogeneous gas. In that case, for obtaining the gradient of the pressure, we promote n_0 to a position-dependent on 2D electronic density, that is, $n_0 \longrightarrow n_{2D}(\mathbf{r}_\parallel)$. With this assumption, the gradient of the pressure as the form

$$\nabla P = 2\gamma_{2D} n_{2D}(\mathbf{r}_\parallel)\nabla n_{2D}(\mathbf{r}_\parallel) \tag{2.31}$$

We now linearize the hydrodynamic equations by assuming $n_0 \gg n_1$, then $\phi(\mathbf{r}_\parallel) \approx \phi_0(\mathbf{r}_\parallel) + \phi_1(\mathbf{r}_\parallel)$ and $n(\mathbf{r}_\parallel) \approx n_0 + n_1(\mathbf{r}_\parallel)$. This leads to the linearized 2-dimensional hydrodynamic equations (Euler's equation, Poisson equation and continuity equation)

$$\frac{\partial \mathbf{v}}{\partial t} = \frac{e}{m}\nabla\phi_1(\mathbf{r},0) - \frac{2\gamma_{2D}}{m}\nabla n_1(\mathbf{r}_\parallel) \tag{2.32a}$$

$$\nabla^2\phi_1(\mathbf{r}) = \frac{e}{\epsilon_0}\delta(z)n_1(\mathbf{r}_\parallel,0) \tag{2.32b}$$

$$0 = \frac{\partial n_1(\mathbf{r}_\parallel)}{\partial t} + n_0\nabla\cdot\mathbf{v} \tag{2.32c}$$

where we divided Euler's equation [eq. (2.32a)] by the mass of the electron in the gas m and by the homogeneous electronic density.

Graphene

It is natural to think that to obtain the hydrodynamic equations for graphene we could just change the mass of the electrons in the 2D electron gas by the effective mass of the electron in graphene $m_g = \hbar k_F/v_F$. However the previous analysis is not entirely consistent for graphene, as the pressure has a different functional form from the 2D electron gas, due to the linear dispersion of the electrons in graphene [17]. Since we are dealing with a 2D material, the method of linearization is the same as the 2D electron gas. Also, the Fermi momentum in graphene is given by $k_F = \sqrt{\pi n_0}$, which follows from the calculation of the number of particles in the graphene layer. It presented the kinetic energy as

$$K_g = 4A\int \frac{kdkd\theta}{(2\pi)^2}v_F\hbar k = v_F\hbar\frac{2}{3\pi}\pi^{3/2}N_e^{3/2}A^{-1/2} \tag{2.33}$$

where A is the area of the graphene layer, v_F is the Fermi velocity of the electron in graphene and N_e is the total number of electrons. In a similar way to the 2D electron gas and assuming a position-dependent electronic density, we get the gradient of the pressure in the form

$$\nabla P = v_F\hbar\frac{1}{2}\sqrt{\pi n(\mathbf{r}_\parallel)}\nabla n(\mathbf{r}_\parallel) \tag{2.34}$$

At last the linearized momentum equation (Euler's equation) in real space can be written in terms of the effective mass for graphene $m_g = \hbar k_F/v_F$ as

$$\frac{\partial \mathbf{v}}{\partial t} = \frac{ev_F}{\hbar k_F}\nabla\phi_1(\mathbf{r}_\parallel, 0) - \frac{v_F^2}{2n_0}\nabla n_1(\mathbf{r}_\parallel) \tag{2.35}$$

The remaining equations are the Poisson's equation and the continuity equation given by (2.32b) and (2.32c), respectively.

2.3 Boundary Conditions

In the latter sections, we described the behavior of an electron gas in an infinite system at the lights of the hydrodynamic model. Now let us recall equation (2.24), this is the wave equation that can be solved for different geometries by writing the Laplacian in an appropriate system of coordinates. This is a physics problem known as Boundary Value Problems (BVPs) and it makes necessary to provide some boundary conditions at the surface of the electron gas to account for the proper solutions for the problems.
In the electrostatic approximation, let us consider an interface S with free surface charge density σ separating two media with different relative permittivity and a vector $\mathbf{n}$ normal to that surface. The first boundary condition follows from the continuity of the potential at the separation of the two media

$$\phi_1^{(medium\ 1)}(\mathbf{r}, t)\Big|_S = \phi_1^{(medium\ 2)}(\mathbf{r}, t)\Big|_S \tag{2.36}$$

The second boundary condition follows from the continuity of the electric displacement vector component perpendicular to the interface, and since $\mathbf{E} = \nabla\phi$ the condition can be expressed as the continuity of the normal derivative of the electrostatic potential at the interface S

$$\epsilon_1 \frac{\partial \phi_1^{(medium\ 1)}(\mathbf{r}, t)}{\partial n}\bigg|_S = \epsilon_2 \frac{\partial \phi_1^{(medium\ 2)}(\mathbf{r}, t)}{\partial n}\bigg|_S \tag{2.37}$$

The hydrodynamic model also provides an extra conditions due to the fact that the current flowing, perpendicular to the interface S, must vanish. In other words, the normal component of the electron velocity field v is zero at S

$$n_0\mathbf{v}\cdot\hat{n} = 0 \tag{2.38}$$

this last condition can be written in a more interesting way. What condition (2.38) tell us, is that the normal component of the velocity to the surface is zero, and consequently so does the time derivative of the velocity. Then, by using equation (2.21), the last boundary condition follows as

$$\frac{\epsilon_0\omega_p^2}{en_0}\frac{\partial\phi_1}{\partial n}\bigg|_S = \frac{\beta^2}{n_0}\frac{\partial n_1}{\partial n}\bigg|_S \tag{2.39}$$

In this way the hydrodynamic equations can be solved with the constrains provided by the boundary conditions given by equations (2.36), (2.37) and (2.39). Now let us consider that medium 2 is a metallic system, in this case, the metal dielectric function is given by the Drude model (see chapter 1.1)

$$\epsilon(\omega) = \epsilon_\infty - \frac{\omega_p^2}{\omega^2} \tag{2.40}$$

where ϵ_∞ is a background permittivity that accounts for all the effects that are not provided by the free electrons, such as high-frequency interband transitions. Note that in equation (2.40) we are not considering damping effects ($\Gamma = 0$). In the hydrodynamic model, it already held all the charges accountable within the theory, so in this case, for a nonlocal metal the boundary condition that states the continuity of the normal derivative of the potential [eq. (2.37)] is changed as

$$\epsilon_1 \frac{\partial \phi_1^{(medium\ 1)}(\mathbf{r}, t)}{\partial n}\bigg|_S = \epsilon_\infty \frac{\partial \phi_1^{(metal)}(\mathbf{r}, t)}{\partial n}\bigg|_S \tag{2.41}$$

If we are in the presence of local metal, it is only necessary to substitute ϵ_∞ for $\epsilon(\omega)$ in the last equation, and that is because the Drude model provides a local Drude dielectric function. Whithin the hydrodynamic equations, we are now in a good position to study the optical properties of some electrostatic configurations and see how the nonlocal effects are present in the electrostatic systems.

Chapter 3

Plasmonic Nanostructures

In this chapter, we will give use to the nonlocal hydrodynamic theory derived in the last section to solve and study some electrostatic boundary-value problems. First, we will review the problem of bounded electron gases in a planar geometry. However, this model can also be generalized to cylindrical and spherical geometries [18, 20]. The case in the study will be of a semi-infinite and finite metal slab embedded in a dielectric. Following these cases, it will be interesting to study the problems in electrostatic approximation involving a 2D electron gas and a graphene layer in vacuum. Finally, the first goal of this thesis will be the study of the plasmon dispersion and the potentials created in a graphene sheet, when the latter is in the vicinity of a semi-infinite and finite nonlocal metal. The metals chosen for this last problem are gold and titanium due to their properties. We solve the problems for a planar geometry in isotropic, homogeneous, and nonmagnetic media.

3.1 Electrostatic configurations

To obtain the dispersion curves of the plasmons in the structures in study, it is first necessary to determine the electronic densities $n_1(\mathbf{r}, t)$ and the potentials $\phi_1(\mathbf{r}, t)$. The wave equation gives the electronic density, while, with this information, the potential follows directly from Poisson's equation. Then we just use the boundary conditions to obtain the plasmon dispersion in the configuration. The dispersion relation of the plasmons is of outermost importance, as it will give the energy spectrum of the plasmons and furthermore the frequencies that this type of particles are found. Although this is the standard procedure for determining the dispersion in metals, the case for the 2D electron gas and the graphene sheet will be different. First, owing to the polarization of the 2D materials, the boundary condition that states the continuity of the normal derivative of the electrostatic potential at the interface S [eq. (2.37)], will have, in this case, a discontinuity at the interface, proportional to the electronic density $n_1(\mathbf{r}_{\parallel}, t)$

$$\epsilon_1 \frac{\partial \phi_1^{(medium\ 1)}(\mathbf{r},t)}{\partial n}\bigg|_S - \epsilon_2 \frac{\partial \phi_1^{(medium\ 2)}(\mathbf{r},t)}{\partial n}\bigg|_S = \frac{e}{\epsilon_0} n_1(\mathbf{r}_\parallel, t) \tag{3.1}$$

Where the index 1 states for first-order perturbation terms, found by linearization of the potential and of the electronic density. To recall we consider the surface S at $z = 0$ and $\mathbf{r}_\parallel$ is the in-plane 2D position vector. For this reason, to solve the hydrodynamic equations we introduce the Fourier transforms in the 2D plane

$$n_1(\mathbf{r}_\parallel, t) = \int \frac{d\omega d\mathbf{k}}{(2\pi)^3} n_1(\mathbf{k},\omega) e^{i(\mathbf{k}\cdot\mathbf{r}_\parallel - \omega t)} \tag{3.2}$$

where $\mathbf{k}$ is here defined as an in-plane 2D wavevector. It is also needed the Fourier transforms of the velocity $\mathbf{v}(\mathbf{r}_\parallel, t)$ and the potential $\phi(\mathbf{r}_\parallel, t)$. Luckily, they have the same form of the last equation but for $\mathbf{v}(\mathbf{k},\omega)$ and $\phi(\mathbf{k},\omega)$. Finally, to obtain the dispersion we just use Euler's equation in the momentum space. So, by using the Fourier transforms in the hydrodynamic equations, we obtain

$$-i\omega \mathbf{v}(\mathbf{k},\omega) = \frac{e}{m} i\mathbf{k}\phi_1(\mathbf{k},0,\omega) - 2\frac{\gamma_{2D}}{m} i\mathbf{k} n_1(\mathbf{k},\omega) \tag{3.3a}$$

$$-i\omega n_1(\mathbf{k},\omega) + n_0 i\mathbf{k}\cdot\mathbf{v}(\mathbf{k},\omega) = 0 \tag{3.3b}$$

$$\left(\frac{\partial^2}{\partial z^2} - k^2\right)\phi_1(\mathbf{k},z,\omega) = \frac{e}{\epsilon_0}\delta(z) n_1(\mathbf{k},\omega) \tag{3.3c}$$

Euler's equation (3.3a) have the constants of the 2D electron gas. For graphene, we have to consider the pre-factors obtained in equation (2.35). Equation (3.3c) is nothing but Green's function that will be useful for chapter 4.

3.1.1 Metal-dielectric interface

Let us assume a planar metal-dielectric interface, with the z coordinate perpendicular to it. The metal occupies the region $z < 0$ and the dielectric region $z > 0$, so the materials are semi-infinite in both regions (see figure 3.1). Assuming an electronic density $n_1(\mathbf{r})$ of the form

$$n_1(\mathbf{r}) = n(z) e^{i(\mathbf{k}\cdot\mathbf{r}_\parallel - \omega t)} \tag{3.4}$$

for $z < 0$ (metal) and zero for $z > 0$ (dielectric), where $\mathbf{k} = k_x\hat{e}_x + k_y\hat{e}_y$ is the 2D wavenumber and $\mathbf{r}_\parallel = x\hat{e}_x + y\hat{e}_y$ is the 2D cartesian position vector. The wave equation given by (2.24) acquires the form

$$\left(\beta^2\frac{\partial^2}{\partial z^2} - \beta^2 k^2 + \omega^2 - \omega_p^2\right) n(z) = 0 \tag{3.5}$$

The solution for this last partial differential equation is chosen as $n(z) = Ae^{\alpha z}$ where A is a constant to be determined. It follows from equation (3.5): $\alpha^2\beta^2 - \beta^2 k^2 + \omega^2 - \omega_p^2 = 0$ and

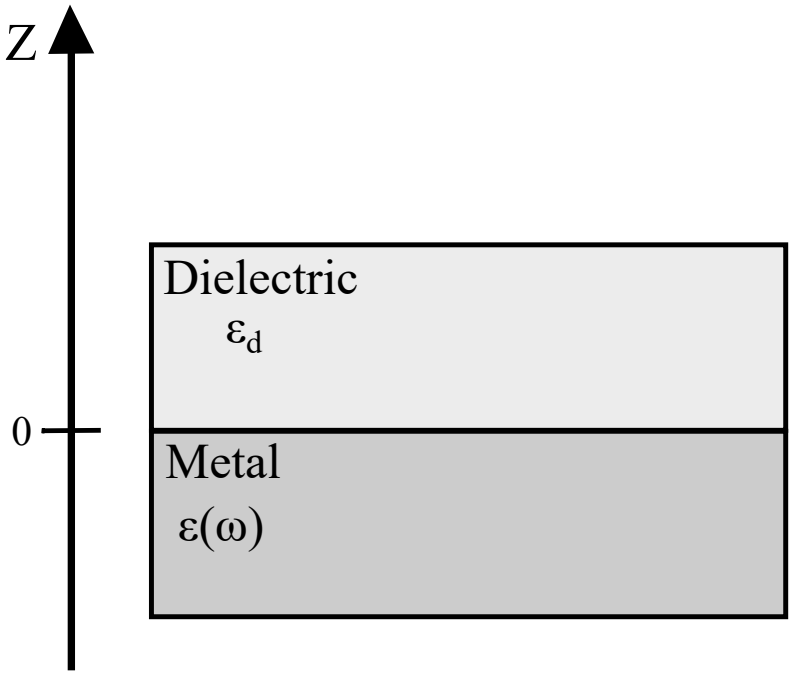

Figure 3.1: Representation of a metal-dielectric interface. Notice that the metal and the dielectric are semi-infinite slabs with permissivity $\epsilon(\omega)$ and ϵ_d, respectively.

$$\alpha^2 = k^2 + \frac{\omega_p^2 - \omega^2}{\beta^2} \tag{3.6}$$

The α parameter provides information about the nature of the SPPs. The solutions for the electronic density correspond to surface plasmons for real values of α, since $\omega < \omega_p$. For imaginary values, we have $\omega > \omega_p$, which corresponds to bulk plasmons.
The electrostatic potencial $\phi_1(\mathbf{r})$ for this system can also be written with a planar wave *ansatz* as

$$\phi_1(\mathbf{r}) = \begin{cases} M(z)e^{i(\mathbf{k}\cdot\mathbf{r}_\parallel - \omega t)} & \text{if } z < 0 \\ D(z)e^{i(\mathbf{k}\cdot\mathbf{r}_\parallel - \omega t)} & \text{if } z > 0 \end{cases} \tag{3.7}$$

where the coefficients $M(z)$ and $D(z)$ can be determined by making use of Poisson's equation (2.22). For the metal case (the region with $z < 0$), we have an electronic density given by (3.4), so in this case, the equation to solve is an inhomogeneous partial differential equation. For the dielectric case (the region with $z > 0$), since there is not a free electric charge and therefore the electronic density in this region is zero, then the partial differential equation to be solved is the Laplace equation $\nabla^2\phi(\mathbf{r}) = 0$. With this in mind, the coefficients are given by

$$\begin{aligned} M(z) &= Be^{\alpha z} + Ce^{kz} \\ D(z) &= De^{-kz} \end{aligned} \tag{3.8}$$

Note that the term proportional to C satisfies the Laplace equation, and we built the solutions, knowing the exponentials must decay as z approaches the infinity limits, or else the potentials would have an exponential growth as $|z|$ increases. Now let's focus our attention on the electrostatic potential inside the metal. It is possible to infer that we are in the presence of a nonlocal metal since the term proportional to B depends on the nonlocal parameter β [see equation (3.4)]. The solution for $M(z)$ is only valid if the following condition is verified

$$A = (\alpha^2 - k^2)\frac{\epsilon_0}{e}B \tag{3.9}$$

this last equation comes directly from solving Poisson's equation with the potential inside the metal and the electronic density $n_1(\mathbf{r})$ given by (3.4). The boundary conditions give the other restrictions at the interface, where $z = 0$. The boundary condition (2.36) reads

$$B + C = D \tag{3.10}$$

the boundary condition (2.37) gives

$$B\alpha + Ck = -\epsilon_d Dk \tag{3.11}$$

where ϵ_d is the dielectric constant for the dielectric. For this case (and for the planar slab in the next section), we will consider $\epsilon_\infty = 1$, and this choice rests on the fact that we are considering the metal as a free electron gas. For this reason, there is no polarization effects and high energy interband transitions contributing to ϵ_∞. So there is no polarization of the medium, and we can use the Drude model described in terms of a free electron gas. The last boundary condition (2.39) states

$$\frac{\epsilon_0}{e}\omega_p^2(B\alpha + Ck) - \beta^2 A\alpha = 0 \tag{3.12}$$

We end it up with a system of four linear equations and four coefficients to be determined. Manipulating the equations given by the boundary conditions will provide us with the following equation

$$\alpha + \epsilon_d k = (\epsilon_d + 1)\alpha\frac{\omega^2}{\omega_p^2} \tag{3.13}$$

For $k = 0$ the solution of the spectrum condition is $\omega = \omega_p/\sqrt{1+\epsilon_d}$, as expected for an electrostatic calculation. In addition, at $k = 0$, there is another solution given by $\omega = \omega_p$, which describes a bulk mode, (see chapter 1.1) that is, the transparent regime where the radiation propagates throughout the metal. The general solution of the spectrum condition for a metal-dielectric interface for an arbitrary value of k reads

$$\omega(k) = \frac{1}{2}\left(\beta k + \sqrt{\beta^2 k^2 + 2\omega_p^2}\right) \tag{3.14}$$

Therefore, since in general we have $\beta k \ll \omega_p$, the dispersion is approximately $\omega(k) = \frac{1}{2}(\beta k + \sqrt{2}\omega_p)$, that is, linear in the wavenumber. In figure 3.2, the spectrum given by equation (3.14) is depicted together with the horizontal line that corresponds to the electrostatic limit for the surface plasmon-polaritons in vacuum as $k \longrightarrow +\infty$.

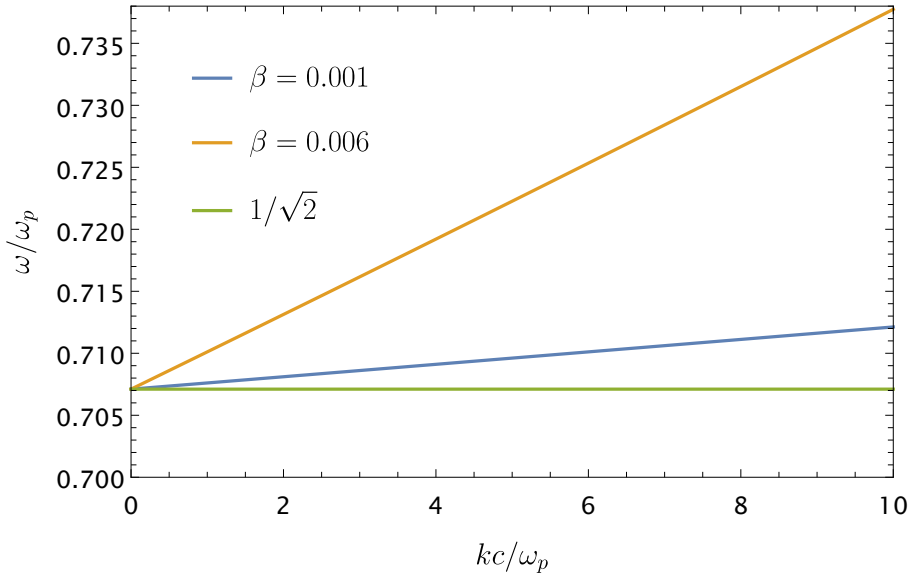

Figure 3.2: Spectrum of surface plasmon-polaritons (SPPs) in the electrostatic limit, given by equation (3.14), for the nonlocal parameters: $\beta = 0.001$ and $\beta = 0.006$. The horizontal line at $1/\sqrt{2}$ is the result for the electrostatic calculations at $k = 0$ where vacuum is the dielectric medium with $\epsilon_d = 1$.

The nonlocal effects are visible in figure 3.2. As the nonlocal parameter β approaches zero, the dispersion behavior becomes more like the horizontal line $1/\sqrt{2}$. This means that the nonlocal effects assist in an increase of the energy of the surface plasmon-polaritons. The curves presented in figure 3.2 exist with values lower than the bulk plasmon frequency, that is $\omega < \omega_p$, which means that we are in the presence of excitations bounded to the interface between the metal and the dielectric, which corresponds to SPPs (recall chapter 1.1).

3.1.2 Planar Slab

Now that we gathered the dispersion relation of the SPPs for a semi-infinite metallic slab, let's study the case for a finite metallic slab embedded in vacuum ($\epsilon_d = 1$). In figure 2 it is presented a representation for the finite slab with thickness $2a$ and with the surface oriented perpendicular to the z axis. For the other directions (x and y) the slab is infinite. For this geometry, the potentials and the electronic densities are given by

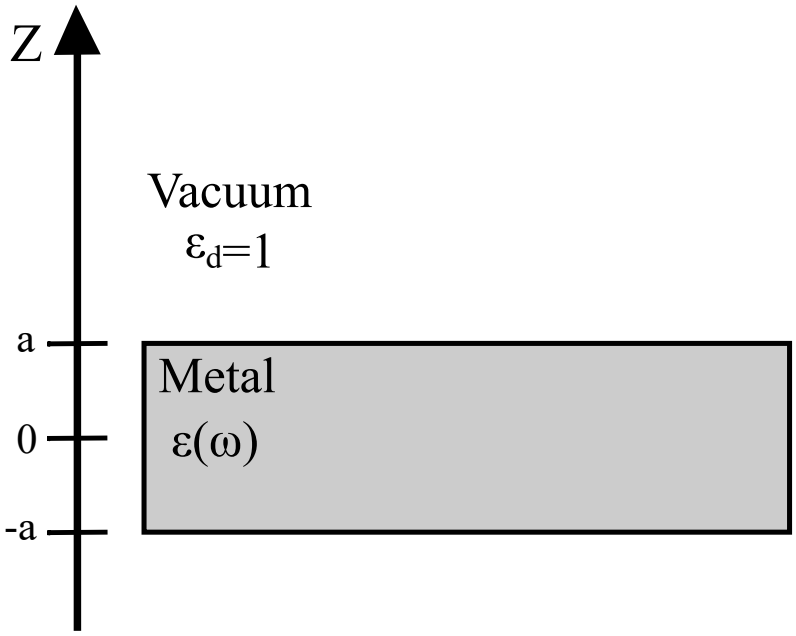

Figure 3.3: Representation of a finite metal slab with thickness $2a$ surrounded by vacuum ($\epsilon_d = 1$).

$$n_1(\mathbf{r},t) = \begin{cases} 0 & \text{if } z < -a \\ n(z)e^{i(\mathbf{k}\cdot\mathbf{r}_\parallel - \omega t)} & \text{if } -a < z < a \\ 0 & \text{if } z > a \end{cases} \tag{3.15}$$

$$\phi_1(\mathbf{r},t) = \begin{cases} D_1(z)e^{i(\mathbf{k}\cdot\mathbf{r}_\parallel - \omega t)} & \text{if } z > a \\ M(z)e^{i(\mathbf{k}\cdot\mathbf{r}_\parallel - \omega t)} & \text{if } -a < z < a \\ D_2(z)e^{i(\mathbf{k}\cdot\mathbf{r}_\parallel - \omega t)} & \text{if } z < -a \end{cases} \tag{3.16}$$

Similar to the metal-dielectric interface case, let's solve equation (2.24) in cartesian coordinates, obtaining for $n_1(\mathbf{r},t)$

$$n_1(z) = A_1 n_0 \cosh(\alpha z) + A_2 n_0 \sinh(\alpha z) \tag{3.17}$$

with α given by equation (3.6) and n_0 is the static electronic density (see chapter 2.2). As explained in the last section, the surface plasmon-polaritons will appear for real values of α and the bulk plasmons for imaginary values.

Now we determine the potentials with Poisson's equation (2.22) by solving the appropriate differential equations for each specific region. The coefficients are then given by

$$D_1(z) = D_1 e^{kz} \tag{3.18}$$

$$M(z) = B_1 \cosh(kz) + C_1 \cosh(\alpha z) + B_2 \sinh(kz) + C_1 \sinh(\alpha z) \tag{3.19}$$

$$D_2(z) = D_2 e^{-kz} \tag{3.20}$$

Just like the metal-dielectric interface, the potential outside the metal must decay as $|z| \to \infty$. Inside the metal, we write the potential as a linear combination of $\sinh$ and $\cosh$ functions because we have a finite metal and two surfaces at $z = \pm a$. We could also write the solution as exponential functions [20]. The coefficient for $M(z)$ remains valid if

$$C_1 = \frac{e}{\epsilon_0} \frac{n_0}{\alpha^2 - k^2} A_1 \tag{3.21}$$

$$C_2 = \frac{e}{\epsilon_0} \frac{n_0}{\alpha^2 - k^2} A_2 \tag{3.22}$$

To determine the dispersion for this system we first apply the boundary conditions (2.36) and (2.37) to the surface of the slab at $z = \pm a$.

$$D_1 = \left[\sinh(ka)\cosh(\alpha a) - \frac{\alpha}{k}\cosh(ka)\sinh(\alpha a)\right] C_1 + \left[\frac{\alpha}{k}\sinh(ka)\cosh(\alpha a) - \cosh(ka)\sinh(\alpha a)\right] C_2 \tag{3.23}$$

$$D_2 = \left[\sinh(ka)\cosh(\alpha a) - \frac{\alpha}{k}\cosh(ka)\sinh(\alpha a)\right] C_1 - \left[\frac{\alpha}{k}\sinh(ka)\cosh(\alpha a) - \cosh(ka)\sinh(\alpha a)\right] C_2 \tag{3.24}$$

$$B_1 = -\left[\cosh(\alpha a) + \frac{\alpha}{k}\sinh(\alpha a)\right] e^{-ka} C_1 \tag{3.25}$$

$$B_2 = -\left[\cosh(\alpha a) + \frac{\alpha}{k}\sinh(\alpha a)\right] e^{-ka} C_2 \tag{3.26}$$

Finally, the dispersion relation for the plasmons for this system within the nonlocal hydrodynamic model is obtained by applying the last boundary condition (2.39)

$$\alpha \sinh(\alpha a)\left[\frac{\omega^2}{\omega_p^2} - \frac{1}{2}\left(1 - e^{-2ka}\right)\left(1 + \frac{k}{\alpha \tanh(\alpha a)}\right)\right] A_1 \pm \alpha \cosh(\alpha a)\left[\frac{\omega^2}{\omega_p^2} - \frac{1}{2}\left(1 + e^{-2ka}\right)\left(1 + \frac{k}{\alpha \coth(\alpha a)}\right)\right] A_2 = 0 \tag{3.27}$$

The finite metal slab contains two types of solutions for the potential: even and odd modes. For an even mode $A_2 = 0$ and

$$\Omega^2 = \frac{1}{2}\left(1 - e^{-2x}\right)\left(1 + \frac{x}{y\tanh(y)}\right) \tag{3.28}$$

On the contrary, for an odd mode $A_1 = 0$ and the dispersion equation reads

$$\Omega^2 = \frac{1}{2}\left(1 + e^{-2x}\right)\left(1 + \frac{x}{y\coth(y)}\right) \tag{3.29}$$

To simplify the expressions, we defined some dimensionless variables: $\Omega = \omega/\omega_p$; $x = ka$ and $\zeta = a\omega_p/\beta$. In this case, ζ is the nonlocal parameter, but different from β this parameter defines the local case for $\zeta \longrightarrow \infty$, which is also called the non-dispersive limit [18]. Let's also define the variable $y = \alpha a = \sqrt{x^2 - \zeta^2(\Omega^2 - 1)}$ which determines the surface plasmon-polaritons modes, for real y, and the bulk plasmons modes for imaginary y. We can find the plasmon dispersion for the even and odd modes by solving the transcendental equations (3.28) and (3.29).

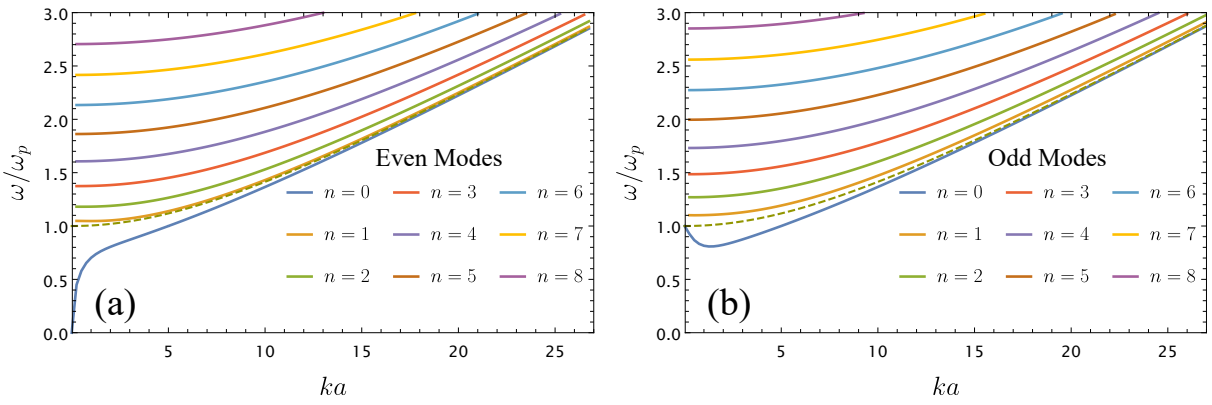

Figure 3.4: Dispersion curves in a finite metal slab with thickness $2a$ for $\zeta = 10$. (**a**) Even modes given by equation (3.28). (**b**) Odd modes given by equation (3.29). The curve with $n = 0$ corresponds to the surface mode, while the curves with $n > 0$ corresponds to bulk modes. The dashed curve is the dispersion for the infinite medium given by equation (2.25).

Let's now study the dispersion curves presented in figure 3.4. For a fixed wavenumber k there is more than one root to the transcendental equations. In that order, we found all the solutions falling in the frequency interval $0 \leqslant \Omega \leqslant 3$. We presented the solutions for the even (a) and the odd (b) modes. Depicted with the dispersion relations is also computed the dispersion for an infinite homogeneous medium given by equation (2.25). The first difference between the even and odd modes comes from the frequency at $ka = 0$. For this frequency, the lowest curves with $n = 0$, which corresponds to surface modes (α real), are different from zero in the odd modes dispersion. Actually the surface plasmon dispersion at $ka = 0$ takes the value of $\omega \sim \omega_p$. For higher values of the wavenumber, the surface mode tends to disperse similarly to the infinite medium.

To study the nonlocal effects, we provide it in figure 3.5 the dispersion relation for the surface modes and the first volume mode ($n = 1$) for different values of ζ. Our analysis shows the differences already known for the surface modes. For the even surface mode, all the curves have a null frequency at $ka = 0$ while for the odd surface modes the dispersion takes $\omega \sim \omega_p$ at $ka = 0$, no matter the value of the nonlocal parameter ζ. The volume modes are very similar to the even and odd modes. However, when the nonlocal parameter increases, the curves converge to the non-dispersive case where $\zeta \longrightarrow \infty$ (or $\beta \longrightarrow 0$), this is the local behavior of the plasmon dispersion. Actually, for this limit, the volume modes disperse to $\Omega = 1$. For the surface modes, the even and odd curves start to behave, respectively, as

$$\Omega^2 = \frac{1}{2}\left(1 - e^{-2x}\right) \tag{3.30}$$

$$\Omega^2 = \frac{1}{2}\left(1 + e^{-2x}\right) \tag{3.31}$$

This equations corresponds to the dashed curves in figure 3.5.

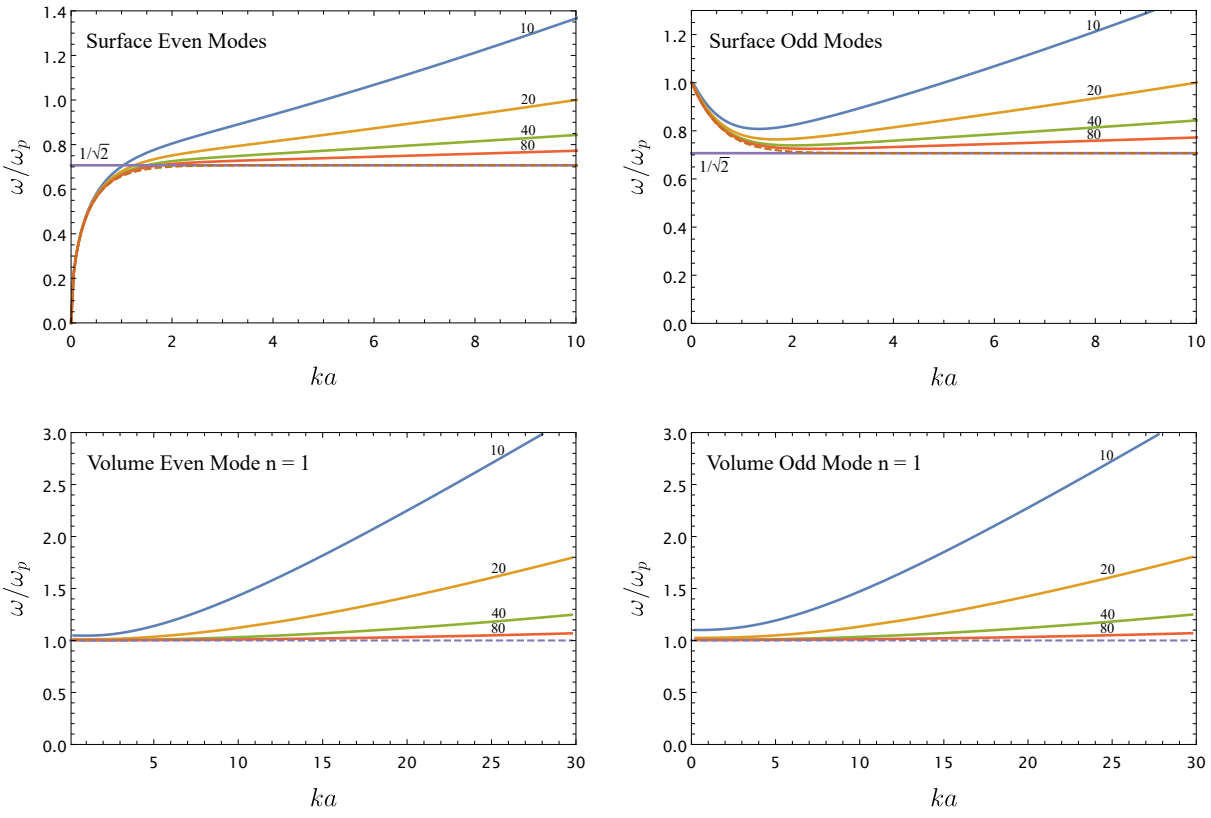

Figure 3.5: Dispersion curves in the slab for different values of the parameter $\zeta = a\omega_p/\beta(10, 20, 40, 80)$. it is represented the surface modes and the volume mode $n = 1$ for the even (left) and odd (right) cases. The dashed curve corresponds to the non-dispersive model ($\zeta = \infty$).

Consider now the induced electrostatic potential $\phi_1(z)$ in the various regions given by the equation system (3.16). In figure 3.6, we show the potential profile for the even and odd modes for different values

of ζ. Each figure shows the potential for the three regions in the study. For $z/a < -1$ and $z/a > -1$, we have the electrostatic potential in vacuum. For the metal region ($-1 < z/a < 1$) the potential is delimited by the grey vertical lines. To draw the surface mode potential, we normalize them to a specific z/a point. For the even mode, we normalize the potential at $z = 0$ and for the odd surface mode at $z = 0.5a$. This normalization became necessary to have a better comparison between the different curves. For the potential in the volume modes, the normalization did not show necessary. It is also interesting to note that the odd modes possess a node at the center of the slab, which does not occur in the even modes. Once again, as the nonlocal parameter increases, the potential tends to the non-dispersive limit (dashed line).

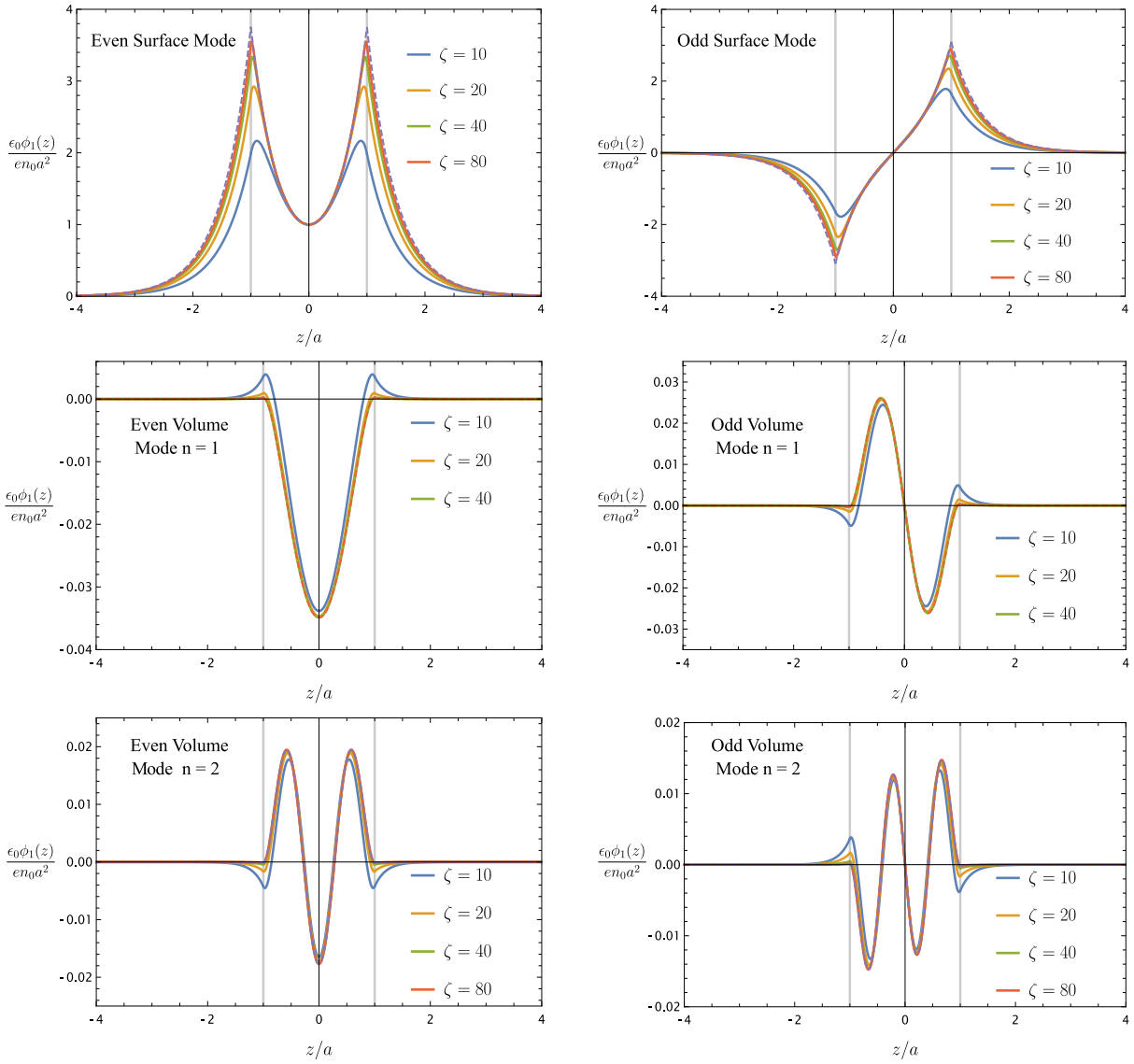

Figure 3.6: Electrostatic potential $\phi_1(z)$ in a slab for various values of $\zeta(10, 20, 40, 80)$. To plot the surface mode we took $ka = 2$ and for the volume modes $ka = 5$. The dashed line corresponds to the non-dispersive model ($\zeta \longrightarrow \infty$).

3.1.3 2D electron gas

To start the study of 2D materials, let us consider the simple case of a 2D electron gas surrounded by vacuum with his interface perpendicular to the z axis and located at $z = 0$. We now consider the potential in the momentum space $\phi_1(\mathbf{k}, z, \omega)$, assuming $\phi_1(\mathbf{k}, z, \omega) = Ae^{-kz}$ for $z > 0$ and $\phi_1(\mathbf{k}, z, \omega) = Ae^{kz}$ for $z < 0$ (note the potentials satisfy Poisson's equation (3.3c) in vacuum). The coefficients A and B need to be determined by the boundary conditions (2.36) and (3.1). Which gives the relations

$$A = B \tag{3.32}$$

$$-k(A + B) = \frac{e}{\epsilon_0} n_1(\mathbf{k}, \omega) \tag{3.33}$$

which provides

$$A = -\frac{e}{2k\epsilon_0} n_1(\mathbf{k}, \omega) \tag{3.34}$$

With these last new relations, equation (3.3a) gives an expression for the velocity $\mathbf{v}(\mathbf{k}, \omega)$ written in terms of the electronic density $n_1(\mathbf{k}, \omega)$. At last, the continuity equation (3.3b) with the expression for the velocity gives

$$\omega^2 = \frac{n_0 e^2}{2\epsilon_0 m} k + \pi n_0 \frac{\hbar^2 k^2}{m^2} \tag{3.35}$$

which is the well-known expression for the surface plasmons in a 2D electron gas [21]: $\omega \propto k$ at high wavenumber and $\omega \propto \sqrt{k}$ at small wavenumbers. Here $\hbar$ is the Planck's constant an c the velocity of light. For low frequencies, the result for the dispersion is only given by the first term, since for realistic parameters $k < k_F$. We can write the expression in a simpler and more intuitive form by considering the electronic density $n_0 = k_F^2/2\pi$ and the mass of the electron gas as $m = \hbar k_F / v_F$, where v_F is the Fermi velocity. With these definitions, the dispersion for the 2D electrons becomes,

$$\omega^2 = \frac{e^2 k_F}{4\pi\epsilon_0 \hbar} k + \frac{v_F^2}{2} k^2 \tag{3.36}$$

In [21] it is seen the dispersion given by equation (3.36). The plasmon dispersion obtained is proportional to $\sqrt{k}$ and the SPPs are seen in the range of frequencies of Gigahertz (GHz).

3.1.4 Graphene

Obtaining the dispersion of the surface plasmon in graphene is a lot similar to the calculations made for the 2D electron gas. We consider a graphene sheet (2-dimensional) in vacuum located at $z = 0$ and with the normal vector parallel to the z axis. Of course the potential is the same as before: $\phi_1(\mathbf{k}, z, \omega) = Ae^{-kz}$ for $z > 0$ and $\phi_1(\mathbf{k}, z, \omega) = Ae^{kz}$ for $z < 0$. From the boundary conditions follows equations (3.32) and (3.33), but in this case $n_1(\mathbf{k}, \omega)$ is the electronic density for graphene. Recalling that

$$\phi_1(\mathbf{k}, 0, \omega) = -\frac{e}{2k\epsilon_0} n_1(\mathbf{k}, \omega) \tag{3.37}$$

Once more, we apply the potential in Euler's equation to obtain a relation between the velocity and the electronic density $n_1(\mathbf{k}, \omega)$. Then the continuity equation provides the expression for the dispersion

$$\hbar^2\omega^2 = 2\alpha_{FS}E_F\hbar ck + \frac{v_F^2\hbar^2}{2}k^2 \approx 2\alpha_{FS}E_F\hbar ck \tag{3.38}$$

with the approximate result valid for realistic parameters ($k < k_F$). The last term in equation (3.38) is the hydrodynamic correction to the dispersion relation of plasmons in graphene. Recall the Fermi momentum for graphene $k_F = \sqrt{\pi n_0}$ and the Fermi energy $E_F = \hbar k_F v_F$. The fine structure constant is given by $\alpha_{FS} = e^2/4\pi\epsilon_0\hbar c$.

In figure 3.7 is represented the dispersion of the surface plasmons in graphene given by equation (3.38) for different values of the Fermi energy. The energy of the plasmons in graphene it is in the order of $0 - 80$ meV as seen in (a), which corresponds to a frequency plasmon in the $0 - 15$ terahertz region (b). As expected, the plasmons have a dispersion proportional to $\sqrt{k}$ for low momentum frequencies, while for larger k the curves tend to a linear dispersion. In [20] is stated that the validity of the hydrodynamic model is limited to the frequency values of $kv_F \ll \omega \ll k_F v_F$. The typical value for the homogeneous electronic density in graphene is in the order of $n_0 \leqslant 10^{-13}$ cm^{-2}, and the corresponding Fermi energy must respect the condition $E_F \leqslant 0.4$ eV. This will allow us to study the plasmonic properties of graphene in the THz to a mid-infrared range of frequencies, which is confirmed by figure 3.7 (b).

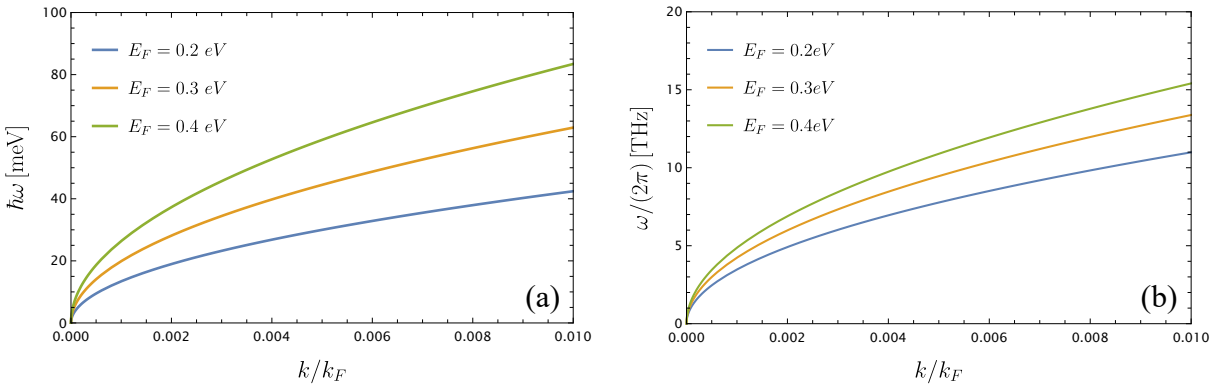

Figure 3.7: Dispersion relation [eq. (3.38)] for a single layer of graphene in vacuum for different values of the Fermi energies $E_F = (0.2, 0.3, 0.4)$ eV and a typical Fermi velocity of $v_F = c/300$. **(a)** Dispersion in terms of energy of the surface plasmons in the graphene layer. **(b)** Dispersion of plasmons in graphene regarding frequencies. Plasmonic effects are found in the THz to mid-infrared range of frequencies.

3.2 Graphene-Metal Interface

The electrostatic boundary-value problems solved in the latter sections are already known by literature [17, 18, 20, 21]. Our attention must go now to the problem of the generation of plasmons in a graphene

sheet when it is in the vicinity of a metal. At a first approach, this section will focus on the study of the nonlocal effects in the dispersion of the surface plasmons and the potentials created in graphene for two different planar configurations: first we will consider a semi-infinite nonlocal metal slab and then we generalize the results for a finite nonlocal metal slab. To simplify the algebra, graphene will always be located at $z = 0$ in the next problems.

Graphene in the vicinity of a semi-infinite metal

Let's then consider a planar configuration perpendicular to the z-axis and infinite for the x and y axis, as we can see in figure 3.8. The layered heterostructure is embedded in vacuum ($\epsilon_d = 1$). For this geometry, we have graphene separated from metal through a dielectric of thickness d. The metal occupies the region $z < -d$ while the dielectric is placed at $-d < z < 0$.

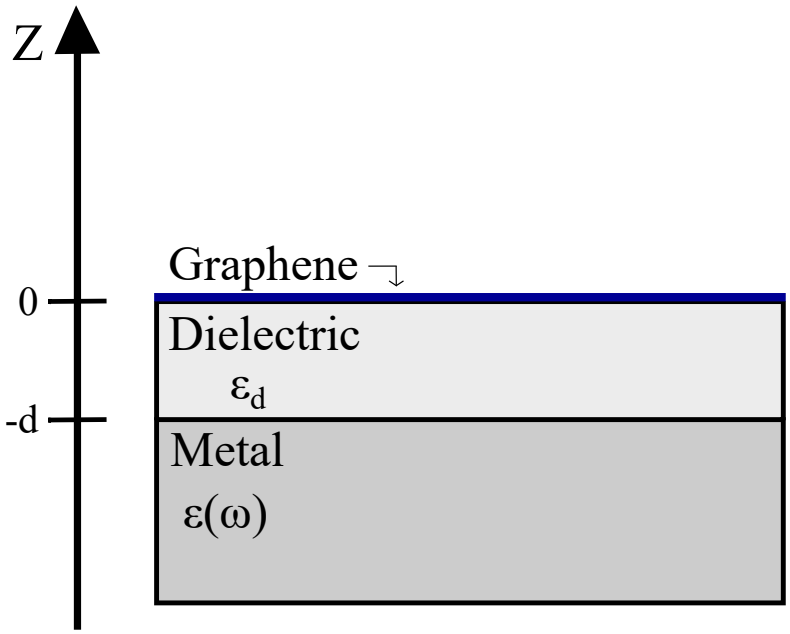

Figure 3.8: Schematic representation of graphene in the vicinity of a semi-infinite metal. Between the graphene sheet and the metal exists a dielectric of thickness d and dielectric constant ϵ_d.

For this planar geometry the electronic density and the potentials are given, respectively, by

$$n_1(\mathbf{r},t) = \begin{cases} 0 & \text{if } z > 0 \\ 0 & \text{if } -d < z < 0 \\ n(z)e^{i(\mathbf{k}\cdot\mathbf{r}_\parallel - \omega t)} & \text{if } z < -d \end{cases} \tag{3.39}$$

$$\phi_1(\mathbf{r},t) = \begin{cases} M(z)e^{i(\mathbf{k}\cdot\mathbf{r}_\parallel - \omega t)} & \text{if } z < -d \\ D(z)e^{i(\mathbf{k}\cdot\mathbf{r}_\parallel - \omega t)} & \text{if } -d < z < 0 \\ G(z)e^{i(\mathbf{k}\cdot\mathbf{r}_\parallel - \omega t)} & \text{if } z > 0 \end{cases} \tag{3.40}$$

Note that the electronic density for graphene is given by: $n_1(\mathbf{r},t) = \delta(z)n_1(\mathbf{r}_{||},t)$, however, for now, we are interested in the study of the potential for $z > 0$ (in vacuum) where the electronic density is zero, since there are no charge carriers. Graphene density will play an important role in the boundary conditions as already seen in section 3.1.4. The term $n(z)$ in the electronic density of the metal ($z < -d$) can be determined by recalling the differential equation (3.5) and the parameter $\alpha = \sqrt{k^2 + (\omega_p^2 - \omega^2)/\beta^2}$ [eq. (3.6)]. Of course, the local metal is rescued when we take $\beta \longrightarrow 0$. The differential equation as a solution of the form

$$n(z) = n_0 A e^{\alpha z} \tag{3.41}$$

For the potential, we solve Poisson's equation [eq. (2.22)] inside the metal, where the electronic density is given by the last equation, and we solve the Laplace equation for the other regions. This provides

$$M(z) = Be^{\alpha z} + Ce^{kz} \tag{3.42}$$

$$D(z) = De^{-kz} + Fe^{kz} \tag{3.43}$$

$$G(z) = Ge^{-kz} \tag{3.44}$$

In this case, the boundary conditions must apply to the surfaces at $z = 0$ (graphene/dielectric) and $z = -d$ (metal/dielectric). For the graphene-dielectric interface, the boundary conditions are given by equations (2.36) and (3.1), this last condition, we already know that due to the polarization of graphene, the normal derivative of the potential at the interface becomes discontinuous. For the metal-dielectric interface, we solve equations (2.36) and (2.37) and for the metal, the hydrodynamic model provide us with equation (2.39). Contrary to the problem of the metal-dielectric interface and the planar slab, we will consider $\epsilon_\infty \neq 1$. In this section, we will compare the strength of the nonlocal effects in two distinct metals: gold (Au) and titanium (Ti). In both cases, the background permittivity is different from 1. Within this thesis, we will only consider these two metals, even though this study is not restricted to them and we can extend the theory to other types of metals.

Solving the BCs equations is essential to determine the coefficients in the potentials. In latter electrostatic problems solved, until now, the equations were quite simple to solve through algebraic methods. However, in this case we are presented with a certain level of complexity, but luckily we have five coefficients for five boundary conditions and so we can use matricial methods to solve the linear system of equations. This is, it is only necessary to confirm the equality $M \cdot V = N$, where V is the coefficient matrix $V = [B, C, D, F, G]$ and N the matrix of the free-coefficient terms $N = [0, 0, 0, (e/\epsilon_0)n_1(\mathbf{k},\omega), 0]$. The matrix M is given by

$$M = \begin{bmatrix} e^{-\alpha d} & e^{-kd} & -e^{kd} & -e^{-kd} & 0 \\ \epsilon_\infty \alpha e^{-\alpha d} & \epsilon_\infty k e^{-kd} & \epsilon_d k e^{kd} & -\epsilon_d k e^{-kd} & 0 \\ 0 & 0 & 1 & 1 & -1 \\ 0 & 0 & \epsilon_d k & -\epsilon_d k & -k \\ (\omega^2/\omega_p^2)(\alpha/k)e^{(k-\alpha)d} & 1 & 0 & 0 & 0 \end{bmatrix}$$

The solution for all coefficients and consequently the potentials can be consulted in appendix A. For our purposes, we only need the potential in graphene to determine the dispersion of the surface plasmons in it. By that, in graphene (at $z = 0$) we have

$$\phi_1(\mathbf{k}, 0, \omega) = G(0) = \frac{e}{\epsilon_0} n_1(\mathbf{k}, \omega)[D(k, \omega) + F(k, \omega)] \tag{3.45}$$

with the auxiliary function $D(k, \omega)$ and $F(k, \omega)$, respectively

$$D(k, \omega) = -\frac{\epsilon_d(\alpha\omega^2 - k\omega_p^2) + \alpha(\omega_p^2 - \omega^2)\epsilon_\infty}{k[\epsilon_d(1 - \epsilon_d + e^{2dk}(1 + \epsilon_d))(\alpha\omega^2 - k\omega_p^2) + \alpha(\epsilon_d - 1 + e^{2dk}(1 + \epsilon_d))(\omega^2 - \omega_p^2)\epsilon_\infty]} \tag{3.46}$$

$$F(k, \omega) = -\frac{e^{2dk}(\epsilon_d(\alpha\omega^2 - k\omega_p^2) + \alpha(\omega^2 - \omega_p^2)\epsilon_\infty)}{k[\epsilon_d(1 - \epsilon_d + e^{2dk}(1 + \epsilon_d))(\alpha\omega^2 - k\omega_p^2) + \alpha(\epsilon_d - 1 + e^{2dk}(1 + \epsilon_d))(\omega^2 - \omega_p^2)\epsilon_\infty]} \tag{3.47}$$

Finally, the potencial (3.45) goes into the Euler's equation (3.3a) for graphene, and the dispersion relation follows from the continuity equation (3.3b)

$$\hbar^2\omega^2 = \left[-4\alpha_{FS}\hbar c E_F(D(k, \omega) + F(k, \omega)) + \frac{\hbar^2 v_F^2}{2}\right] k^2 \tag{3.48}$$

Figure 3.9 and 3.10 represent the energy spectrum of the surface plasmon-polaritons, given by the last equation when a graphene layer is in the vicinity of a nonlocal semi-infinite metal. The spectrum is shown for two different values of the separation between the metal and graphene, this is the dielectric thickness d. As already said, we consider two different metals, gold (Au) and titanium (Ti). The nonlocal parameter β in our model is given by $\beta = v_F/\sqrt{3}$, which for gold and titanium take the values $0.0027c$ and $0.0035c$, respectively. Gold is described by the plasma frequency $\omega_p = 8.84$ eV and by the background permittivity $\epsilon_\infty = 9.84$. While for titanium, the parameters are: $\omega_p = 2.80$ eV and $\epsilon_\infty = 2.2$ [15]. In both figures, we study the impact of the nonlocal effects probed by the metal in the spectrum of the surface plasmons in graphene and we compare the respective curves with the spectrum for the local case ($\beta \to 0$)

For gold and titanium, a linear character describes the spectrum of the surface plasmons. This means that the SPPs dispersion for graphene in a vicinity of a semi-infinite metal is proportional to the wavenumber, $\omega \propto k$. This is in contrast with the spectrum obtained for graphene in vacuum (figure

3.7), where the plasmons disperse by following the law $\sqrt{k}$. Looking now at the differences between the spectrum of the two metals, it is visible that the strength of the nonlocal effects is more enhanced in the titanium figures, where the dispersion curves has a higher separation when regarding the local spectrum.

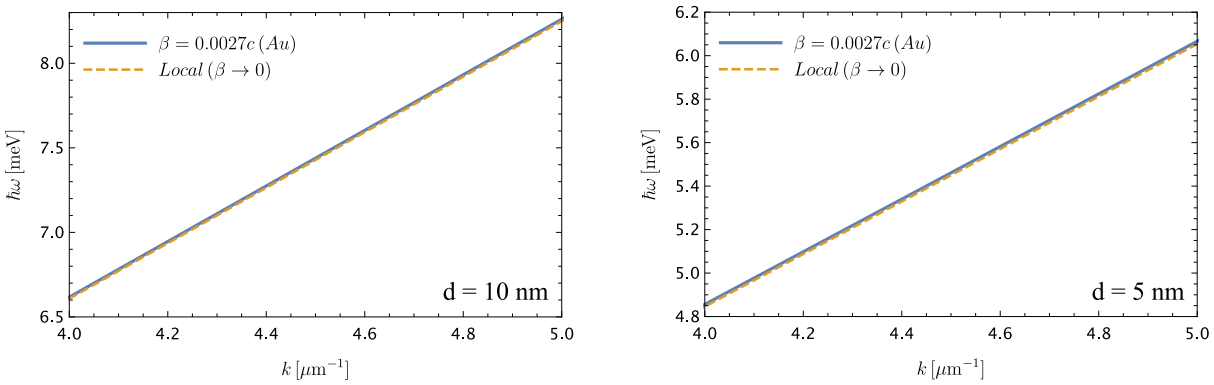

Figure 3.9: Spectrum of the graphene surface plasmon-polaritons given by equation (3.48) when in a graphene-metal interface, where the metal in case was gold. To improve the visualization of the nonlocal effects it was necessary approximate the spectrum, so note that it does not start at $k = 0$. The dielectric chosen was silicon dioxide, $\epsilon_d = 3.9$ and with thickness $d = 10$ nm and $d = 5$ nm. The nonlocal effects are studied for the nonlocal parameter $\beta = 0.0027c$. We also computed the local spectrum ($\beta \longrightarrow 0$). The other parameters are: $\omega_p = 8.84$ eV, $\epsilon_\infty = 9.84$ and $E_F = 0.17$ eV.

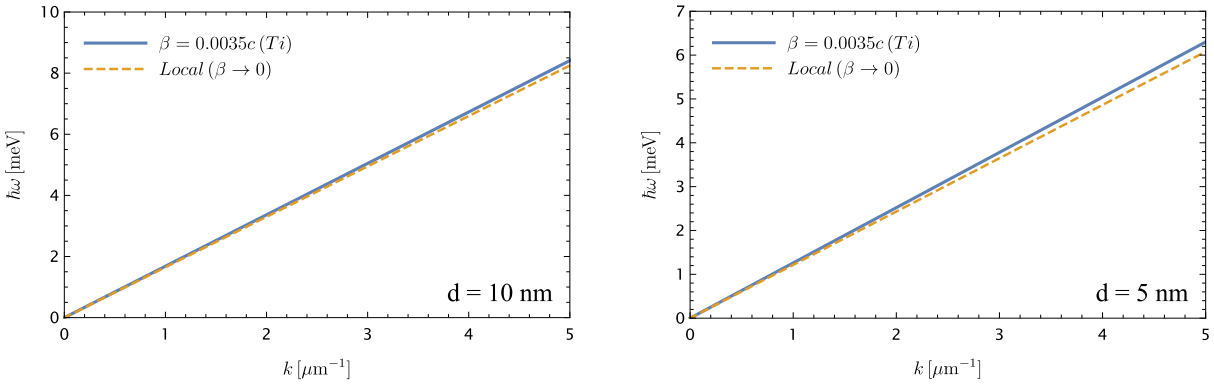

Figure 3.10: Spectrum of the graphene surface plasmon-polaritons given by equation (3.48) when in a graphene-metal interface, where the metal in case was titanium. The dielectric chosen was silicon dioxide, $\epsilon_d = 3.9$ and with thickness $d = 10$ nm and $d = 5$ nm. The nonlocal effects are studied for the nonlocal parameter $\beta = 0.0035c$. We also computed the local spectrum ($\beta \longrightarrow 0$). The other parameters are: $\omega_p = 2.80$ eV, $\epsilon_\infty = 2.20$ and $E_F = 0.17$ eV.

The nonlocality is more distinguishable in titanium due to their smaller plasma frequency ω_p and background permittivity ϵ_∞. Actually, we have $\omega_{p,Ti}/\omega_{p,Au} \simeq 0.32$ and $\epsilon_{\infty,Ti}/\epsilon_{\infty,Au} \simeq 0.22$. These two factors are crucial for the presence of nonlocal effects in the system. Furthermore, in our case we are not considering relaxation frequencies ($\gamma = 0$), however, this variable also plays an important role in the study of nonlocal effects, more information about this parameter can be found in ref. [15]. All this leads to a

higher β parameter in titanium ($\beta_{Ti}/\beta_{Au} \simeq 1.29$), which enhances the nonlocal effects. These nonlocal effects are all provenient from the characteristics of the metal, however, the dielectric between the metal and graphene also plays a role in the nonlocal spectrum. Specifically, in the proximity of the metal and graphene, or in other words, the thickness d of the dielectric change the behavior of the surface plasmon dispersion. Figures 3.9 and 3.10 shows the difference between the local and nonlocal spectrum for $d = 10$ nm and $d = 5$ nm, where we observe an increase in the nonlocal effects as the space between the metal and graphene is decreased. This effect is more perceptible for titanium. This occurs due to greater spatial confinement of the fields inside the configuration [15]. Nevertheless, when we increase the thickness of the dielectric spacer, the system tends to behave as local, and we retrieve the dispersion proportional $\sqrt{k}$.

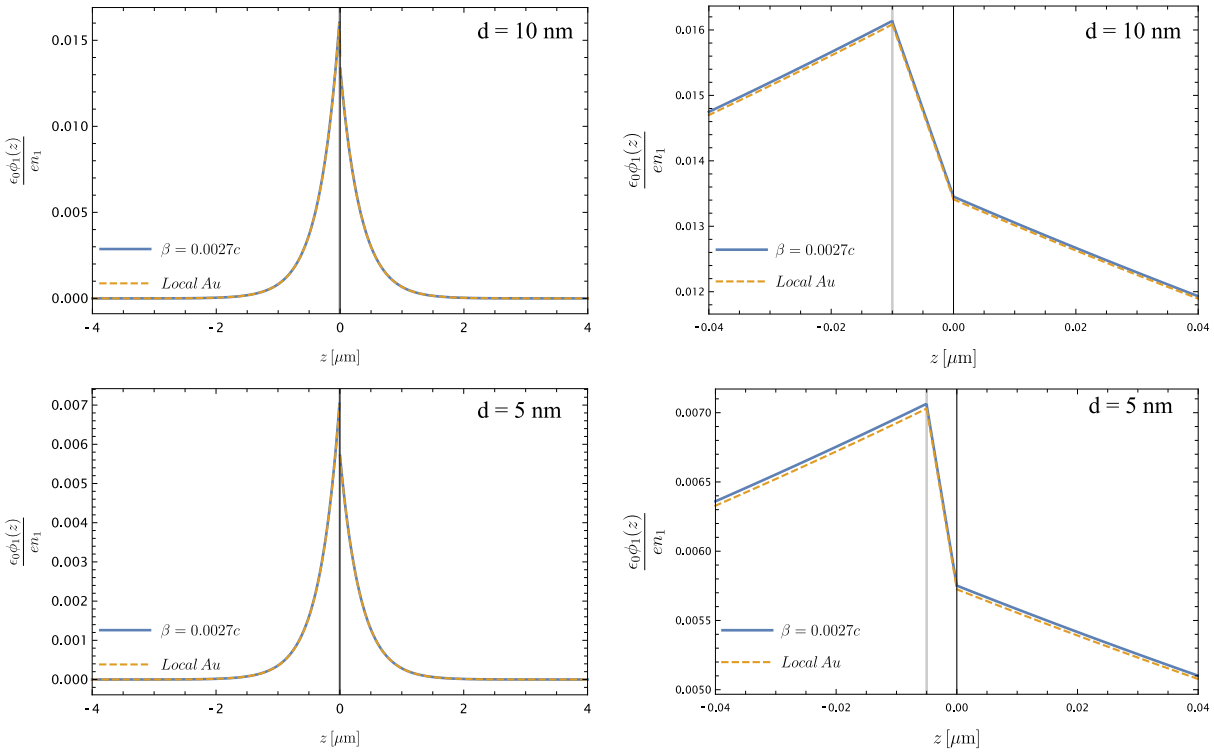

Figure 3.11: Potential curves for gold given by equation (3.40) for $k = 3\ \mu$m and $\beta = 0.0027c$. The dashed curve corresponds to the local model ($\beta \longrightarrow 0$). Note the continuity of the potentials in all regions. The right figures show an approximation to the plots on the left, so we can see the potential in the dielectric where the vertical gray lines represent the dielectric with thickness $d = 10$ nm and $d = 5$ nm. The Fermi energy has a value of $E_F = 0.17$ eV.

Finally, the potentials $\phi_1(z)$ are represented in figure 3.11 for gold and in figure 3.12 for titanium. The dielectric has thickness of $d = 10$ nm and $d = 5$ nm, fixing $k = 3\ \mu$m. It is possible to observe the behavior of the metal for $z < -d$, where, as expected, approaches zero at infinity and has an exponential growth as it becomes closer to the dielectric, where at $-d < z < 0$ we observe a descending and linear behavior for the potential. In this region, the behavior is linear because we are in a region where $z \ll 1$ (and, of course, $d \ll 1$), so we can expand the potential in a Taylor series. In this way, we obtain a

reasonable approximation by choosing only linear terms (first-order terms). At last, as we move away from the graphene layer ($z > 0$) the potential tends to zero. We also verify the continuity of the potential at all the interfaces, and for a lower nonlocal parameter β, the potential tends towards a local character.

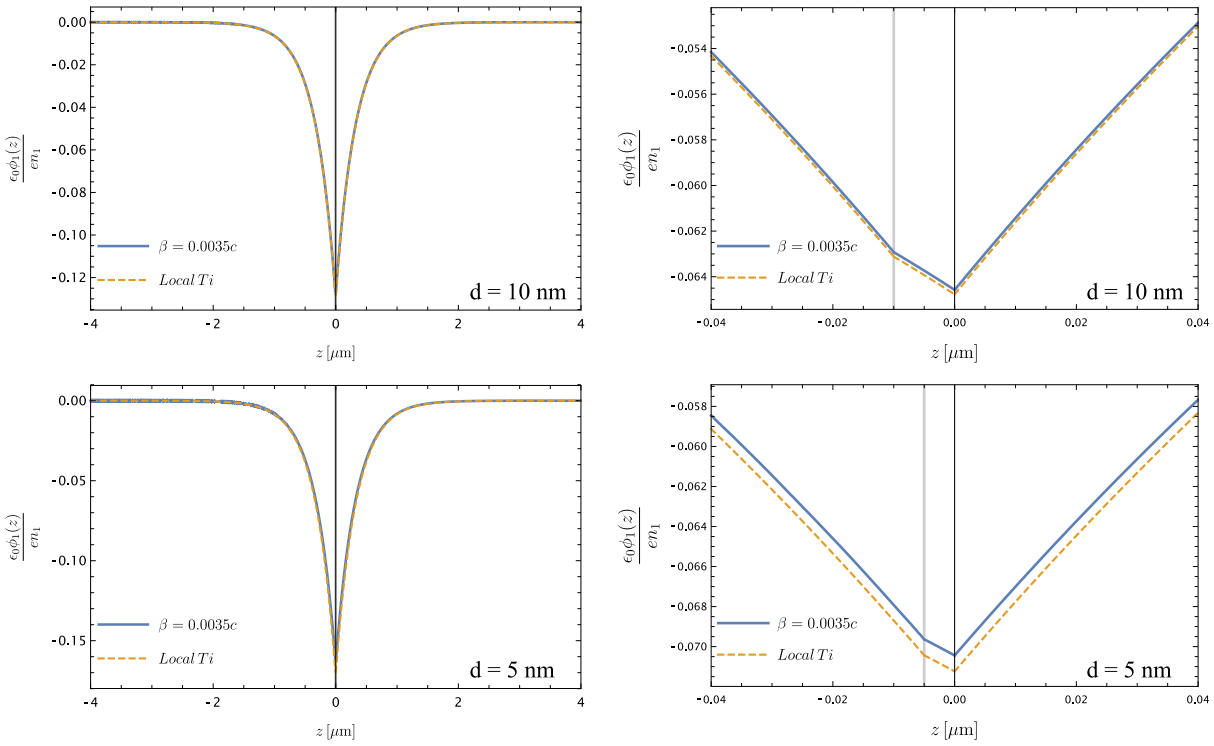

Figure 3.12: Potential curves for titanium given by equation (3.40) for $k = 3\ \mu$m and $\beta = 0.0035c$. The dashed curve corresponds to the local model ($\beta \longrightarrow 0$). Note the continuity of the potentials in all regions. The right figures show an approximation to the plots on the left, in order to study the potential in the dielectric where the vertical gray lines represent the dielectric thickness of $d = 10$ nm and $d = 5$ nm. The Fermi energy has a value of $E_F = 0.17$ eV.

Graphene in the vicinity of a finite metal

For our last electrostatic problem we retrieve the configuration in figure 3.8 but with the following additions: we take the metal as finite with thickness a and we add a semi-infinite dielectric, with dielectric constant ϵ_{d_1}, just below the metal as represented in figure 3.13. In this case, we have: dielectric 1 located at $z < -(d + a)$, the finite metal at $-(d + a) < z < -d$, and dielectric 2 at $-d < z < 0$ just between the metal and graphene. Like the last problem, the graphene layer is located at $z = 0$. Since now we have four regions, the electronic density and the potentials for each one will be

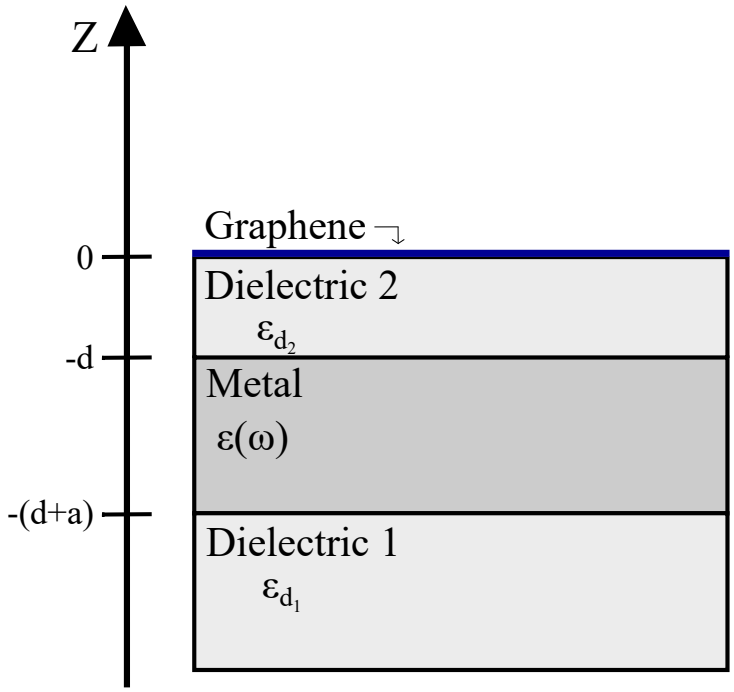

Figure 3.13: Schematic representation of graphene in the vicinity of a finite metal. Between the graphene sheet and the metal exists a dielectric (ϵ_{d_2}) of thickness d. Just below the metal is positioned a semi-infinite dielectric (ϵ_{d_1}).

$$n_1(\mathbf{r},t) = \begin{cases} 0 & \text{if } z < -(d+a) \\ n(z)e^{i(\mathbf{k}\cdot\mathbf{r}_\parallel - \omega t)} & \text{if } -(d+a) < z < -d \\ 0 & \text{if } -d < z < 0 \\ 0 & \text{if } z > 0 \end{cases} \tag{3.49}$$

$$\phi_1(\mathbf{r},t) = \begin{cases} D_1(z)e^{i(\mathbf{k}\cdot\mathbf{r}_\parallel - \omega t)} & \text{if } z < -(d+a) \\ M(z)e^{i(\mathbf{k}\cdot\mathbf{r}_\parallel - \omega t)} & \text{if } -(d+a) < z < -d \\ D_2(z)e^{i(\mathbf{k}\cdot\mathbf{r}_\parallel - \omega t)} & \text{if } -d < z < 0 \\ G(z)e^{i(\mathbf{k}\cdot\mathbf{r}_\parallel - \omega t)} & \text{if } z > 0 \end{cases} \tag{3.50}$$

Through the wave equation (3.5) we now determine the solution for the electronic density as

$$n(z) = n_0 A_1 \cosh(\alpha z) + n_0 A_2 \sinh(\alpha z) \tag{3.51}$$

where n_0 is the homogeneous electronic density. Since now we are in the presence of a finite metal, we have to consider the density solution as a linear combination of both $\cosh$ and $\sinh$ functions. For the potential, we solve Poisson's equation [eq. (2.22)] inside the metal, where the electronic density is given by the last equation. In the regions with no charge (all except the metal), we solve Laplace's equation. This gives

$$D_1(z) = De^{kz} \tag{3.52}$$

$$M(z) = B_1 \cosh(\alpha z) + C_1 \cosh(kz) + B_2 \sinh(\alpha z) + C_2 \sinh(kz) \tag{3.53}$$

$$D_2(z) = F \cosh(kz) + E \sinh(kz) \tag{3.54}$$

$$G(z) = Ge^{-kz} \tag{3.55}$$

Once again, we apply the boundary conditions stating the continuity of the potential [eq. (2.36)], the (dis)continuity of the normal derivative of the potential at the interface [eq. (2.37)], for the surfaces: $z = -(d + a)$ (metal/dielectric 1), $z = -d$ (metal/dielectric 2) and $z = 0$ (graphene/dielectric 2). We must recall equation (3.1) for the graphene-dielectric interface. Also within the metal we have the boundary condition (2.39). Similar to the graphene in the vicinity of a semi-infinite metal, we resort to matricial methods to help us find the coefficients for the potentials. So let's consider equation $M \cdot V = N$, where we have the coefficient matrix $V = [B_1, B_2, C_1, C_2, D, E, F, G]$ and $n = [0, 0, 0, 0, 0, (e/\epsilon_0)n_1(\mathbf{k}, \omega), 0, 0]$. The solution for all the coefficients, the matrix M and the potential auxiliary functions can be consulted in appendix A. The potential in graphene ($z = 0$) is then given by

$$\phi_1(\mathbf{k}, 0, \omega) = -\frac{e}{\epsilon_0} n_1(\mathbf{k}, \omega) \left[\frac{G_1(k, \omega) + G_2(k, \omega)}{T_1(k, \omega) + T_2(k, \omega)} \right] \tag{3.56}$$

Once again, the potential (3.56) goes into the Euler's equation (3.3a) for graphene, and the dispersion relation follows from the continuity equation (3.3b)

$$\hbar^2 \omega^2 = \left[4\alpha_{FS} \hbar c E_F \left(\frac{G_1(k, \omega) + G_2(k, \omega)}{T_1(k, \omega) + T_2(k, \omega)} \right) + \frac{\hbar^2 v_F^2}{2} \right] k^2 \tag{3.57}$$

The spectrum of the SPPs given by the last equation it is represented in figures 3.14 and 3.15. Just like in the last problem, we show the spectrum for the metals gold ($\beta = 0.0027c$) and titanium ($\beta = 0.0035c$). The thickness of the dielectric 2 take the values of $d = 10$ nm and $d = 5$ nm, and we show the dispersion curves for different values of the metal slab thickness. We consider dielectric 1 as vacuum and the dielectric 2 as silicon dioxide ($\epsilon_d = 3.9$). In the figures is also plotted the dispersion for the local semi-infinite metal case. This assures us that this curve will always give us the lowest energy for the surface plasmons in graphene, which is in contradiction with the results for the finite metal case, where the energy decreases as the thickness of the metal slab also decreases. In this case, we were expecting that when decreasing the thickness of the metal slab, the surface plasmons should start to behave like there is no metal in the system and their energy should increase, but that was not verified.

The thickness of the dielectric also plays an important role in the increasing energy of the plasmons. Higher the thickness, the less the effects that the metal will have on the plasmonic waves in graphene and the plasmon energy will increase, as is seen in figure 3.16. Furthermore, if the dielectric thickness between graphene and metal is increased, then the metal effects will become more negligible and the SPPs will start to have a dispersion proportional to $\sqrt{k}$ rather than linear. Since the nonlocal effects are

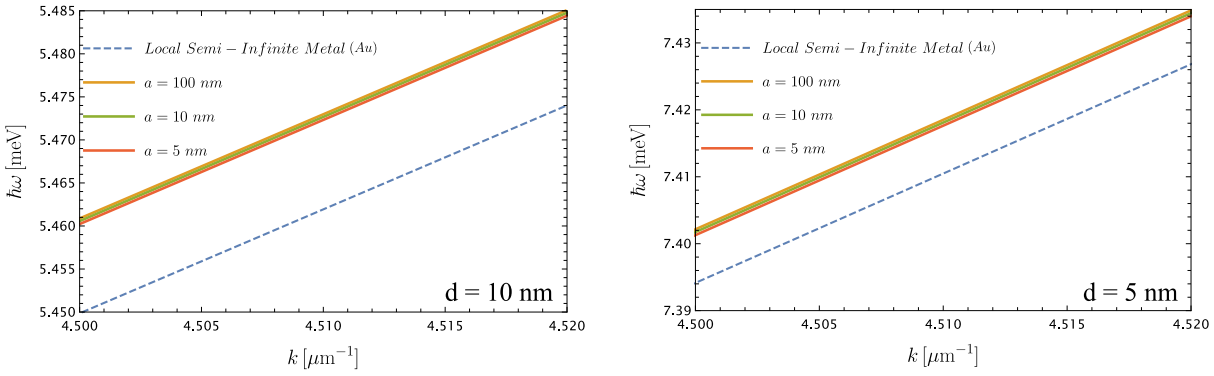

Figure 3.14: Dispersion relation of the SPPs given by equation (3.57) in a graphene/metal interface for the finite metal case (gold). The curves can be observed for different thickness of the metal $a = (100, 10, 5)$ nm. In the left figure are drawn the curves for $d = 10$ nm and in the right figure the curves for $d = 5$ nm. It is also represented the curves for the local semi-infinite metal case (dashed blue line). Note that the scale does not start at $k = 0$ in order to have a better visualization of the nonlocal curves. The parameters for gold are: $\omega_p = 8.84$, $\epsilon_\infty = 9.84$ and $\beta = 0.0027c$. The remaining parameters are: $\epsilon_{d_1} = 1$ (vacuum), $\epsilon_{d_2} = 3.9$ (silicon dioxide) and a Fermi energy of $E_F = 0.17$ eV.

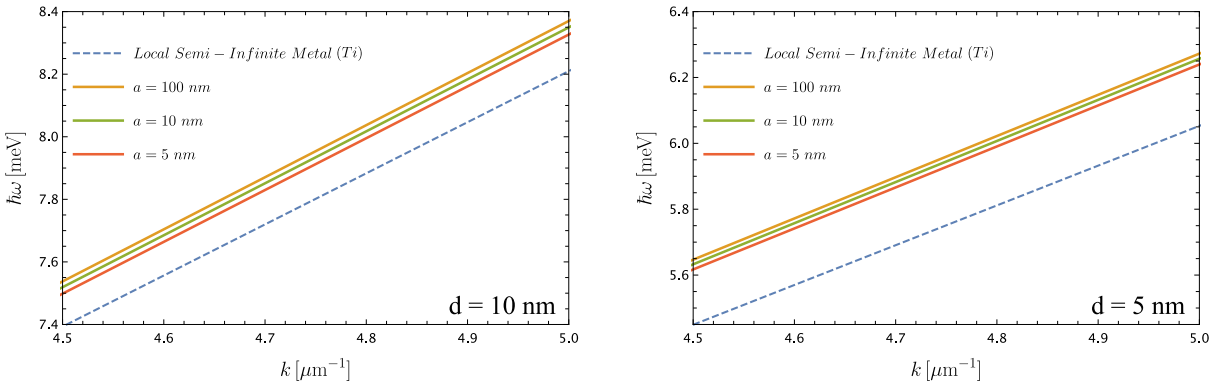

Figure 3.15: Dispersion relation given of the SPPs by equation (3.57) in a graphene/metal interface for the finite metal case (titanium). The curves can be observed for different thickness of the metal $a = (100, 10, 5)$ nm. In the left figure are drawn the curves for $d = 10$ nm and in the right figure the curves for $d = 5$ nm. It is also represented the curves for the local semi-infinite metal case (dashed blue line). Note that the scale does not start at $k = 0$, in order to have a better visualization of the nonlocal curves. The parameters for titanium are: $\omega_p = 2.8$, $\epsilon_\infty = 2.2$ and $\beta = 0.0035c$. The remaining parameters are: $\epsilon_{d_1} = 1$ (vacuum), $\epsilon_{d_2} = 3.9$ (silicon dioxide) and a Fermi energy of $E_F = 0.17$ eV.

more visible in titanium, we shall focus on this metal henceforth to study the dispersion of the SPPs and the electrostatic potentials. Note that we also computed the dispersion $\hbar v_F k$ just to check the validity of the hydrodynamic model, from chapter 3.1.4 we know that the condition $\hbar v_F k \ll \hbar\omega$ must be verified.

The exact dispersion of the SPPs [eq. (3.57)] is very mathematical complex (see appendix A), due to the high number of parameters and materials in the configuration. In that case, to have a better understanding of the dispersion behavior, let us proceed to make some approximations. We start by considering that the metal behave as a perfect metal, this is $\epsilon_\infty \to \infty$. In this case, the auxiliary

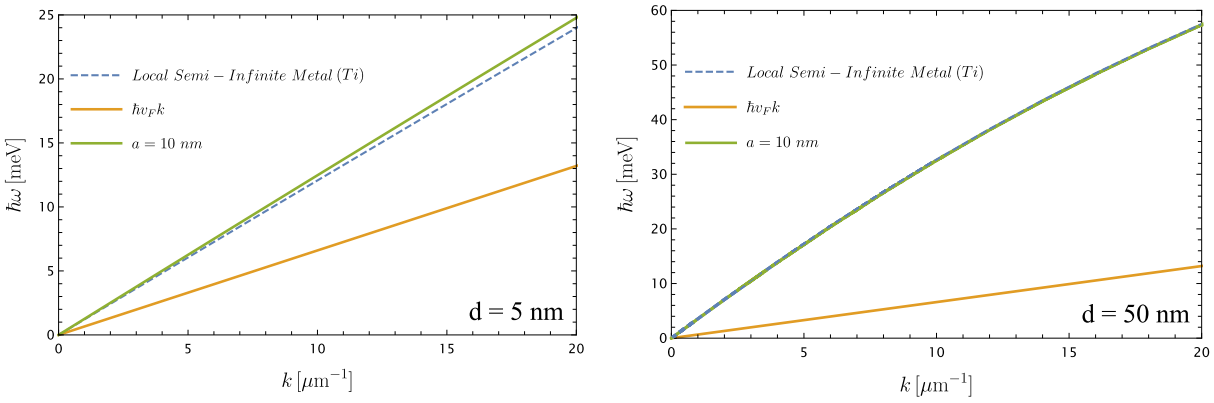

Figure 3.16: Dispersion relation of the SPPs given by equation (3.57) in a graphene/metal interface for the finite metal case (titanium), when the metal thickness has a value of $a = 10$ nm. It is also represented the curves for the semi-infinite local metal ($\beta \longrightarrow 0$) and the curve $\hbar v_F k$. In the left figure the curves are drawn for $d = 5$ nm and in the right figure for $d = 50$ nm. The parameters are: $\omega_p = 2.8$, $\epsilon_\infty = 2.2$, $\beta = 0.0035c$, $\epsilon_{d_1} = 1$, $\epsilon_{d_2} = 3.9$ and $E_F = 0.17$ eV.

functions G_1 and T_1 do not depend on the background permittivity, so their contribution to the dispersion is negligible. Regarding the functions G_2 and T_2, it is seen that they can be written with a term proportional to ϵ_∞ that sums with a term proportional to ϵ_∞^2 in both functions. Since we are taking the infinite limit, the biggest contribution will come from the quadratic term and the linear term can be neglected. In that order, the limit becomes

$$\lim_{\epsilon_\infty \to \infty} \frac{G_2(k,\omega)}{T_2(k,\omega)} = \frac{\sin(kd)}{k[\epsilon_{d_2}\cos(kd) + \sin(kd)]} \tag{3.58}$$

where for a small angle approximation $kd \ll 1$, the dispersion for graphene in the vicinity of a local provided by equation (3.57) becomes

$$\hbar^2\omega^2 = \left(4\alpha_{FS}\hbar c E_F \frac{d}{\epsilon_{d_2}} + \frac{\hbar^2 v_F^2}{2}\right) k^2 \tag{3.59}$$

This equation follows the dispersion of the SPPs in graphene near a local metal, where the separation between them is small enough and we can consider that the metal is also semi-infinite [22]. Notice that the last expression does not depend on the metal thickness. In our last approximation, we will try to recover the expression for graphene in vacuum by considering the limits $a \longrightarrow 0$ and $d \longrightarrow 0$. Of course, the dielectric constant will be $\epsilon_{d_1} = \epsilon_{d_2} = 1$ (vacuum). Let us start by obtaining the expression where the metal thickness approaches zero. In this case, by taking the limit in the hyperbolic sine and cosine terms of the auxiliary function, this will lead to the appearance of terms linear in a and quadratic in a, this last ones are neglected due to $a \longrightarrow 0$ so, for this case only the linear terms in the metal thickness contribute to the dispersion. In that order, we obtain

$$\frac{G_1(k) + G_2(k)}{T_1(k) + T_2(k)} \approx \frac{\cosh(kd) + \sinh(kd)}{2k\cosh(kd) + 2k\sinh(kd)} \tag{3.60}$$

Finally, within this expression we apply the limit $d \longrightarrow 0$ to obtain $1/2k$ and the dispersion for the graphene SPPs in vacuum is given by

$$\hbar^2\omega^2 = 2\alpha_{FS}\hbar c E_F k + \frac{\hbar^2 v_F^2}{2}k^2 \tag{3.61}$$

which is the exact expression obtained for a graphene sheet in vacuum given by equation (3.38). This shows us that the plasmon dispersion obtained when graphene is near a finite metal provide the expected expressions for graphene near a local semi-infinite metal [eq. (3.59)] and a graphene sheet in vacuum [eq. (3.61)] when taking the appropriate limits, respectively. In figure 3.17 is shown the dispersion for this two limits altogether with the dispersion for graphene in the vicinity of a semi-infinite local metal given by equation (3.48), which is expected to be the same as the limit spectrum $\epsilon_\infty \longrightarrow \infty$.

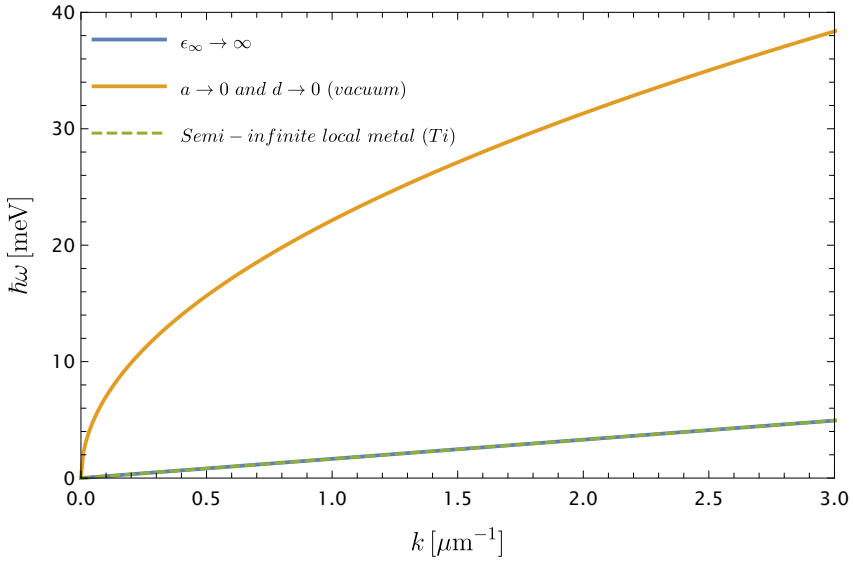

Figure 3.17: Spectrum limits of equation (3.57) that corresponds to graphene near a finite metal. For $\epsilon_\infty \longrightarrow \infty$ we obtain the spectrum of a local semi-infinite metal, that corresponds to the semi-infinite local metal (dashed green line). The dielectric chosen was silicon dioxide ($\epsilon_{d_2} = 3.9$) and a thickness of $d = 10$ nm. The metal chosen was titanium. For the limit $a \longrightarrow 0$ and $d \longrightarrow 0$ we obtain the problem of graphene in a dielectric, which in this case we choose to be vacuum ($\epsilon d_1 = \epsilon d_2 = 1$) and this spectrum agrees with the spectrum of graphene in vacuum represented in figure (3.7). The Fermi energy has a value of $E_F = 0.17$ eV.

At last, we represent the potentials in figure 3.18 for titanium ($\beta = 0.0035c$) with a thickness of $a = 10$ nm. The potentials were drawn by fixing $k = 3\ \mu\mathrm{m}^{-1}$ and for a dielectric thickness of $d = 10$ nm and $d = 5$ nm. It is for $d = 5$ nm that we see a clearer distinction between the local and nonlocal potentials, because as we decrease the dielectric thickness, the nonlocal effects become more enhanced due to the higher spatial confinement of the fields. Once again, there is a continuity for the potential in the various regions.

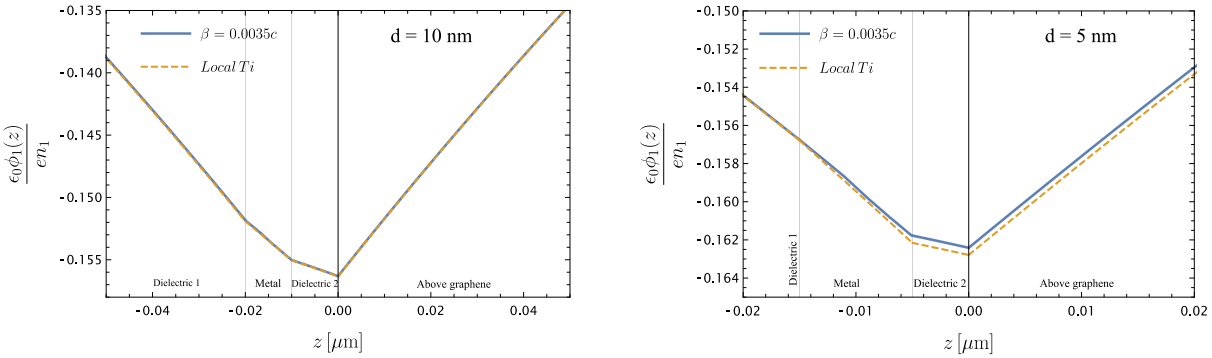

Figure 3.18: Electrostatic potential for titanium (Ti) while fixing $k = 3\ \mu\mathrm{m}^{-1}$ and $a = 10$ nm The dashed curve corresponds to the local model ($\beta \longrightarrow 0$). The thickness of the dielectric 2 is $d = 10$ nm (left) and $d = 5$ nm (right). The Fermi energy takes a value of $E_F = 0.17$ eV, the dielectric constants are $\epsilon_{d_1} = 1$ and $\epsilon_{d_2} = 3.9$. For titanium the parameters are: $\omega_p = 2.80$ and $\epsilon_\infty = 2.2$.

Chapter 4

Hydrodynamic Model in the Presence of External Potentials

In this chapter, we will extend the hydrodynamic model in the electrostatic approximation to describe the plasmonic effects created by the potential of an external charge in graphene. In the latter chapter, the intrinsic potentials of the mediums within the hydrodynamic theory provided the characteristic dispersion curves for the surface plasmons in graphene. Now that we know the typical energy at which the plasmons occur in graphene, it will be interesting to add an external moving charge to the system to study the outcome of the potential in graphene. In this thesis, we will study the potential induced in graphene by a particle moving parallel to it. Of course, the motion perpendicular to the graphene sheet can also be achieved [17] (or any other motion, for that matter). Furthermore, we derive a simple expression for the induced potential $\phi_{in}(\mathbf{r}_{\|}, z, \omega)$ due to a moving charge Ze. The following external charge densities describe this moving charge, regarding the two motion cases

$$\rho_{ex}(\mathbf{r}_{\|}, z, t) = Ze\delta(x)\delta(y)\delta(z - vt) \tag{4.1}$$

$$\rho_{ex}(\mathbf{r}_{\|}, z, t) = Ze\delta(x)\delta(y - vt)\delta(z - z_0) \tag{4.2}$$

where the particle is moving at speed v. Note that delta functions define the direction of the motion. In equation (4.1), the particle has a perpendicular motion to the graphene plane (piercing it). On the other hand, equation (4.2) describes the parallel motion to the graphene plane at a height $z = z_0$, where we also considered that the charge moves in the direction of the y-axis. We will determine the potential through equation (3.3c) having into account the presence of external charges. This equation can be solved with the Green´s function method and the potentials will be given in the momentum space. Therefore, it is necessary to perform a Fourier transforms in $\mathbf{r}$ and t of the charge densities, which gives

$$\rho_{ex}(\mathbf{k}, z, \omega) = Ze \int dt d\mathbf{r}_{\parallel} e^{-i(\mathbf{k}\cdot\mathbf{r}_{\parallel} - \omega t)} \delta(x)\delta(y)\delta(z - vt) = \frac{Ze}{v} e^{i\omega z/v} \tag{4.3}$$

$$\rho_{ex}(\mathbf{k}, z, \omega) = Ze \int dt d\mathbf{r}_{\parallel} e^{-i(\mathbf{k}\cdot\mathbf{r}_{\parallel} - \omega t)} \delta(x)\delta(y - vt)\delta(z - z_0) = 2\pi Ze\delta(z - z_0)\delta(\omega - k_y v) \tag{4.4}$$

As stated we are interested in the motion parallel to the graphene sheet, thus in the next sections we will use equation (4.4) to obtain the induced potential in the graphene sheet for two configurations: graphene in the vicinity of a dielectric and graphene in the vicinity of local metal. The parallel motion of the external charge will induce a dragging of the surface plasmons in graphene, which will lead to the formation of plasmonic wakes on the surface of graphene. First, we will have to reconstruct the hydrodynamic model to account for external charges. The methods to derive the expressions for the external and induced potentials were first deduced by Fetter in [23].

4.1 Motion Parallel to the Graphene Sheet

The additional presence of external electrostatic forces acting on the electron gas must have a description in the hydrodynamic model. This adds extra terms to Euler's and Poisson's equation. The continuity equation remains unchanged. With this external potential, we get

$$\frac{\partial \mathbf{v}}{\partial t} = \frac{ev_F}{\hbar k_F} \nabla \left[\phi_1(\mathbf{r}_{\parallel}, 0) + \phi_{ex}(\mathbf{r}_{\parallel}, 0)\right] - \frac{v_F^2}{2n_0} \nabla n_1(\mathbf{r}_{\parallel}) \tag{4.5a}$$

$$\nabla^2 \left[\phi_1(\mathbf{r}) + \phi_{ex}(\mathbf{r})\right] = -\frac{e}{\epsilon_0} \rho_{ex}(\mathbf{r}) + \frac{e}{\epsilon_0} \delta(z) n_1(\mathbf{r}_{\parallel}, 0) \tag{4.5b}$$

where $\phi_{ex}(\mathbf{r}_{\parallel}, 0)$ is the external potential acting on the electron gas due to the external forces, while $\rho_{ex}(\mathbf{r})$ is the volume density of external charges. Note that we write the last equations for the parameters in graphene. To recall, k_F and v_F are the Fermi momentum and the Fermi velocity, respectively. $n_0 = k_F^2/\pi$ is the homogeneous electronic density for graphene. Of course, we can also do it for the 2D electron gas by using equation (2.32a) instead. Moreover, we are interested in the electronic response of graphene towards an external force. Performing a Fourier transform of the quantities in equations (4.5a) and (4.5b), and we obtain

$$-i\omega \mathbf{v}(\mathbf{k}, \omega) = \frac{ev_F}{\hbar k_F} i\mathbf{k}\phi(\mathbf{k}, 0, \omega) - \frac{v_F^2}{2n_0} i\mathbf{k} n_1(\mathbf{k}, \omega) \tag{4.6a}$$

$$\left(\frac{\partial^2}{\partial z^2} - k^2\right) \phi(\mathbf{k}, z, \omega) = -\frac{1}{\epsilon_0} \rho_{ex}(\mathbf{k}, z, \omega) + \frac{e}{\epsilon_0} \delta(z) n_1(\mathbf{k}, \omega) \tag{4.6b}$$

In this equation we defined the total potential as $\phi(\mathbf{k}, z, \omega) = \phi_1(\mathbf{k}, z, \omega) + \phi_{ex}(\mathbf{k}, z, \omega)$, and $\rho_{ex}(\mathbf{k}, z, \omega)$ is the volume density of external charges. The continuity equation remains the same as equation (3.3b).

To solve equation (4.6b) we use Green's function method to obtain the potential. The free space Green's function is defined as [24]

$$\left(\frac{\partial^2}{\partial z^2} - k^2\right) g(\mathbf{k}, z - z', \omega) = -\delta(z - z') \tag{4.7}$$

where it follows the general solution for the potential

$$\phi(\mathbf{k}, z, \omega) = \frac{1}{\epsilon_0} \int dz' g(\mathbf{k}, z - z', \omega) \rho(\mathbf{k}, z', \omega) \tag{4.8}$$

where the total volume density of charge is given by

$$\rho(\mathbf{k}, z, \omega) = \rho_{ex}(\mathbf{k}, z, \omega) - e\delta(z) n_1(\mathbf{k}, \omega) \tag{4.9}$$

The solution for equation (4.7) gives the usual function (check with appendix B)

$$g(\mathbf{k}, z - z', \omega) = \frac{1}{2k} e^{-k|z-z'|} \tag{4.10}$$

then the total potential in equation (4.8) can be rewritten with the charge densities provided in equation (4.9) as

$$\phi(\mathbf{k}, z, \omega) = \int dz' \frac{1}{2k\epsilon_0} e^{-k|z-z'|} \rho_{ex}(\mathbf{k}, z', \omega) - \frac{e}{2k\epsilon_0} e^{-k|z|} n_1(\mathbf{k}, \omega) \tag{4.11}$$

which can be thought as $\phi(\mathbf{k}, z, \omega) = \Phi_{ex}(\mathbf{k}, z, \omega) - \Phi_1(\mathbf{k}, z, \omega)$. We now replace this result in the hydrodynamic equation (4.6a), obtaining

$$\omega \mathbf{v}(\mathbf{k}, \omega) = \frac{e v_F}{\hbar k_F} \mathbf{k} \left[\Phi_1(\mathbf{k}, 0, \omega) - \Phi_{ex}(\mathbf{k}, 0, \omega)\right] + \frac{v_F^2}{2n_0} \mathbf{k} n_1(\mathbf{k}, \omega) \tag{4.12}$$

With this last equation, we obtain the velocity of the electron gas which we plug into the continuity equation. By that, we obtain an expression for $n_1(\mathbf{k}, \omega)$ that depends on the external charges. This will allow us to write the induced potential in terms of $\rho_{ex}(\mathbf{k}, z, \omega)$. In this way, the induced and external potentials are given, respectively, by

$$\Phi_{in}(\mathbf{k}, z, \omega) = -\Phi_1(\mathbf{k}, z, \omega) = \frac{n_0 e^2 v_F}{4\epsilon_0^2 \hbar k_F} \frac{e^{-k|z|}}{\omega^2 - \omega_{spp}^2} \int dz' e^{-k|z'|} \rho_{ex}(\mathbf{k}, z', \omega) \tag{4.13}$$

$$\Phi_{ex}(\mathbf{k}, z, \omega) = \int dz' \frac{1}{2k\epsilon_0} e^{-k|z-z'|} \rho_{ex}(\mathbf{k}, z', \omega) \tag{4.14}$$

where ω_{spp} is the known dispersion for the surface plasmon-polaritons in graphene. Note the potentials are a function of the external volume density of charges $\rho(\mathbf{k}, z', \omega)$ in the medium. In that case, we just plug equation (4.4) for the parallel motion, to obtain the potential induced in graphene by the external charges

$$\Phi_{in}(\mathbf{k}, z, \omega) = 2\pi Z \frac{n_0 e^3 v_F}{4\epsilon_0^2 \hbar k_F} \frac{e^{-k(|z|+z_0)}}{\omega^2 - \omega_{spp}^2} \delta(\omega - k_y v) \tag{4.15}$$

$$\Phi_{ex}(\mathbf{k}, z, \omega) = \frac{2\pi Z e}{2k\epsilon_0} e^{-k|z-z_0|} \delta(\omega - k_y v) \tag{4.16}$$

To obtain the last potentials in real space, we only need to perform an inverse Fourier transform, as will be done in the next sections.

4.2 Graphene in the vicinity of a dielectric

When graphene is in the vicinity of a dielectric (ϵ_d), the calculations are similar to graphene in vacuum. However, in such case, the Green function must differ from that of the free space [eq. (4.10)], moreover, the method to get the potential remains the same. To determine the potentials when a charge is moving parallel to a graphene sheet in the vicinity of a dielectric, it is necessary to first calculate the Green's function in graphene. By that, we have graphene at $z = 0$ and the dielectric with dielectric constant ϵ_d at $z < 0$ as seen in figure 4.1. Consider that we have vacuum at $z > 0$.

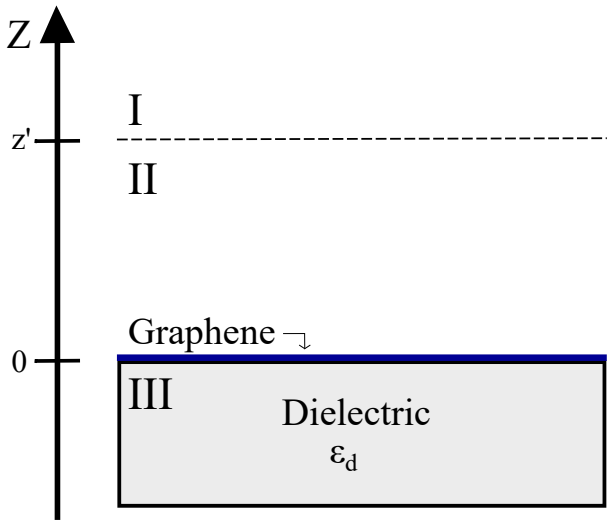

Figure 4.1: Graphene in the vicinity of a dielectric configuration. Graphene is at $z = 0$, while the dielectric is present at $z < 0$. Vacuum ($\epsilon_d = 1$) extends for $z > 0$. We want to find the Green function at an arbitrary z'.

Once again, the Green function is defined in equation (4.7). Where we consider an exponential behavior for these functions

$$g(z, z') = \begin{cases} g_I(z, z') = A(z')e^{-kz} & \text{if } z > z' \\ g_{II}(z, z') = C_1(z')e^{-kz} + C_2(z')e^{kz} & \text{if } 0 < z < z' \\ g_{III}(z, z') = B(z')e^{kz} & \text{if } z < 0 \end{cases} \tag{4.17}$$

The Green functions in equation (4.17) must, at all cases, decay as $|z| \longrightarrow \infty$. In particular, $g_I(z,z')$ must decay as z tends to positive values of infinity, while $g_{III}(z,z')$ decays for negative values of infinity. Of course, this is like the calculations done in chapter 3 for the potentials, and as in that case, it is also necessary to apply some boundary conditions to the different regions, as to obtain the coefficients in the Green function. These conditions are just the continuity of the Green function and the discontinuity of the normal derivative to the function at the boundaries (the mathematical formulation is clear in appendix B). Because the Green function is like a point charge potential, only at $z = z'$ are the derivatives not continuous. We consider all the remaining charges of the configuration when we calculate the potential with equation (4.8). Solving the linear system of the equation provided by the boundary conditions we get for the Green functions

$$g(z,z') = \begin{cases} g_I(z,z') = \frac{e^{-k(z-z')}}{2k} + r_d \frac{e^{-k(z+z')}}{2k} & \text{if } z > z' \\ g_{II}(z,z') = r_d \frac{e^{-k(z+z')}}{2k} + \frac{e^{k(z+z')}}{2k} & \text{if } 0 < z < z' \\ g_{III}(z,z') = t_d \frac{e^{k(z-z')}}{2k} & \text{if } z < 0 \end{cases} \tag{4.18}$$

By thinking of the Green functions as propagating waves through the mediums, we can express these with the "reflection"(r_d) and "transmission"(t_d) coefficients as

$$r_d = \left(\frac{1-\epsilon_d}{1+\epsilon_d} \right) \tag{4.19}$$

$$t_d = \left(\frac{2}{1+\epsilon_d} \right) \tag{4.20}$$

We now want the potential created due to the parallel motion of an external particle (at $z > 0$) to the graphene sheet. Since graphene is at $z = 0$ we want the Green function for this region, so we also admit $z' = 0$. Here $g_{II}(z,z')$ vanishes, because this region cease to exist and the induced potential in graphene is given by $g_I(z,z')$ and $g_{III}(z,z')$. However, if we want the external potential, then we have to consider $0 < z < z'$ and we must make use of the Green function $g_{II}(z,z')$. Equation (4.8) demonstrates the total potential and the external and induced potentials are, respectively

$$\Phi_{ex}(\mathbf{k},z,\omega) = \frac{1}{\epsilon_0} \int dz' \left(\frac{e^{k(z-z')}}{2k} + r_d \frac{e^{-k(z+z')}}{2k} \right) \rho_{ex}(\mathbf{k},z',\omega) \tag{4.21}$$

$$\Phi_{in}(\mathbf{k},z,\omega) = -\Phi_1(\mathbf{k},z,\omega) = -\frac{e}{\epsilon_0} t_d \frac{e^{-k|z|}}{2k} n_1(\mathbf{k},\omega) \tag{4.22}$$

Notice that $\epsilon_d = 1$ then the "reflection"coefficient is $r_d = 0$, and the "transmission"coefficient obtained is $t_d = 1$, and the potentials in the last equations are reduced to the expressions in equations (4.13) and (4.14).

Using the results for the potentials in the hydrodynamic equation (4.12), we obtain a relation for the velocity which, once again, we put in the continuity equation (3.3b) which get us the following equation

$$0 = -\omega^2 n_1(\mathbf{k},\omega) + n_0 k^2 \left[-\frac{e v_F}{\hbar k_F}\Phi_{ex}(\mathbf{k},0,\omega) + \left(\frac{e^2 v_F}{k(1+\epsilon_d)\epsilon_0 \hbar k_F} + \frac{v_F^2}{2n_0} \right) n_1(\mathbf{k},\omega) \right] \tag{4.23}$$

where the term in curve brackets multiplied by $n_0 k^2$ is the dispersion of the surface plasmon-polariton ω_{spp}, for graphene in this configuration. Recall that we can write the dispersion in terms of the Fermi energy $E_F = \hbar k_F v_F$ and the fine structure constant $\alpha_{FS} = e^2/4\pi\epsilon_0\hbar c$, by considering the homogeneous electronic density as $n_0 = k_F^2/\pi$. So the relation for the SPPs in graphene is given by

$$\omega_{spp}^2 = \frac{4\alpha_{FS} E_F \hbar c}{(1+\epsilon_d)\hbar^2} k + \frac{v_F^2}{2} k^2 \tag{4.24}$$

Note that if we take $\epsilon_d = 1$ we have graphene in vacuum and the dispersion obtained through this method is the same as the one obtained in equation (3.38). Also, resorting to this last equation, we can get the inhomogeneous electronic density $n_1(\mathbf{k},\omega)$ through equation (4.23)

$$n_1(\mathbf{k},\omega) = -\frac{(2\alpha_{FS} E_F \hbar c/e)}{\hbar^2\omega^2 - \hbar^2\omega_{spp}^2} k \int dz' t_d e^{-kz'} \rho_{ex}(\mathbf{k},z',\omega) \tag{4.25}$$

Since the induced potential in graphene depends on $n_1(\mathbf{k},\omega)$ we can write it as

$$\Phi_{in}(\mathbf{k},z,\omega) = \frac{1}{\epsilon_0}\alpha_{FS} E_F \hbar c \frac{t_d^2 e^{-k|z|}}{\hbar^2\omega^2 - \hbar^2\omega_{spp}} \int dz' e^{-kz'} \rho_{ex}(\mathbf{k},z',\omega) \tag{4.26}$$

Now we want to study the parallel motion to the graphene sheet, where the volume density of external charge (4.4) provides

$$\Phi_{in}(\mathbf{k},z,\omega) = 2\pi v^2 \Phi_0 \frac{t_d^2 e^{-k(|z|+z_0)}}{\omega^2 - \omega_{spp}^2} \delta(\omega - k_y v) \tag{4.27}$$

where the prefactor $\Phi_0 = \frac{Ze}{\epsilon_0}\frac{\alpha_{FS} E_F \hbar c}{\hbar^2 v^2}$ has units of electric potential and we defined it to make the potentials easier to read. Note that the delta function implies that the particle disperses with a frequency given by $\omega = k_y v$. Fourier transforming to real space and time equation (4.27), we obtain for $\Phi_{in}(\mathbf{r},z,t)$

$$\Phi_{in}(\mathbf{r},z,t) = v^2 \Phi_0 \int_{-\infty}^{\infty} \frac{d\omega d\mathbf{k}}{(2\pi)^2} \frac{t_d^2 e^{-k(|z|+z_0)} e^{i(\mathbf{r}_\parallel\cdot\mathbf{k}-\omega t)}}{\omega^2 - \omega_{spp}^2} \delta(\omega - k_y v) \tag{4.28}$$

This last equation finally gives us the potential induced in the surface of the graphene sheet. However, the expression as such, still needs to be resolved, so as to provide us with results for the problems in question. We will work out a method to calculate the integral in a more convenient form. The calculation method is based on a mathematical description given to us by [17], where the Sokhotski-Plemelj formula will allow us to divide the integral into two distinct new integrals: a principal value integral and an imaginary integral. Before we start the calculation of the integral, let us compute the phase velocity $v_p = \omega/k$ of the plasmons in graphene

$$v_p = \frac{\sqrt{ak}}{k} = \left(\frac{\omega}{a}\right)^{\kappa} \tag{4.29}$$

with $\kappa = -1$. Thus, plasmons in graphene behave as gravity waves [25], with an acceleration a. The argument of the δ-function in equation (4.28) implies that $\omega = kv\cos\theta$, which also gives us the following condition

$$\cos\theta = \frac{\omega}{vk} = \frac{v_p}{v} \leq 1 \tag{4.30}$$

by that, the velocity v of the charge must be larger than v_p. Using $\omega = \sqrt{ak}$, we must also have

$$\frac{a}{v^2} \leq k \tag{4.31}$$

This means that the k integral has domain $k \in [a/v^2, \infty[$. Now that we have defined the domain of integration of the potential integral in equation (4.28), let us write it in polar coordinates for simplicity

$$\Phi_{in}(\mathbf{r}_{\parallel}, z, t) = v^2 t_d^2 \Phi_0 \int_0^{2\pi} \frac{d\theta}{2\pi} \int_0^{\infty} \frac{kdk}{2\pi} \frac{e^{-k(|z|+z_0)} e^{ik[r\cos(\theta-\theta')-vt\cos\theta]}}{(kv\cos\theta)^2 + i\mathrm{sgn}(\cos\theta)\eta - ak} \tag{4.32}$$

In this last integral we made some important considerations, where the polar angle θ is the angle that the vector $\mathbf{k}$ makes with the y-axis. While the angle θ' is the polar angle of $\mathbf{r}_{\parallel}$, and by that end the scalar product $\mathbf{k}\cdot\mathbf{r}$ is given by $kr\cos(\theta-\theta')$. Note that the delta function implies $\omega = k_y v$, but the y-component of $\mathbf{k}$ can be written as $k_y = k\cos\theta$. To treat the dispersion of the surface plasmon-polaritons in graphene [eq. (4.24)], we know that for real parameters ($k \ll k_F$) the hydrodynamic term can be neglected. So we get $\omega_{spp}^2 = ak$, where $a = \frac{4\alpha_{FS}E_F\hbar c}{(1+\epsilon_d)\hbar^2}$ is a parameter with units of acceleration and characterizes the 2D electron gas in graphene. Finally, to solve the integral in the complex plane we get the term $i\mathrm{sgn}(\cos\theta)\eta$, where $\eta \longrightarrow 0$ and $\mathrm{sgn}(\cos\theta)$ is the sign function for cosine. Equation (4.29) can be resolved by using the Sokhotski-Plemelj theorem

$$\begin{aligned}\Phi_{in}(\mathbf{r}_{\parallel}, z, t) = {} & t_d^2\Phi_0 \int_0^{2\pi} \frac{d\theta}{2\pi} \fint_0^{\infty} \frac{dk}{2\pi} \frac{e^{-k\mu}e^{ik\nu}}{k\cos^2\theta - a/v^2} \\ & - i\pi t_d^2\Phi_0 \int_0^{2\pi} \frac{d\theta}{2\pi} \int_0^{\infty} \frac{dk}{2\pi} e^{-k\mu}e^{ik\nu}\mathrm{sgn}(\cos\theta)\delta(k\cos^2\theta - a/v^2)\end{aligned} \tag{4.33}$$

where the symbol $\fint$ stands for the principal value of the integral. The parameters μ and ν are given by

$$\mu = |z| + z_0 \tag{4.34}$$

$$\nu = [r\cos(\theta-\theta') - vt\cos\theta] \tag{4.35}$$

Now let's perform a variable change of the form $k\cos^2\theta - a/v^2 = \kappa$, then the last integral can be written as

$$\Phi_{in}(\mathbf{r}_{\parallel}, z, t) = \Phi_0 t_d^2 \int_0^{2\pi} \frac{d\theta}{(2\pi)^2} \frac{e^{-f(\theta)}}{\cos^2\theta} \fint_{-a/v^2}^{\infty} d\kappa \frac{e^{-v^2 f(\theta)\kappa/a}}{\kappa} - i\pi t_d^2 \Phi_0 \int_0^{2\pi} \frac{d\theta}{(2\pi)^2} \frac{e^{-f(\theta)}}{\cos^2\theta} \mathrm{sgn}(\cos\theta) \tag{4.36}$$

In this case the sign function constrains the limits of integration, that is, if the cosine function is positive the sign function takes the value of $+1$ within the integration limits $[-\pi/2, \pi/2]$, while for negative values of $\cos\theta$ the sign function takes -1 in the range of integration $[\pi/2, 3\pi/2]$. We also defined the function $f(\theta)$ as

$$f(\theta) = \frac{a}{\cos^2\theta v^2}[\mu - i\nu(\theta)] \tag{4.37}$$

with μ and ν defined in equations (4.34) and (4.35), respectively. The principal value of the integral in κ is a known special function, called the exponential integral function $\mathrm{Ei}(x)$. So we write the integral as

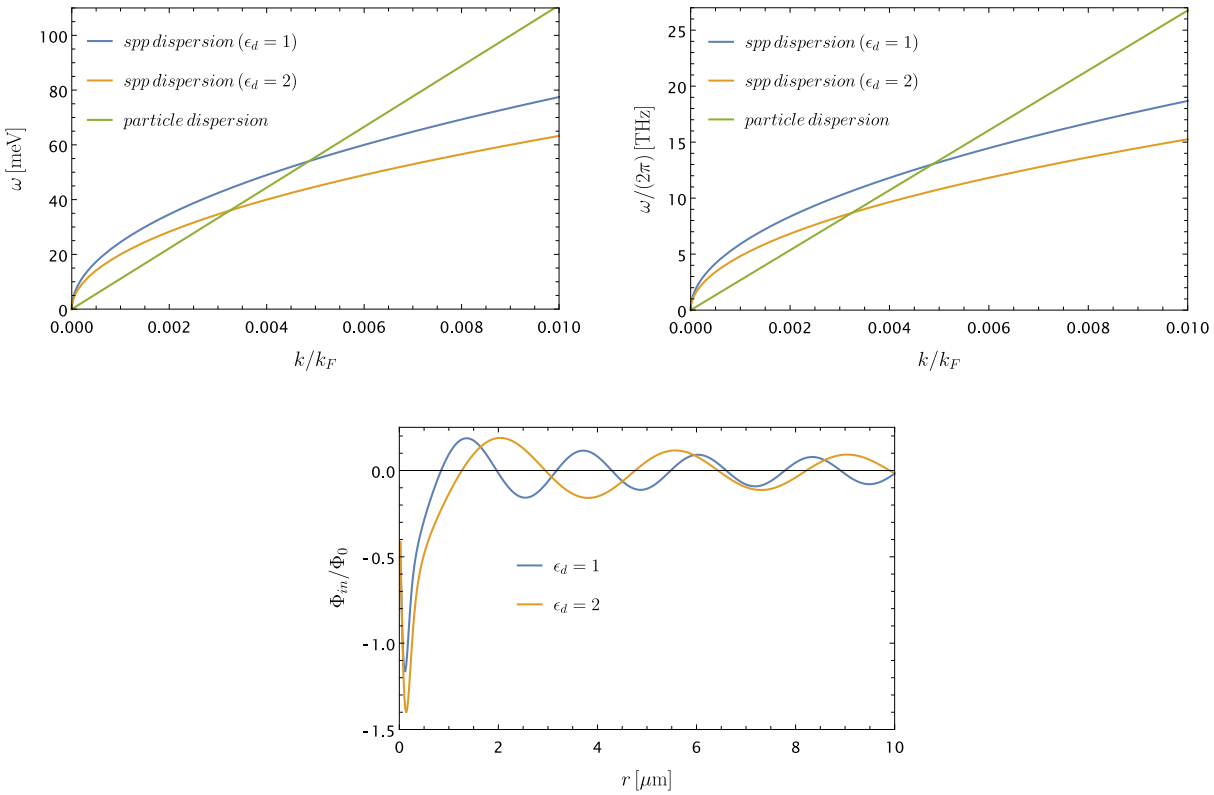

Figure 4.2: Top: Dispersion relation of the graphene SPPs, when in the vicinity of a dielectric given by equation (4.24) in terms of energy (left) and frequency (right). The green curve corresponds to the particle dispersion that follows the law $\omega = kv$, along the direction of the moving particle (y-axis). Note that the velocity of the moving particle v gives the slope of the spectrum. Bottom: Induced electrostatic potential along the direction of propagation of the moving particle. The parameters are: an electronic density of 10^5 μm^{-2} which gives a Fermi energy of $E_F = 0.37$ eV ,$v = 0.1c$, $z_0 = 0.01$ μm and $t = 0$ s. The plots show the curves for two distinct values of the dielectric constant, $\epsilon_d = 1$ and $\epsilon_d = 2$.

$$\Phi_{in}(\mathbf{r}_{\parallel}, z, t) = t_d^2 \Phi_0 \int_0^{2\pi} \frac{d\theta}{(2\pi)^2} \frac{e^{-f(\theta)}}{\cos^2\theta} \mathrm{Ei}[f(\theta)] - i\pi t_d^2 \Phi_0 \int_0^{2\pi} \frac{d\theta}{(2\pi)^2} \frac{e^{-f(\theta)}}{\cos^2\theta} \mathrm{sgn}(\cos\theta) \tag{4.38}$$

In figure 4.2 we can see the spectrum of the surface plasmon-polaritons in graphene given by equation (4.24) in terms of energy and frequency of the plasmons plotted with the external particle dispersion given by $\omega = kv$. See that if we change the velocity of the external particle, this will also change the slope of this curve (since it is given by v). From the particle dispersion, we see it intercepts the SPPs dispersion in graphene, when in the vicinity of a dielectric, at $k/k_F = 0.00488$ for $\epsilon_d = 1$, corresponding to a SPP wavelength of $\lambda_{spp} = 2\pi/k = 2.3$ μm. The successive crest of the potential in vacuum (blue line), gives value of $\triangle y \approx 2.3$ μm which matches well with the value obtained by the dispersion plot. For the case were $\epsilon_d = 2$ the interception occurs at $k/k_F = 0.00322$, corresponding to a SPP wavelength of $\lambda_{spp} = 2\pi/k = 3.48$ μm, which, as expected, matches the successive crests in the potential of the orange line, where $\triangle r \approx 3.48$ μm. If we change the velocity of the particle, those interceptions will occur at different values, and consequently, this will also change the wavelength of the SPP as it alters the distance between crests in the potential. Some transversal and longitudinal cuts were also made to represent the induced potential. Hence if the coordinate y is fixed to a certain value, then we get a transversal representation of the potential for all values of the coordinate x. Meanwhile, in the longitudinal cut, what is fixed is the coordinate x and the potential is represented for all values of y. In figure 4.3 is represented the transverse (left) and longitudinal potential (right), for the fixed values $y_0 = -10$ μm and $x_0 = 0$ μm, respectively. These representations also allow us to see the oscillatory character of the potential.

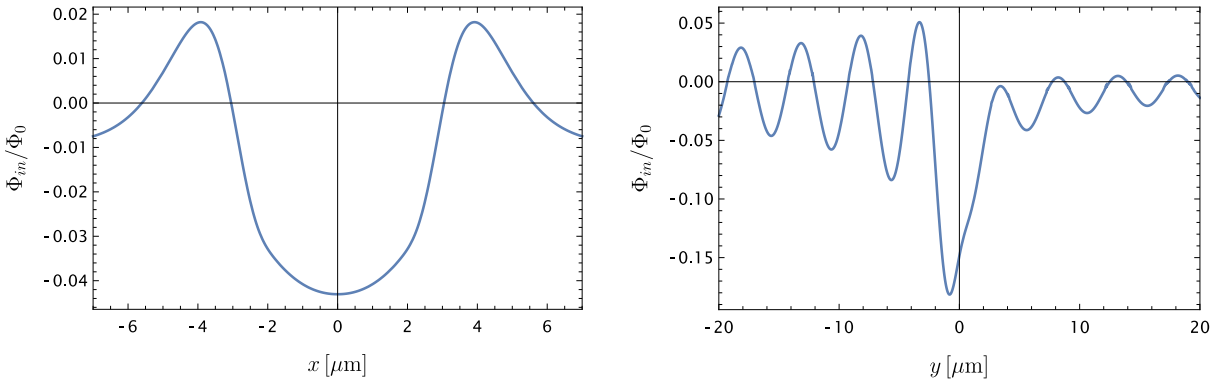

Figure 4.3: Induced potential in graphene given by equation (4.38). The left figure shows the transversal cut for $y_0 = -10$ μm, while the right figure shows the longitudinal cut for $x_0 = 0$ μm. The longitudinal cut allows us to observe the oscillatory nature of the potential, which is in agreement with method 1. The potentials were obtained with the parameters: $E_F = 0.17$ eV, $v = 0.1c$ and $z_0 = 1$ μm for graphene in vacuum ($\epsilon_d = 1$).

4.3 Graphene in the vicinity of a local metal

For our last electrostatic problem, it will be interesting to study the parallel motion of an external charge to a graphene sheet when this last is in the vicinity of a local metal. Note that for a local metal, the nonlocal parameter β is zero, so the electrostatic potential in the metal will only be proportional to $e^{kz}e^{i(\mathbf{k}\cdot\mathbf{r}_{\parallel}-\omega t)}$. Even though the metal is local, the system will still provide nonlocal effects due to the presence of graphene. Since we now add a metal region to the system, we will have to calculate the Green function taking this material into consideration. The configuration for this problem is represented in figure 4.4, where we have graphene at $z = 0$. The dielectric slab has thickness d for $0 < z < -d$ and the metal region is semi-infinite at $z < 0$. Like in the last problem, for $z > 0$ we have vacuum.

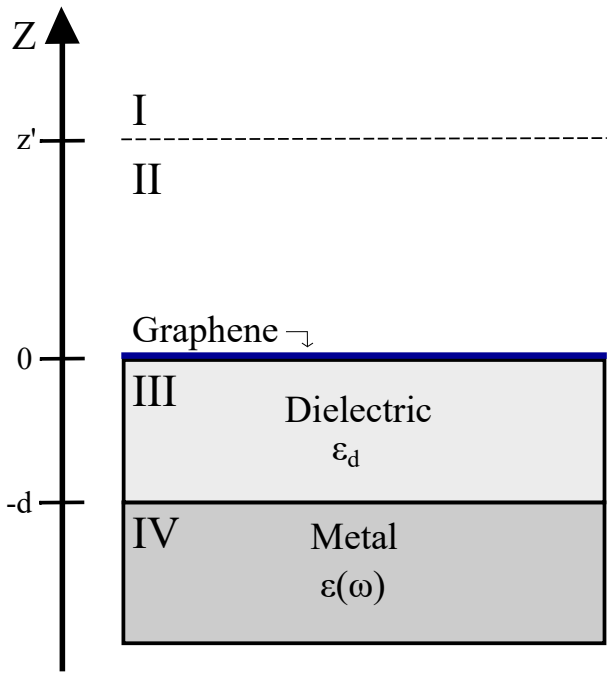

Figure 4.4: Configuration for graphene in the vicinity of a local metal. Graphene is located at $z = 0$, while in-between graphene and the metal is present a dielectric with thickness d and dielectric constant ϵ_d. The local metal is semi-infinite at $z < -d$. The Vacuum ($\epsilon_d = 1$) extends for $z > 0$. We want to find the Green function at an arbitrary z'.

With the Green function defined in equation (4.7), we can write for each region

$$g(z,z') = \begin{cases} g_I(z,z') = A(z')e^{-kz} & \text{if } z > z' \\ g_{II}(z,z') = B_1(z')e^{-kz} + B_2(z')e^{kz} & \text{if } 0 < z < z' \\ g_{III}(z,z') = D_1(z')e^{-kz} + D_2(z')e^{kz} & \text{if } -d < z < 0 \\ g_{IV}(z,z') = M(z')e^{kz} & \text{if } z < -d \end{cases} \tag{4.39}$$

The Green functions in equation (4.17) must, at all cases, decay as $|z| \longrightarrow \infty$. In particular, $g_I(z,z')$ must decay as z tends to positive values of infinity, while g_{IV} decays for negative values of infinity. To obtain the

coefficients in Green's functions, we already know from the last section what boundary conditions should be applied. Having that in mind, we have a local metal with dielectric function given by $\epsilon(\omega)$ [eq. (2.40)]. Solving the linear system of the equations provided by the boundary conditions we obtain for the Green functions

$$g(z,z') = \begin{cases} g_I(z,z') = \frac{e^{-k(z-z')}}{2k} + \frac{e^{-k(z+z')}}{2k}\left(\frac{r_D + r_d e^{2kd}}{r_d r_D + e^{2kd}}\right) & \text{if } z > z' \\ g_{II}(z,z') = \frac{e^{-k(z+z')}}{2k}\left(\frac{r_D + r_d e^{2kd}}{r_d r_D + e^{2kd}}\right) + \frac{e^{k(z-z')}}{2k} & \text{if } 0 < z < z' \\ g_{III}(z,z') = \frac{e^{-k(z+z')}}{2k}\left(\frac{t_d r_D}{r_d r_D + e^{2kd}}\right) + \frac{e^{k(z-z')}}{2k}\left(\frac{t_d e^{2kd}}{r_d r_D + e^{2kd}}\right) & \text{if } -d < z < 0 \\ g_{IV}(z,z') = \frac{e^{k(z-z')}}{2k}\left(\frac{t_d t_D e^{2kd}}{r_d r_D + e^{2kd}}\right) & \text{if } z < -d \end{cases} \tag{4.40}$$

Where r_d and t_d are the "reflection"and "transmission"coefficients given by equations (4.19) and (4.20), respectively. However, the presence of the metal will provide a new type of "reflection"and "transmission"coefficients, because of the Drude dielectric function

$$r_D = \left(\frac{\epsilon_d - \epsilon(\omega)}{\epsilon_d + \epsilon(\omega)}\right) \tag{4.41}$$

$$t_D = \left(\frac{2\epsilon_d}{\epsilon_d + \epsilon(\omega)}\right) \tag{4.42}$$

where r_D and t_D are functions of ω.

Let us now study the potential created due to the parallel motion of an external particle (at $z > 0$) to the graphene sheet, when this last is in the vicinity of a local metal. For the induced potential, we will assume $z' = 0$ and the Green function that will contribute to the potential will be $g_I(z,z')$. For the external potential, we are interested in region II so we use $g_{II}(z,z')$. Note that we have followed the same reasoning as in the problem of graphene near a dielectric. By that, the total potential is given by equation (4.8) and the external and induced potentials are, respectively

$$\Phi_{ex}(\mathbf{k},z,\omega) = \frac{1}{\epsilon_0}\int dz' \left[\frac{e^{k(z-z')}}{2k} + \frac{e^{-k(z+z')}}{2k}\left(\frac{r_D + r_d e^{2kd}}{r_d r_D + e^{2kd}}\right)\right]\rho_{ex}(\mathbf{k},z',\omega) \tag{4.43}$$

$$\Phi_{in}(\mathbf{k},z,\omega) = -\Phi_1(\mathbf{k},z,\omega) = -\frac{e}{\epsilon_0}t_d\frac{e^{-kz}}{2k}\left(\frac{r_D + e^{2kd}}{r_d r_D + e^{2kd}}\right)n_1(\mathbf{k},\omega) \tag{4.44}$$

Using the results for the potentials in the hydrodynamic equation (4.12), we obtain a relation for the velocity which, once again, we put in the continuity equation (3.3b) and obtain

$$\begin{aligned} 0 &= -\omega^2 n_1(\mathbf{k},\omega) \\ &+ n_0 k^2\left[-\frac{e v_F}{\hbar k_F}\Phi_{ex}(\mathbf{k},0,\omega) + \left(\frac{e^2 v_F}{(1+\epsilon_d)\epsilon_0 \hbar k_F}\left(\frac{r_D + e^{2kd}}{r_d r_D + e^{2kd}}\right)\frac{1}{k} + \frac{v_F^2}{2n_0}\right)n_1(\mathbf{k},\omega)\right] \end{aligned} \tag{4.45}$$

In the same way as graphene in the vicinity of a dielectric (section 4.2), the dispersion for the SPPs in this configuration is given in the last equation, by the expression in curve brackets multiplied by $n_0 k^2$, which gives

$$\omega_{spp}^2 = \left[\frac{4\alpha_{FS} E_F \hbar c}{(1+\epsilon_d)\hbar^2} \left(\frac{r_D(\omega) + e^{2kd}}{r_d r_D(\omega) + e^{2kd}} \right) \frac{1}{k} + \frac{v_F^2}{2} \right] k^2 \tag{4.46}$$

Note that we write the dispersion in terms of the Fermi energy $E_F = \hbar k_F v_F$ and the fine structure constant $\alpha_{FS} = e^2/4\pi\epsilon_0\hbar c$, by considering the homogeneous electronic density as $n_0 = k_F^2/\pi$. The inhomogeneous electronic density is now easily obtained through equation (4.45), where the external potential for this configuration is expressed in equation (4.43)

$$n_1(\mathbf{k}, \omega) = -\frac{(2\alpha_{FS} E_F \hbar c/e)}{\hbar^2\omega^2 - \hbar^2\omega_{spp}^2} k \int dz' t e^{-kz'} \left(\frac{r_D(\omega) + e^{2kd}}{r_d r_D(\omega) + e^{2kd}} \right) \rho_{ex}(\mathbf{k}, z', \omega) \tag{4.47}$$

By that, the induced potential of graphene in the vicinity of a local metal is given by

$$\Phi_{in}(\mathbf{k}, z, \omega) = \frac{1}{\epsilon_0} \alpha_{FS} E_F \hbar c \frac{t_d^2 e^{-kz}}{\hbar^2\omega^2 - \hbar^2\omega_{spp}^2} \left(\frac{r_D(\omega) + e^{2kd}}{r_d r_D(\omega) + e^{2kd}} \right) \int dz' e^{-kz'} \rho_{ex}(\mathbf{k}, z', \omega) \tag{4.48}$$

Now we want to study the parallel motion to the graphene sheet, where the volume density of external charge (4.4) provides

$$\Phi_{in}(\mathbf{k}, z, \omega) = 2\pi v^2 \Phi_0 \frac{t_d^2 e^{-k(z+z_0)}}{\hbar^2\omega^2 - \hbar^2\omega_{spp}^2} \left(\frac{r_D(\omega) + e^{2kd}}{r_d r_D(\omega) + e^{2kd}} \right) \delta(\omega - k_y v) \tag{4.49}$$

Remember the delta-function implies that the particle disperses with a frequency given by $\omega = k_y v$ and the prefactor Φ_0 given by $\Phi_0 = \frac{Ze}{\epsilon_0} \frac{\alpha_{FS} E_F \hbar c}{\hbar^2 v^2}$. Fourier transforming to real space and time equation (4.27), we obtain for $\Phi_{in}(\mathbf{r}, z, t)$

$$\Phi_{in}(\mathbf{r}, z, t) = v^2 \Phi_0 \int_{-\infty}^{\infty} \frac{dk_x dk_y}{(2\pi)^2} \frac{t_d^2 e^{-k(z+z_0)} e^{i(\mathbf{r}\cdot\mathbf{k} - k_y v t)}}{\omega^2 - \omega_{spp}^2} \left(\frac{r_D(\omega) + e^{2kd}}{r_d r_D(\omega) + e^{2kd}} \right) \delta(\omega - k_y v) \tag{4.50}$$

Now we are in a position to develop the induced potential in graphene. The calculations are similar to those of the last section, however, in this case, we will have to find an approximate solution to the ω_{spp}, since equation (4.46) is not analytical and its solutions are found numerically. But the method to determine the potential is the same. Once again, let us compute the phase velocity $v_p = \omega/k$ of the plasmons in graphene. Since we know the dispersion is linear in the wavenumber k, the phase velocity will be the slope of the spectrum represented in figure 4.5 (of course, the slope will change for different parameters). Note that this is true only if the dispersion is linear, which only happens for small dielectric thickness d, as such we write $\omega_{spp} = v_0 k$, where v_0 is the slope of the spectrum and the phase velocity. By that, we can write

$$v_p = v_0 \omega^{\kappa} \tag{4.51}$$

with $\kappa \longrightarrow 0$. If we increase the dielectric thickness, we will have a plasmon dispersion of the form $\sqrt{k}$, and the value of κ will be the same as in the graphene in the vicinity of a dielectric case ($\kappa = -1$). The argument of the δ-function implies that $\omega = kv\cos\theta$, which also gives us the lower limit for the integral in k

$$\cos\theta = \frac{\omega}{vk} = 1 \Leftrightarrow \omega_{spp}(k) = vk \tag{4.52}$$

In figure 4.5, the dispersion is only equal to vk at $k = 0$. The equality shown in equation (4.52) won't be satisfied, provided that the dispersion of the SPPs remains linear in the wavevector k. So, we can perform the integral in k in the domain $k \in]0, \infty[$. Once again, let us start by taking the potential integral in equation (4.50) and write it in polar coordinates

$$\Phi_{in}(\mathbf{r}_{\parallel}, z, t) = v^2 t_d^2 \Phi_0 \int_0^{2\pi} \frac{d\theta}{2\pi} \int_0^{\infty} \frac{kdk}{2\pi} \frac{e^{-k(|z|+z_0)} e^{ik[r\cos(\theta-\theta')-vt\cos\theta]}}{(kv\cos\theta)^2 + i\mathrm{sgn}(\cos\theta)\eta - \omega_{spp}^2} \times \left(\frac{r_D(kv\cos\theta) + e^{2kd}}{r_d r_D(kv\cos\theta) + e^{2kd}} \right) \tag{4.53}$$

For this integral, we can already infer some important differences between the metal configuration and the dielectric configuration that provide the induced potential (4.29). First of all, the dispersion for the SPPs in graphene is proportional to $\sqrt{k}$ in the graphene/dielectric case, while for the graphene/metal structure, if the distance between the metal and graphene is small enough, then the dispersion is proportional to k, as we have already seen in section 3.2. The last difference is also due to the presence of metal, moreover, it has to do with the Drude dielectric function $\epsilon_D(\omega)$, which allows the appearance of a Drude type term in equation (4.53). The other terms and parameters in this integral are obtained in the same way as in section 4.2. The first step in calculating the integral is to obtain an analytical form for the surface plasmon-polaritons dispersion. Luckily, it is possible to expand r_D in powers of ω, since $\omega \ll \omega_p$. In that way, the dispersion of the SPPs only depends on the wavenumber k. So we approximate equation (4.46) in the following way

$$\omega_{spp}^2 \approx \frac{1}{4\hbar\epsilon_d(\epsilon_d - 1)} \left[-D(k) + \sqrt{(D(k))^2 + F(k)} \right] \tag{4.54}$$

where we define some auxiliary functions

$$D(k) = 8\alpha_{FS} E_F c \epsilon_d (1+\epsilon_d) k + \frac{\omega_p^2[\epsilon_d - 1 + e^{2dk}(1+\epsilon_d)]}{\hbar} - v_F^2 \hbar \epsilon_d (\epsilon_d - 1) k^2 \tag{4.55}$$

$$F(k) = 4\omega_p^2 \hbar^{-1} k \epsilon_d (\epsilon_d - 1)[8\alpha_{FS} E_F c(e^{2dk} - 1)(1+\epsilon_d) + k\hbar v_F^2(\epsilon_d - 1 + e^{2dk}(1+\epsilon_d))] \tag{4.56}$$

It is possible to see in figure 4.5 that equation (4.54) gives us a very good approximation to the spectrum of the surface plasmon in graphene, in a way that provides the same behavior as the exact solution given by equation (4.46) for the plasmons. Altogether, the figure also shows the particle dispersion ($\omega = kv$).

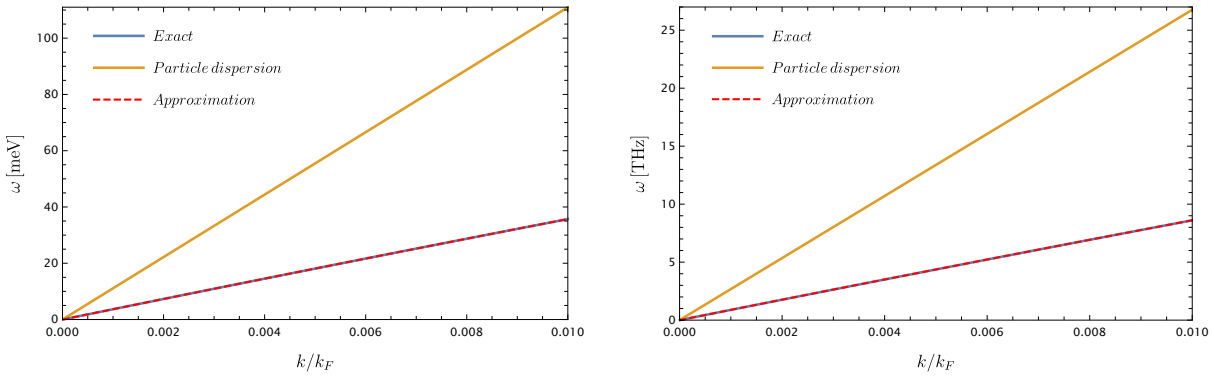

Figure 4.5: Dispersion relation for the surface plasmon-polaritons in graphene when in a vicinity of a local metal. We built the spectrum based on the energy (left) and frequency (right) of the plasmons. Depicted with the exact solution [eq. (4.46)] the approximate solution given by equation (4.54) and the external particle dispersion ($\omega = kv$) are also represented. The parameters are: $E_F = 0.37$ eV, $v = 0.1c$, $z_0 = 1$ μm and a dielectric thickness of $d = 0.01$ μm in vacuum ($\epsilon_d = 1$). The dispersion was plotted having into consideration the titanium as the metal: $\omega_p = 2.80$ and $\epsilon_\infty = 2.20$.

Now we apply the sokhotsky-Plemelj formula to the equation (4.53) we get for the induced potential in graphene

$$\Phi_{in}(\mathbf{r}_\parallel, z, t) = v^2 t_d^2 \Phi_0 \fint_0^{2\pi} \frac{d\theta}{2\pi} \int_0^\infty \frac{dk}{2\pi} \frac{e^{-k\mu} e^{ikv}}{kv^2 \cos^2\theta - \omega_{spp}^2} \left(\frac{r_D(kv\cos\theta) + e^{2kd}}{r r_D(kv\cos\theta) + e^{2kd}} \right)$$
$$- i\pi v^2 t_d^2 \Phi_0 \int_0^{2\pi} \frac{d\theta}{2\pi} \int_0^\infty \frac{dk}{2\pi} e^{-k\mu} e^{ikv} \left(\frac{r_D(kv\cos\theta) + e^{2kd}}{r r_D(kv\cos\theta) + e^{2kd}} \right) \mathrm{sgn}(\cos\theta) \delta(kv^2\cos^2\theta - \omega_{spp}^2) \tag{4.57}$$

where the parameters μ and ν are the same as (4.34) and (4.35), respectively. To solve the principal value, it is necessary to find out the poles of the function contained in the integral, in this case, we have to solve $(k\cos(\theta)v)^2 - \omega_{spp}^2 = 0$ for θ. Then the poles are the set of angles which $\theta \in (\arccos(\frac{\omega_{SPP}}{kv}), \pi - \arccos(\frac{\omega_{SPP}}{kv}), \pi + \arccos(\frac{\omega_{SPP}}{kv}), 2\pi - \arccos(\frac{\omega_{SPP}}{kv}))$. The next step is to simplify the imaginary integral by solving the polar integral with the delta function. In this case, we call for the following function

$$g(k,\theta) = k e^{-k\beta} e^{ik\gamma} \left(\frac{r_D(kv\cos\theta) + e^{2kd}}{r r_D(kv\cos\theta) + e^{2kd}} \right) \tag{4.58}$$

and the imaginary integral becomes

$$-i\pi v^2 t_d^2 \Phi_0 \int_0^{2\pi} \frac{d\theta}{2\pi} \int_0^\infty \frac{dk}{2\pi} g(k,\theta) \mathrm{sgn}(\cos\theta) \delta((kv\cos\theta)^2 - \omega_{spp}^2) \tag{4.59}$$

Having in mind the sign term, the polar integral can be written in two parts

$$2\int_0^{\pi/2} d\theta g(k,\theta)\sum_{i=1}^{4}\frac{\delta(\theta-\theta_i)}{|2v^2k^2\cos\theta_i\sin\theta_i|} - 2\int_{\pi/2}^{\pi} d\theta g(k,\theta)\sum_{i=1}^{4}\frac{\delta(\theta-\theta_i)}{|2v^2k^2\cos\theta_i\sin\theta_i|} \tag{4.60}$$

where we have used the following mathematical property

$$\delta(f(\theta)) \longrightarrow \sum_{i=1}^{N}\delta(\theta-\theta_i)\frac{1}{|f'(\theta_i)|} \tag{4.61}$$

The factor of two appears in each integral because we are only dealing with cosine functions, and in that case, the sign function will provide that for the region of integration where $\cos\theta$ has the same sign, the value of the integral will be the same. At last, we need to look at the angles θ_i to see which one falls in the angle interval of integration. The integral is zero for the angles θ_i that are not in the range of the limits of integration. In that case figure 7, shows us that for $\theta \in \left[0, \frac{\pi}{2}\right]$ only θ_1 contributes for the integral and for $\theta \in \left[\frac{\pi}{2}, \pi\right]$ only θ_2 gives a solution different from zero. This means that the solution of the polar integral is

$$\frac{g(k,\theta_1)}{|v^2k^2\cos\theta_1\sin\theta_1|} - \frac{g(k,\theta_2)}{|v^2k^2\cos\theta_2\sin\theta_2|} \tag{4.62}$$

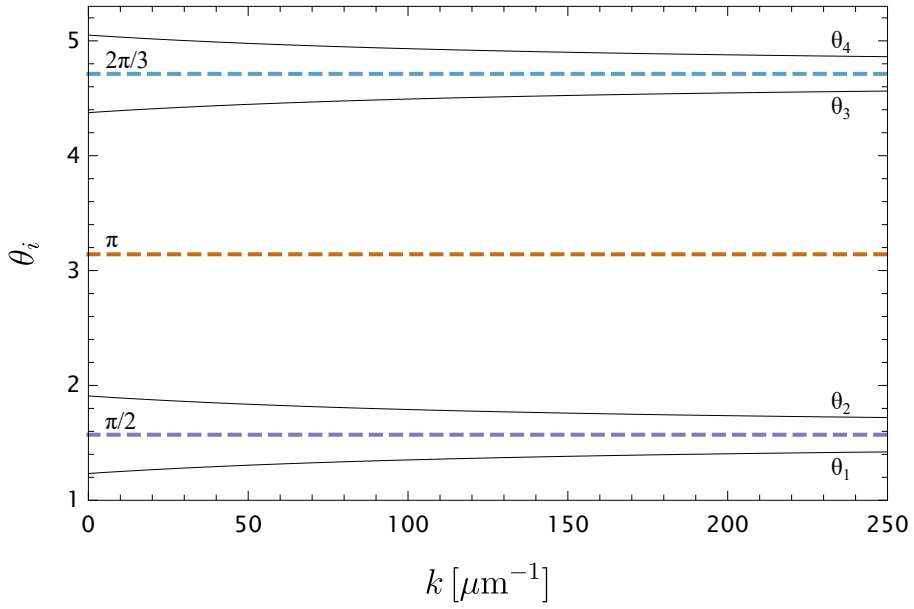

Figure 4.6: Contribution of the polar angles for each interval of the polar integral (4.59). The black lines represented in the figures are the polar angles $\theta_i = (\theta_1, \theta_2, \theta_3, \theta_4) = \theta \in (\arccos(\frac{\omega_{SPP}}{kv}), \pi - \arccos(\frac{\omega_{SPP}}{kv}), \pi + \arccos(\frac{\omega_{SPP}}{kv}), 2\pi - \arccos(\frac{\omega_{SPP}}{kv}))$. Only the angles θ_1 and θ_2 are in the range of the limits of integration, however, the factor of 2 in the integral covers the polar angles of the upper branch (θ_3 and θ_4). The parameters are the same as in figure 4.5.

Finally, the induced potential when graphene is in the vicinity of a local metal is given by

$$\Phi_{in}(\mathbf{r},z,t) = v^2 t_d^2 \Phi_0 \int_0^{2\pi} \frac{d\theta}{2\pi} \oint_0^{\infty} \frac{kdk}{2\pi} \frac{e^{-k\beta} e^{ik\gamma}}{(kv\cos\theta)^2 - \omega_{spp}^2} \left(\frac{r_D(kv\cos\theta) + e^{2kd}}{r r_D(kv\cos\theta) + e^{2kd}} \right)$$
$$- iv^2 t_d^2 \Phi_0 \int_0^{\infty} \frac{dk}{4\pi} \left(\frac{g(k,\theta_1)}{|v^2 k^2 \cos\theta_1 \sin\theta_1|} - \frac{g(k,\theta_2)}{|v^2 k^2 \cos\theta_2 \sin\theta_2|} \right) \tag{4.63}$$

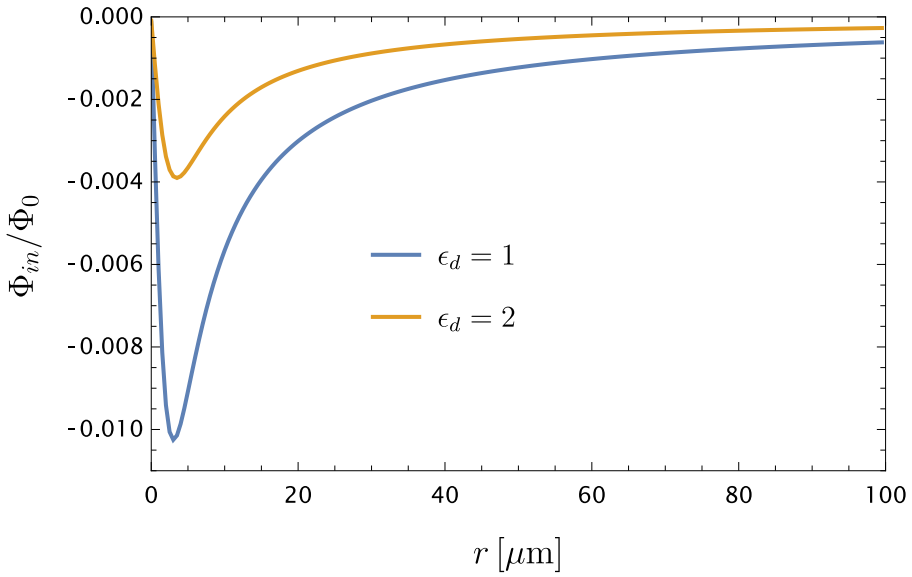

Figure 4.7: Induced electrostatic potential along the direction of propagation of the moving particle given by equation (4.63). The parameters are: an electronic density of $10^5 \mu m^{-2}$ which gives a Fermi energy of $E_F = 0.37$eV ,$v = 0.1c$, $z_0 = 1$ μm ,$t = 0$ s and for a dielectric thickness of $d = 0.01$ μm. The plots show the curves for two distinct values of the dielectric constant, $\epsilon_d = 1$ and $\epsilon_d = 2$. Note that in this problem the potential is continuous rather than oscillatory, like in the graphene in the vicinity of a dielectric problem.

Contrary to the case of the dielectric, the potential of graphene in the vicinity of a local metal is not oscillatory, but rather presents a peak and then goes from zero to higher values of r. This means that the metal breaks the oscillatory behavior of the potential, as seen in figure 4.7. However, this happens because the dispersion relation of the SPPs plays an important role in the potential's behavior.
Let us recall the dispersion for graphene in the vicinity of a dielectric (fig. 4.2), in this case, the spectrum is proportional to $\sqrt{k}$ and the potential is oscillatory, but when we add metal to the configuration, the dispersion changes to a behavior proportional to k and the potential ceases to present an oscillatory nature. Moreover, when we increase the thickness d of the dielectric, the dispersion tends to $\sqrt{k}$ and the oscillations in the graphene surface are recovered. This argument was also confirmed by [25] where the differences of waves propagating on the surface of the water are directly related to the dispersion of those waves in the media.

The transversal and longitudinal cuts for the induced potential are represented in figure 4.8. The longitudinal representation shows us that the presence of the metal altogether with a small enough separation between the metal and graphene, suffices for the potential to behave more continuously, rather than

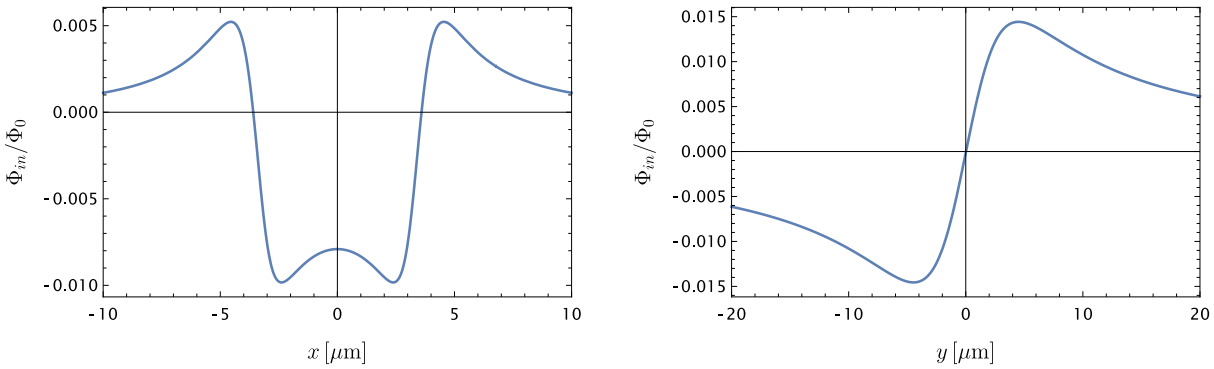

Figure 4.8: Induced potential in graphene given by equation (4.63). The transversal cut (left) was done for $y_0 = -15$ μm and the longitudinal cut (right) for $x_0 = 0$ μm. In this case, the longitudinal representation shows the break of the oscillatory behavior. The potentials were obtained with the parameters: $E_F = 0.17$ eV, $v = 0.1c$, $z_0 = 1$ μm and for a dielectric thickness of $d = 0.01$ μm with a dielectric constant of $\epsilon_d = 1$. The metal chosen was titanium: $\omega_p = 2.80$ eV and $\epsilon_\infty = 2.20$.

present an oscillatory nature. In appendix 3, we show that the integrals in equation (4.63) have approximately the same numerical value and we can use only the second integral multiplied by a factor of two to compute the induced potential. This becomes necessary, because the second integral is computationally faster to evaluate than the first integral.

Chapter 5

Plasmonic Kelvin and Mach wakes

In the previous chapter, we deduced the expressions for the induced potential in graphene created by an external particle moving parallel to it, with constant velocity v (along the y-axis). The presence of this external particle will give rise to plasmonic wakes on the surface of graphene. Our aim for this chapter is to study the shape and the proprieties of this type of wakes. In [17] the same study was conducted for graphene in vacuum, and it was uncovered that the external particle creates a V-shape pattern on the surface of graphene. By that it is possible to make an analogy with the waves created on the surface of a liquid, having been disturbed by a moving object at a uniform pace (like the external particle for graphene). The half-angle that encloses this V-shape wake is commonly known to be of $\arcsin(1/3) = 19.47°$, which means that the angle of the wake remains constant, at any speed of the moving object. Since this angle was first proved by Lord Kelvin, this type of waves are known as Kelvin waves. However, recent studies have suggested that the angle decreases with the increase of the velocity of the moving perturbation. The measure of the angles for different velocities of the moving perturbation will let us know, where the Kelvin region ends and where another one begins. It was found that for higher velocities the angle decreases with the law $1/v$, which is indicative of the Mach type waves [25–28]. We are now interested to see, if these studies for the classical Kelvin and Mach waves can be transferred to the plasmonic wakes created on the surface of graphene, for the configurations of the previous chapter. Furthermore, we will study the half-angle of the V-shaped potential, in order to make a parallelism between the Kelvin and Mach wakes in graphene. Firstly, within this chapter, we will discuss about classical Kelvin and Mach waves, so as to have a starting point in the study of this type of wakes in graphene. In particular, the plasmonic wakes will be analyzed in two cases: graphene in the vicinity of a dielectric and graphene in the vicinity of a local metal (the same configurations in chapter 4).

5.1 Classical Kelvin and Mach wakes

Let us consider a plane-free surface of steady liquid in equilibrium and in a gravitational field. This field is characterized by the gravitational field strength g. To the surface of the liquid, a moving external disturbance can be applied in order to disturb the state of equilibrium of the liquid at a given point. The effects of this perturbation will then extend to the entire surface and a specific pattern will appear on the surface of the liquid. This pattern depends on the shape and on the motion of the object, which is perturbing the surface. Since we wish to study the parallel motion of an external perturbation in graphene, it is quite clear that we have to analyze and understand the parallel motion on the surface of a liquid, where the moving object has a rectilinear motion. For simplicity, let us consider the surface of the water. When a perturbation is applied, this will create water wakes, which will propagate through all the free surface. Various studies describe this type of wakes by looking at the waves produced by a moving ship or by a duck swimming in a pond with velocity v [28]. It is not only interesting to study this physical phenomenon in water, but it is also a fairly suitable method to probe the surface of soft systems, where some usual techniques, such as electron microscopy, impose some constraints. In the paper [29] it is precisely shown that, a moving tip with speed v parallel to the surface of the soft system will induce a local distortion, which will dissipate in the liquid surface through the form of waves. The study was also made for a point-like particle, such as an electron or a proton moving at a nanoscale distance from the surface, similar to our plasmonic problem [30].

A moving ship with velocity v traveling along a calm water surface creates a V-shaped wave moving in an opposite direction from that of the moving ship. These waves have some properties that make them a very interesting object of study. One of the theories that explains the propagation and creation of this type of wake pattern is the Kelvin theory, which studies Kelvin type waves. However, some studies suggest that this theory only works for small velocities of the ship. This implies that as the velocity increases, the waves cannot be described by the Kelvin theory but by another one called Mach theory, which studies Mach type of waves. We will now analyze these two theories in order to understand when we can use them and how the waves are affected by the velocity of the moving perturbation. Note that to create these types of waves we could choose a different perturbation other than the ship, as long as the perturbation was able to create waves on the surface of the water. The majority of the studies use the waves created by ships because it is easy to obtain real satellite images (see figure 5.1) from these waves as well as distinguish the different structures in the ship wakes depending on different velocities of the ship. Furthermore, we will define an important parameter that describes the drag (also related to the velocity) of the wave. This parameter is the Froude number, which is adimensional

$$F = \frac{v}{\sqrt{gL}} \tag{5.1}$$

where g is the gravitational acceleration and L is the hull length of the ship. The Froude number will help us interpret the moment when the transition between a Kelvin wave and the Mach wave occurs, for what

Froude number, and consequently for what velocity the waves change their behavior.

A Kelvin wave pattern is composed of two types of waves: transverse waves and divergent waves. Transverse waves are waves that appear in the middle of the ship's wake and are aligned perpendicular to the ship's course, following its crests. Divergent waves belong in the outer region, on the sides of the wave pattern, where the wave behaves differently from those in the middle region (figure 5.1 right). It was observed in [28] that the amplitudes of the transverse and divergent waves depend directly on the Froude number (5.1). This implies that, as the Froude number increases (increasing velocities), the amplitude of the divergent wave dominates the wake pattern, and the amplitude of the transverse wave becomes increasingly smaller, looking like it vanishes for higher Froude numbers. Therefore, for high Froude numbers, we are expecting a wave pattern dominated by divergent waves. Another propriety of this type of wave is the wake angle, which is the opening angle of the wake cone. Kelvin theory suggests that the half-angle that encloses the Kelvin wave is constant, independent of the velocity of the ship (or any other perturbation), and takes the value

$$\theta_K = \arctan\left(\frac{1}{\sqrt{8}}\right) \approx 19.47^\circ \tag{5.2}$$

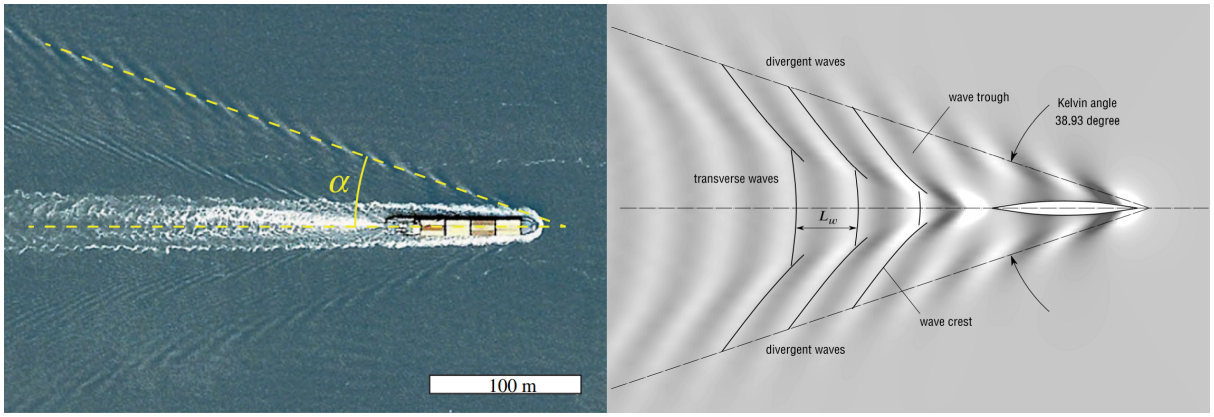

Figure 5.1: (Left) Real image of ship wake created on the surface of the water by a ship traveling with velocity v. α is the wake angle defined from the slope of the dashed yellow line, which gives the maximum amplitude of the wake. The wake angle is half of the angle of the wave produced by the ship for a Froude number $F = 0.15$. Figure adapted from [27]. (Right) Wave pattern of a moving ship at $F = 0.26$. There are some wave structures represented in the figure, such as the wave crest and the wave trough that correspond to the maximum and minimum amplitudes of the wave, respectively, and the wavelength L_w. It is also possible to see that half of the cone angle is the Kelvin angle of about 19.47° (total angle of 38.93°). Figure retrieved from [31].

However, some recent observations and calculations have shown that for fast-moving ships, the angle of the wave decreases with velocity [27]. The decrease in the angle can be explained by assuming that a ship cannot generate a wavelength greater than its hull length. However, this hypothesis is still not well established and is open to questioning. Another explanation for the decrease of the wake angle resides in the fact that the wave pattern is defined by the location of its highest peaks, which means that for

fast-moving ships, the highest peaks don't lie on the outermost divergent waves anymore, resulting in a smaller apparent angle. This also happens, because when the Froude number increases, so does the velocity and the ship enters the planning regime and moves away less mass of water, which results in a smaller apparent angle. In figure 5.2, various waves produced by the ship for different Froude numbers are represented. We see that for higher Froude numbers the highest peaks of the wakes no longer lie on the outermost divergent waves, which means that the angle of the ship wakes decreases as the velocity of the ship increases.

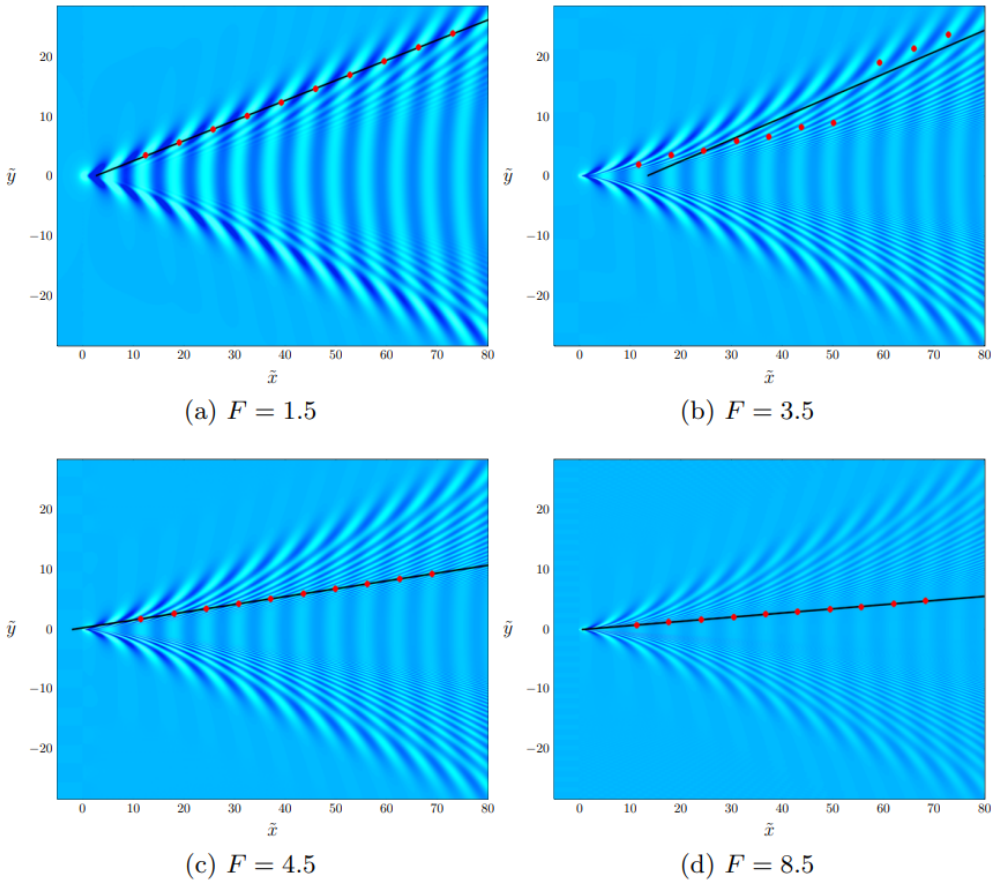

Figure 5.2: Plan view of the ship wakes produced for different Froude numbers. The solid red dots represent the highest peaks, and the black line is the best fit for those points. Clearly, for higher Froude numbers, the highest peaks do not lie anymore in the outermost divergent waves. For an easy comparison, the figures are scaled as $\tilde{y} = y/F^2$ and $\tilde{x} = x/F^2$. This figure was retrieved from [26].

This clearly demonstrates a transition from the Kelvin regime to a different regime. In figure 5.3 we see that for higher velocities, the angle of the cone follows the law F^{-1} (or $1/v$) which is consistent with the Mach regime, where the wake angles follow this specific law. For smaller Froude numbers, the Kelvin regime behavior is clearly perceived, as the wake angles are constant and their numerical value is very close to the Kelvin angle (accounting for the error, the numerical angle interval is within the Kelvin angle). Therefore, it is clear that a transition between these two regimes mirrors a change of behavior for a specific

Froude number.

From figure 5.3 the Froude numbers in the range $0.8 < F < 3$ are in the Kelvin region, where the angles are constant and slightly below the Kelvin angle. For Froude numbers bigger than 4 there is a transition to the Mach region where the angles decrease by the law F^{-1}. This is consistent with figure 5.2 (c) and (d), where half of the cone angle decreases with the increase of the Froude number.

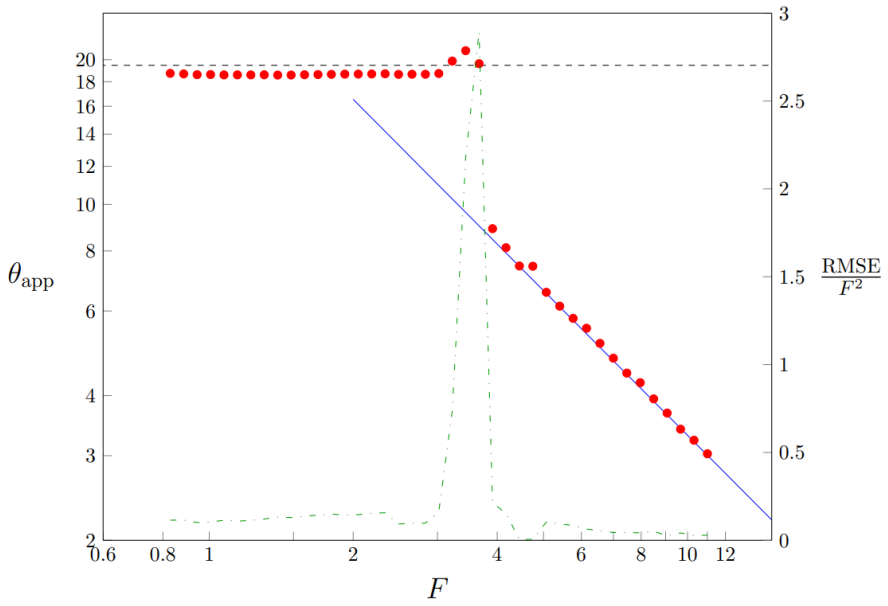

Figure 5.3: Apparent wake angles θ_{app} in degrees as a function of the Froude number. The blue line is the best fit to the angles for the Mach region as it follows the law $F^{-}1$. The black dashed line is Kelvin's angle $19.47°$. The green dot-dashed curve is the root mean squared error, scaled by F^2. Figure retrieved from [26].

It is important to notice that the description of such waves presented in this chapter was assumed to be linear and the perturbation on the water was created by a single source (in this case a ship). However, in [26] is also studied the problem for nonlinear solutions as well for other kinds of sources, like source doublets. In the nonlinear regime, the apparent wake angle increase and becomes greater than the Kelvin angle.

In the following sections of this chapter, we will provide a mathematical description for this type of wakes, starting with the study of the dispersion of water waves and then proceeding to get an expression for the surface displacement brought by the moving ship.

5.1.1 Dispersion of water waves

The complexity of studying the formation and the dispersion of water waves, in particular those caused by a moving disturbance, is well known, due to external and internal factors. Such factors, like the surface tension and the depth of the water, can lead to complicating dispersion for the waves we wish to study. Not to mention that the study of ships in open air can be rather difficult due to winds and perturbations

of the water, which can cause turbulence and, in that way, interfere with the wake pattern produced by a moving ship. However, let us consider the perfect conditions for the observation of these wakes. In that case, the dispersion relation between angular frequency and the wave number k is given by [25, 32]

$$\omega^2(k) = \left(gk + \frac{\sigma k^3}{\rho}\right)\tanh(kh) \tag{5.3}$$

where g is the gravitational field strength, σ the surface tension, ρ the density of the water, and h the water depth. Equation (5.3) provides us with waves of different characteristics, regarding the parameters chosen: if the surface tension is null on the interface air-water ($\sigma = 0$), we are in the presence of pure gravity waves. While for $\sigma \neq 0$ the capillary gravity waves dominate the wave pattern.

For pure gravity waves short compared to the depth of the water, that is $h \longrightarrow \infty$, we get the limit $\lim_{h\to\infty} \tanh(kh) = 1$ and the dispersion relation (5.3) reduces to

$$\omega^2(k) = gk \tag{5.4}$$

The phase velocity can now be taken through $v_p = \omega/k$, which gives

$$v_p = \sqrt{\frac{g}{k}} = \frac{g}{\omega} = \left(\frac{\omega}{g}\right)^{-1} \tag{5.5}$$

This is a lot similar to the phase velocity of plasmons in graphene in the vicinity of a dielectric (section 4.2), obtained in equation (4.37). That is why we consider that plasmons behave as gravity waves in graphene with acceleration given by $a = \frac{4\alpha_{FS}E_F\hbar c}{(1+\epsilon_d)\hbar^2}$. Where α_{FS} is the fine structure constant, E_F is the Fermi energy, and ϵ_d is the dielectric constant.

For pure gravity waves with wavelengths greater than the water depth, we have $\tanh(kh) \approx kh$, we get for the dispersion relation

$$\omega^2 = ghk^2 \tag{5.6}$$

and the phase velocity v_p is given by

$$v_p = \sqrt{gh} = \sqrt{gh}\omega^0 \tag{5.7}$$

Once again, we can make an analogy with the phase velocity of graphene in the vicinity of a local metal [equation (4.51)]. Where the phase velocity is equal to the group velocity $v_g = \partial\omega/\partial k$. In the problem described in the last chapter, the phase velocity was given by v_0, which we obtained as the slope of the plasmonic spectrum in figure 4.5. The slope can be taken as $\partial\omega/\partial k$ so we infer that the phase velocity is equal to the group velocity for gravity waves in shallow water depth and for the graphene in the vicinity of a local metal. For gravity waves of any kind, the waves created are V-shaped waves that stretch behind the moving object. With this study, we can already see, that this kind of wake pattern will appear on the surface of graphene when an external particle is moving parallel to it, as we will analyze in the next section.

For capillary gravity waves ($\sigma \neq 0$) in deep water, the dispersion (5.3) gets the form

$$\omega^2 = \frac{\sigma k^3}{\rho} \tag{5.8}$$

where we neglect gk in comparison to the capillary term. Of course, this gives a phase velocity of

$$v_p = \sqrt{\frac{\sigma k}{\rho}} = \left(\frac{\omega\sigma}{\rho}\right)^{1/3} \tag{5.9}$$

If we define the limiting cases for $\kappa = 0, -1, 1/3$ then, the general phase velocity for water waves can be written as

$$v_p = v_0 \left(\frac{\omega}{\omega_0}\right)^{\kappa} \tag{5.10}$$

where v_0 and ω_0 are constants: for pure gravity waves in deep water ($\kappa = -1$) we get $v_0\omega_0 = g$, for gravity waves in shallow water ($\kappa = 0$) the constants are $v_0 = \sqrt{gh}$ and finally, for capillary waves ($\kappa = 1/3$) the phase velocity gives $v_0^3/\omega_0 = \sigma/\rho$. The authors of [25] also found an expression to calculate the Kelvin angle, which is based on the geometry of the wakes and the group velocity. For the wake half-angle, it was discovered

$$\theta_K = \arctan\left(\frac{1}{2}\sqrt{\frac{1}{\kappa(\kappa-1)}}\right) \tag{5.11}$$

What this expression tells us, is that the kelvin angle depends on the type of wake that we are studying. For $\kappa = -1$ the angle is of $\theta_K = 19.47°$, which is the angle found by Kelvin. In opposite, for $\kappa = 0$ the Kelvin angle occurs at $\theta_K = 90°$. However, for this last limit, the pattern wakes only develops at longer times and becomes less evident, further losing its meaning.

The dispersion relation for the limiting cases ($\kappa = 0, -1, 1/3$), altogether with the exact solution [eq. (5.3)] can be seen in figure 5.4. It shows us that for pure gravity waves in infinite water depth ($\kappa = -1$), the spectrum follows the law $\sqrt{k}$, just like graphene in the vicinity of a dielectric. For gravity waves in shallow water ($\kappa = 0$), the waves are linear in the wavenumber, similar to when we add a local metal to a graphene configuration. This tells us we can make an analogy between these waves and the plasmonic cases studied in chapter 4.

5.1.2 Surface displacement

A mathematical approach is necessary to have a better understanding of the V-shape wave pattern generated by a moving perturbation. For that, we will determine the shape of the surface displacement generated by a pressure field $p(x, y)$. Let us also consider a moving perturbation traveling in x-direction with velocity v. The free equilibrium surface is the plane xy and the z-axis is oriented perpendicular to the surface. We want to find the displacement of the free xy surface, $z = \zeta(x, y, t)$, from the equilibrium position. Assuming an irrotational fluid motion [29], the velocity can be expressed as a velocity potential

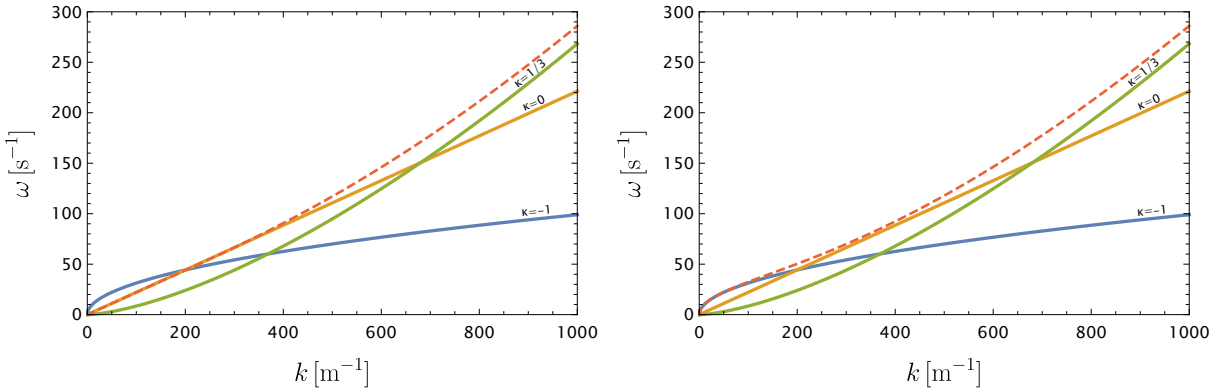

Figure 5.4: Relation dispersion of water waves for the exact (dashed red curve) and for the limiting cases ($\kappa = 0, -1, 1/3$) given by equations (5.6), (5.4) and (5.8), respectively. The exact solution is given by equation (5.3). The left figure shows the exact dispersion (red dashed curve) for a water depth of $h = 5$ mm, which for smaller wavenumbers follows the dispersion of gravity waves in shallow water. For the right figure, we have a depth of $h = 1$ m, and the dispersion behaves as a pure gravity wave in an infinite water depth. The surface water-air tension admitted was $\sigma = 72$ mN/m [33] and the density of water $\rho = 1000$ kg/m^3. The gravity acceleration is the known 9.8 m/s^2.

$v = \nabla\varphi$. The problem is to find the velocity potential, $\varphi(x, y, z)$, and then proceed to find the surface displacement $\zeta(x, y, t)$. We will thoroughly follow the calculations and the notation made by [26], however, for extensive readings and calculations, we must look at [31]. The velocity potential is determined by solving Laplace's equation

$$\nabla^2\varphi = \frac{\partial^2\varphi}{\partial x^2} + \frac{\partial^2\varphi}{\partial y^2} + \frac{\partial^2\varphi}{\partial z^2} = 0 \tag{5.12}$$

where $z < \zeta(x, y)$ for the nonlinear case or $z < 0$ for the linear case. Also, we have the following boundary conditions [26, 34]

$$\varphi_x\zeta_x + \varphi_y\zeta_y = \varphi_z \tag{5.13}$$

$$(\varphi_x^2 + \varphi_y^2 + \varphi_z^2) + \frac{2\zeta}{F^2} + \delta p(x, y) = 1 \tag{5.14}$$

both for $z = 0$. Here we have $\zeta = \sqrt{\zeta_x + \zeta_y}$ and the Froude number given by (5.13). Where the term $\delta p(x, y)$ is, in addition to the atmospheric pressure, the applied pressure on the surface. For ease of notation, the subscripts on this last equation and the following equations are the partial derivatives in order of the coordinate represented. These last two equations are nonlinear and work for $z < \zeta(x, y)$. Equation (5.13) is the kinematic condition, that states there is no current flowing through the free surface, while equation (5.14) is the dynamic condition that combines Bernoulli's equation with constant atmospheric pressure on the free surface, $\zeta(x, y)$ [26]. Since we have been talking about the linear theory (even the hydrodynamic model was linearized), it is important to provide the linear version of the last two conditions

$$\zeta_y = \phi_z \tag{5.15}$$

$$\phi_y + \frac{\zeta}{F^2} = 1 \tag{5.16}$$

for $z = 0$. This problem also gives us a special set of conditions, known as far-field conditions [26, 31], and these states

$$\left(\frac{\partial\varphi}{\partial x}, \frac{\partial\varphi}{\partial y}, \frac{\partial\varphi}{\partial z}\right) \to (1, 0, 0),\ \zeta \to 0 \quad \text{as} \quad x, z \to -\infty \tag{5.17}$$

The condition for x indicates that the gravity wave cannot propagate ahead of the disturbance, while for z the condition indicates a uniform flow stream in the infinitely deep limit. These conditions are known as the far-field boundary conditions. Finally, following Peter study [34], the linearization provides the exact solution for the shape of the Kelvin and Mach waves given by

$$\begin{aligned}\zeta(x, y) = &-\frac{\epsilon F^2 \text{sgn}(x)}{\pi^2}\int_0^{\pi/2}\cos\theta\int_0^{\infty}\frac{ke^{-k|x|}\cos(ky\sin\theta)g(k,\theta)}{F^4k^2+\cos^2\theta}dkd\theta \\ &+\frac{\epsilon H(x)}{\pi}\int_{-\infty}^{\infty}\xi e^{-F^2\xi^2}\cos(x\xi)\cos(y\xi\lambda)d\lambda\end{aligned} \tag{5.18}$$

where

$$g(k, \theta) = F^2 k\sin(k\cos\theta) + \cos\theta\cos(k\cos\theta) \tag{5.19}$$

$$\xi(\lambda) = \frac{\sqrt{\lambda^2+1}}{F^2} \tag{5.20}$$

The parameter $\epsilon = m/(vL^2)$ is the dimensionless source strength, where m is the source strength. For the linear case, $\epsilon \ll 1$. We also have $\text{sgn}(x)$ as the signal function and $\text{H}(x)$ as the Heaviside function. The wave pattern can be obtained by making a numerical evaluation of the equation (5.18) and it was found that the second integral dominates the first integral far downstream. So, the wave pattern appears to be stationary. In that order, it is possible to provide an analytical approximation to the wave pattern. For large $r = \sqrt{x^2+y^2}$ we get the far-field approximation in polar coordinates

$$\zeta(r, \theta) \sim a_1(r, \theta)\cos\left(rg(\lambda_1(\theta), \theta) + \frac{\pi}{4}\right) + a_2(r, \theta)\cos\left(rg(\lambda_2(\theta), \theta) - \frac{\pi}{4}\right) \tag{5.21}$$

where we define the following auxiliary functions

$$\begin{cases}\lambda_1(\theta) = \frac{-1+\sqrt{1-8\tan^2\theta}}{4\tan\theta} & \lambda_2(\theta) = \frac{-1-\sqrt{1-8\tan^2\theta}}{4\tan\theta} \\ f(\lambda) = \frac{\sqrt{\lambda^2+1}}{F^2}e^{\frac{\lambda^2+1}{F^2}} & g(\lambda, \theta) = \frac{\sqrt{\lambda^2+1}}{F^2}(\cos\theta + \lambda\sin\theta)\end{cases} \tag{5.22}$$

Finally, the functions $a_1(r,\theta)$ and $a_2(r,\theta)$ describe the transverse and divergent waves, respectively. Of course, as the Froude number increases, the wave pattern is mainly composed of divergent waves. These functions are given by

$$a_1(r,\theta) = \sqrt{\frac{2}{\pi}} \frac{\epsilon f(\lambda_1(\theta))}{\sqrt{r\left|\frac{\partial^2 g(\lambda_1(\theta),\theta)}{\partial^2 \lambda}\right|}} \tag{5.23}$$

$$a_2(r,\theta) = \sqrt{\frac{2}{\pi}} \frac{\epsilon f(\lambda_2(\theta))}{\sqrt{r\left|\frac{\partial^2 g(\lambda_2(\theta),\theta)}{\partial^2 \lambda}\right|}} \tag{5.24}$$

Since the contribution from $a_2(r,\theta)$ dominates the development of the wave pattern, we can make a small angle ($\theta \ll 1$) perturbation to this amplitude [26, 28], which gives

$$a_2(r,\theta) \approx \frac{\epsilon}{2F\sqrt{\pi r}} \left(\theta^{-3/2} + \frac{7}{4}\theta^{1/2} + ...\right) e^{(\theta^{-2}+2/3+...)/4F^2} \tag{5.25}$$

To find the maximum angle of the wave pattern, we just differentiate equation (5.25) concerning θ and set the result to zero so as to obtain the angle as

$$\theta_{app} \approx \frac{1}{\sqrt{3}F} \tag{5.26}$$

as $F \longrightarrow \infty$. This last expression for the angle shows us that the angle does not follow the constant Kelvin angle, and thus a new regime appears. We already know that the Mach theory tells us that for higher Froude numbers, the wave angle follows the law F^{-1}. As such it was expected that this approximation would turn exactly that. The question that remains is if the two theories studied in this section could be transferred to the plasmonic case, to study the Kelvin and Mach waves in graphene.

5.2 Kelvin and Mach wakes in graphene

Let us recall the electrostatic problems solved in chapter 4. We discovered that when an external particle is moving parallel to a graphene sheet, this will lead to oscillations of the electron gas that will give rise to plasmonic wakes. For our final goal, we wish to understand the shape of the potential created in graphene and see if the angle of the wake follows the theories for ship waves in water, and at what Froude number the transition between Kelvin and Mach theory occurs. In that way, we will study the wake pattern and the aperture angles for two distinct cases: graphene in the vicinity of a dielectric and graphene in the vicinity of a local metal. The external particle is moving parallel to graphene at a height z_0 with velocity v in the y-direction. In the following section, we will show the density plots for the potential using equations (4.35) and (4.63), for the dielectric and local metal cases, respectively. This will give the plan view of the wake induced in graphene for different Froude numbers. To calculate the wake angle, the maximum point of the transverse cut for the potential must be determined (figures 4.3 and 4.8). This is similar to

the criterion used in [26], where the wake angle is given by the best fit of the highest peak points and the center line ($y = 0$).

5.2.1 Graphene in the vicinity of a dielectric

When graphene is in the vicinity of a dielectric (configuration 4.1) we know that the induced potential created by an external particle will create a wake pattern characterized by an oscillatory behavior (see fig. 4.2). The integral form in equation (4.35) gives the induced potential in graphene. The shape of the wake pattern is given by the potential plots in figure 5.5.

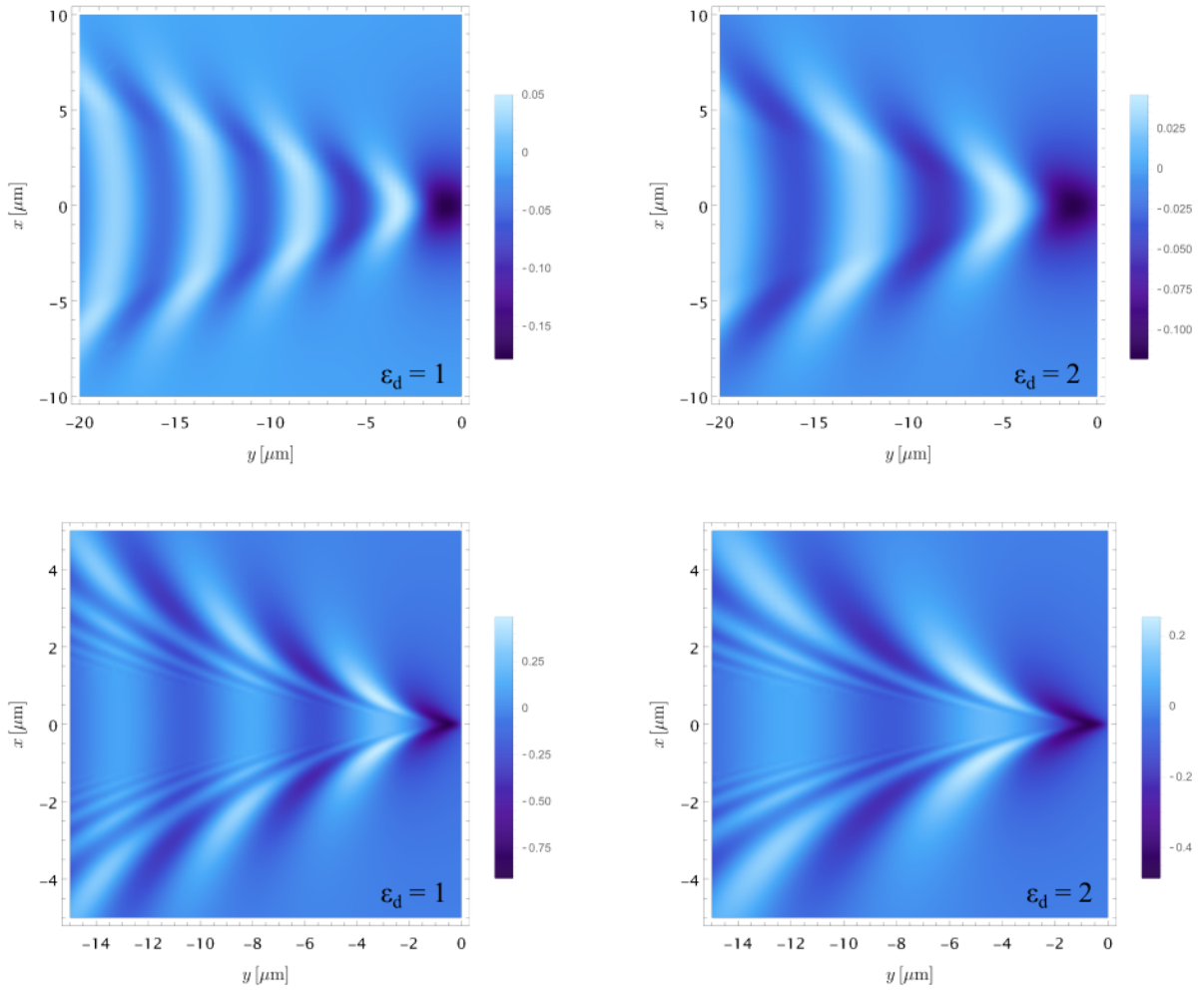

Figure 5.5: Wake pattern of the induced electrostatic potential, in units of Φ_0, given by equation (4.35), when graphene is in the vicinity of a dielectric. The top figures show the density plots for a particle moving at a height $z_0 = 1\ \mu$m above graphene. The bottom ones represent the potential created by the traveling particle at $z_0 = 0.1\ \mu$m. In this figure, the oscillatory behavior of the induced potential is visible. Note the presence of the transverse and divergent waves in the pattern, which makes this case very similar to the ship wakes generated in the water. The velocity of the moving particle is given by $v = 0.1c$ and a Fermi energy of $E_F = 0.17$ eV.

The V-shape pattern in graphene shows us a behavior similar to the water waves created by a moving perturbation (see figure 5.2). Where the electron gas excitation gains an oscillatory nature. In figure 5.5 it is also possible to see the transverse and divergent waves that compose the pattern, for two values of the dielectric constant: $\epsilon_d = 1$ (vacuum) and $\epsilon_d = 2$. We observe that the wavelength of the wake increases as the dielectric constant of the dielectric material increases and the apparent wake angle θ_{app} becomes slightly smaller. Note that the potential fluctuations are more outstanding in the bottom figures because in such case, the external particle is moving closer to graphene ($z_0 = 0.1$ μm). That makes the transverse and divergent waves more distinguishable in this case. In figure 5.6 we present the V-shape pattern for higher Froude numbers (or higher velocities). The first observable difference from the wakes in figure 5.5 is that the transverse wakes cease to exist, and it is only seen in the divergent waves the pattern. In terms of the wake angle, it becomes evident that it does not remain constant, as the Kelvin theory states, but rather decreases with the increase of the Froude number, which can be an indication of a transition to the Mach theory. However, it is necessary to study the wake angle for different values of the particle velocity.

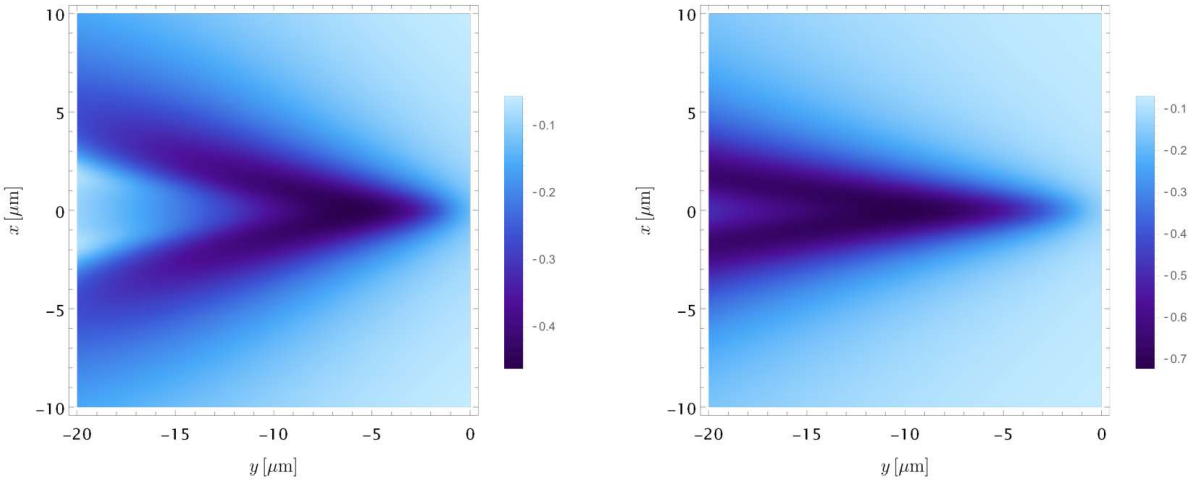

Figure 5.6: Wake pattern of the induced electrostatic potential, in units of Φ_0, given by equation (4.35) for different Froude numbers: $F_{pl} = 2.7$ (left) and $F_{pl} = 4.5$ (right), which corresponds to an external particle velocity ($z_0 = 1$ μm) of $v = 0.3c$ and $v = 0.5c$, respectively. Qualitatively is possible to see a decrease in the wake angle for higher Froude numbers and the dominance of the divergent waves in the wake pattern. The Fermi energy is of $E_F = 0.17$ eV.

The apparent angle θ_{app} is the half opening angle of the wake pattern. To obtain the angle we can just use simple geometry intuition, by finding the point in x (and fixing a point in y) that corresponds to the maximum aperture of the cone. In that order, the tangent gives the angle of the wake pattern, such as

$$\tan \theta_{app} = \frac{x}{y} \tag{5.27}$$

Of course, this method can originate some systematic errors. That happens because of our difficulty in understanding where the maximum aperture of the cone is, since this method depends on our perception of the wake pattern. This can lead to an uncertainty value for the wake angle. However, we can complement

Table 1: Apparent half wake angle θ_{app} (in degrees) of the cone produced by the moving plasmons in graphene induced by an external particle with parallel motion at a height $z_0 = 1$ μm. The Fermi energy of the electron gas is $e_F = 0.17$ eV. The last line of the table gives the Froude number for this problem obtained to the expression $F_{pl} = \sqrt{v^2/z_0 a}$.

v/c	0.075	0.1	0.125	0.15	0.2	0.25	0.3	0.4	0.5	0.6	0.7	0.8	0.9
θ_{app}	22.6	22.6	21.7	21.3	20.1	19.0	17.7	14.4	11.9	9.2	8.3	7.5	6.0
F_{pl}	0.67	0.89	1.1	1.3	1.8	2.2	2.7	3.6	4.5	5.4	6.3	7.2	8.0

this method with another one, that states that the angle of the wake pattern is given by the line that passes through the highest peaks of the wake and the center line $x = 0$. The apparent angles θ_{app} of the wake cone, for different velocities are depicted in table 1. For each velocity, the Froude number $F_{pl} = \sqrt{v^2/z_0 a}$ is also shown, calculated for $z_0 = 1$ μm. To recall a_d is a parameter with units of acceleration and characterizes the 2D electron gas in graphene, given by $a = \frac{4\alpha_{FS} E_F \hbar c}{(1+\epsilon_d)\hbar^2}$. A graphical representation of the angles in the table is found in figure 5.7, where the half wake angle is plotted with the respective plasmonic Froude number, F_{pl}.

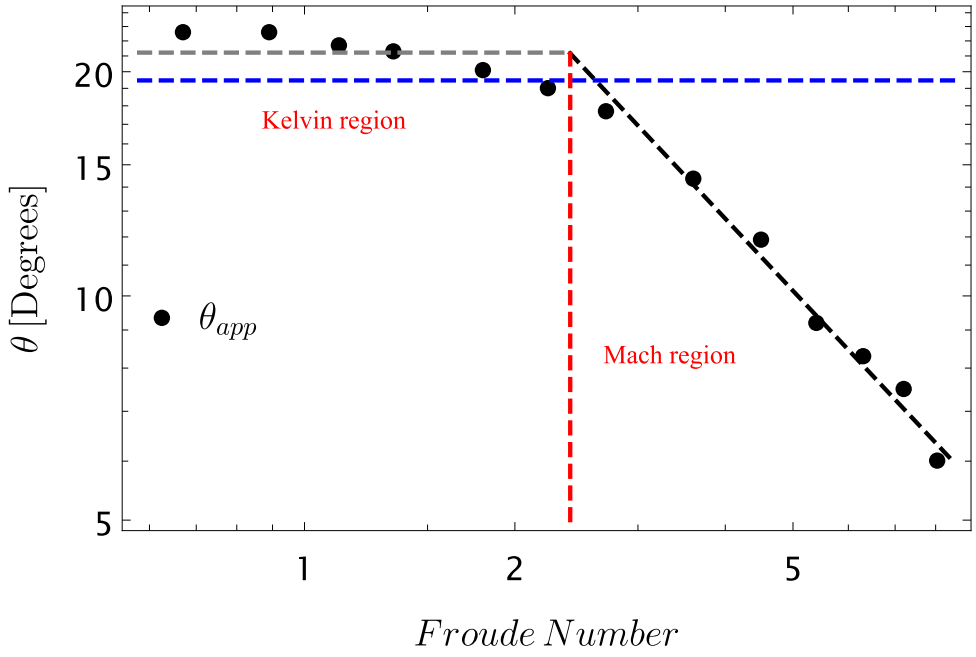

Figure 5.7: Graphical representation of half angle of the plasmonic cone for graphene in the vicinity of a dielectric for $\epsilon_d = 1$ (vacuum), given by table 1. There is a transition from a Kelvin-type wake to a Mach-type wake at $F_{pl} \sim 2.2$ as the Froude number increases. The other parameters were: $E_F = 0.17$ eV and $z_0 = 1$ μm. The dashed black line corresponds to the angle given by $\theta = 1/(\delta F_{pl})$ and $\delta = 0.020$, which only holds for angles in the Mach region. The dashed blue line is the Kelvin angle given by Kelvin's theory ($\theta_K = 19.47°$). The dashed grey line is a fit performed to the angles enclosed in the Kelvin region, with an angle value of $\theta_{app} = 21°$. The transition between the two regions occurs at the interception of the dashed black and grey lines.

From this figure, it is clear that there are two distinct regions with different behaviors. In the Kelvin

region, the angle of the plasmonic wake pattern is almost constant and with a value of $\theta_{app} = 21^\circ$ (grey line), which is slightly above the Kelvin angle of $\theta_K = 19.47^\circ$ (blue line) produced in water waves. For $F_{pl} \gg 1$ the wake angle starts to change behavior and the angles start to decrease by following the law $1/F_{pl}$, which indicates a Mach-type region. In that order, we study the angles by producing a fitting function of the type

$$\theta_{app} \approx \frac{1}{\delta}\sqrt{\frac{z_0 a}{v^2}} = \frac{1}{\delta}\frac{1}{F_{pl}} \tag{5.28}$$

that gives the apparent wake angles as the Froude number increases. A transition from the Kelvin region to the Mach region is clear at $F_{pl} \sim 2.2$ (red line), where δ is a real constant that was found to be the order of $\delta = 0.020$ for $\epsilon_d = 1$ (vacuum). These results are consistent with the study of the formation of plasmonic wakes in graphene provided by [17].

5.2.2 Graphene in the vicinity of a local metal

For graphene in the vicinity of a local metal (configuration 4.4) the oscillatory behavior of the plasmons in graphene vanishes and a rather continuous nature will become more distinct. We already studied this phenomenon in chapter 4.3. Equation (4.63) gave the results in figure 4.7, which precisely shows the continuous nature of the potential. In a similar manner to the problem of graphene in the vicinity of a dielectric we show, in figure 5.8, a plan view of the plasmonic wakes in graphene in the presence of a local metal for different dielectric thickness d and different dielectric constants ϵ_d.

From the density plots, it is possible to infer the cease of the oscillatory behavior of the potential in graphene but is replaced by a somewhat continuous behavior in the cone. Note that in this case there are not any transverse and divergent waves in the pattern. All these differences come from the presence of the metal, which is chosen to be titanium. If the distance between the metal and the graphene sheet (in other words, the dielectric thickness d) increases, it is expected the appearance of the oscillatory nature of the plasmons in graphene, due to the weak effect that the metal will provide to the configuration. However, for the dielectric thickness chosen ($d = 0.01$ μm and $d = 0.1$ μm) the effects of the metal are quite evident as seen in figure 5.8. We also observe that the wake angle decreases with the increase of the dielectric thickness ϵ_d, just like in the case of graphene in the vicinity of a dielectric. The dielectric thickness d, also plays an important role in the variation of the wake angle, in such a way that for $d = 0.01$ μm the cone angle is smaller than for $d = 0.1$ μm. This means that the wake angle is greater for a higher separation between the metal and graphene.

To study the V-shaped pattern of the potential created in graphene, in figure 5.9, it is shown the wake pattern for two different velocities of the external particle. Similar to graphene near a dielectric, the wake angle decreases with the increase of the velocity of the particle (and with the increase of the Froude number). However, the continuous nature of the potential remains, even for higher particle speeds. It remains to be seen if, in such case, we can depict a Kelvin and Mach region by measuring the half angle

of the V-shaped pattern. In tables 2 and 3, the apparent wake angles for different velocities, and an external particle height of $z_0 = 1\ \mu$m and $z_0 = 0.1\ \mu$m are respectively presented.

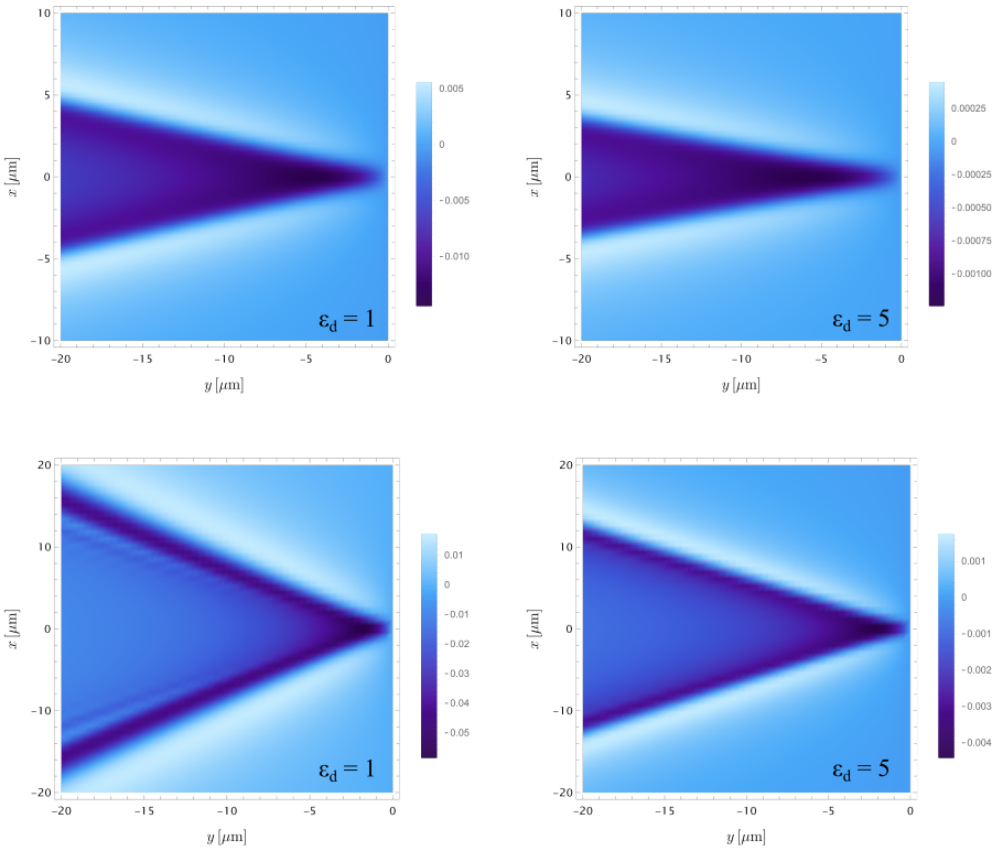

Figure 5.8: Wake pattern of the induced electrostatic potential, in units of Φ_0, given by equation (4.63), when graphene is in the vicinity of a local metal. The top figures show the density plots for a distance between metal and graphene of $d = 0.01\ \mu$m. The bottom ones represent the potential created in graphene for a dielectric thickness of $d = 0.1\ \mu$m. It is possible to understand the continuous nature of the potential in all plots and the nonexistence of transverse and divergent waves. The wake angles are smaller for a higher dielectric constant ϵ_d and a smaller separation of metal/graphene d. The velocity of the moving particle is $v = 0.1c$, the Fermi energy is of $E_F = 0.17$ eV and the external particle is moving at a height of $z_0 = 1\ \mu$m above graphene. The chosen metal was titanium: $\omega_p = 2.80$ eV and $\epsilon_\infty = 2.2$.

In figure 5.10 is represented how the half wake angle of the potential cone created by an external particle moving parallel to graphene at a distance $z_0 = 1\ \mu$m from it, changes with the plasmonic Froude number. Contrary to the dielectric case, there is not a Kelvin region and a Mach region visible in the whole domain. However, following an inverse quadratic law where the best fit to the angle points has to do the law $1/\delta_0 + 1/\delta_1 F_{pl} + 1/\delta_2 F_{pl}^2$, or in other words, the half angle of the wake pattern in graphene near a metal can be taken as

$$\theta_{app} \approx 3.87 + \frac{9.92}{F_{pl}} + \frac{0.77}{F_{pl}^2} \tag{5.29}$$

where $\delta_0 = 0.26$, $\delta_1 = 0.10$ and $\delta_2 = 1.30$. In this case there is no transition for a different angle behavior, since there are no Kelvin and Mach regions. Also, from equation (5.11) the Kelvin angle was expected to be at $\theta_K = \pi/2$, because in this case $\kappa = 0$, which means that the angle increases for lower Froude numbers. Of course, for lower Froude numbers the linear and quadratic terms have a bigger contribution to the angle and as such their value increases. For higher Froude numbers the quadratic term has a small contribution to the angle and equation (5.29) is dominated by linear and the constant terms. This behavior was also perceived in classical water waves in [35]. In this study, a disturbance with a certain length L and a width B was considered, as for axisymmetric disturbances the aspect ratio parameter $A = L/B$ must be one. The Kelvin and Mach regions are reached, which means the angle starts to behave consistently, and for higher speeds it scales as $\theta_{app} \propto F_{pl}^{-1}$. In the case where $A \gg 1$, we find ourselves in the presence of nonaxisymmetric disturbances and angle scales as $\theta_{app} \propto F_{pl}^{-2}$, which show the quadratic nature of some water wakes. For figure 5.11 the apparent angles of the wake pattern in graphene for a particle traveling at a height $z_0 = 0.1$ μm above graphene are drawn. In this case, the whole domain can be described by the law $1/v$ [equation (5.28]. Once again, the Kelvin region ceases to exist and the angles are contained within the Mach region, where the angle is given, once again, by equation (5.28), with $\delta = 0.027$. As the velocity of the external particle increases, and consequently the Froude number, the apparent wake angle θ_{app} decreases, such as in the dielectric case.

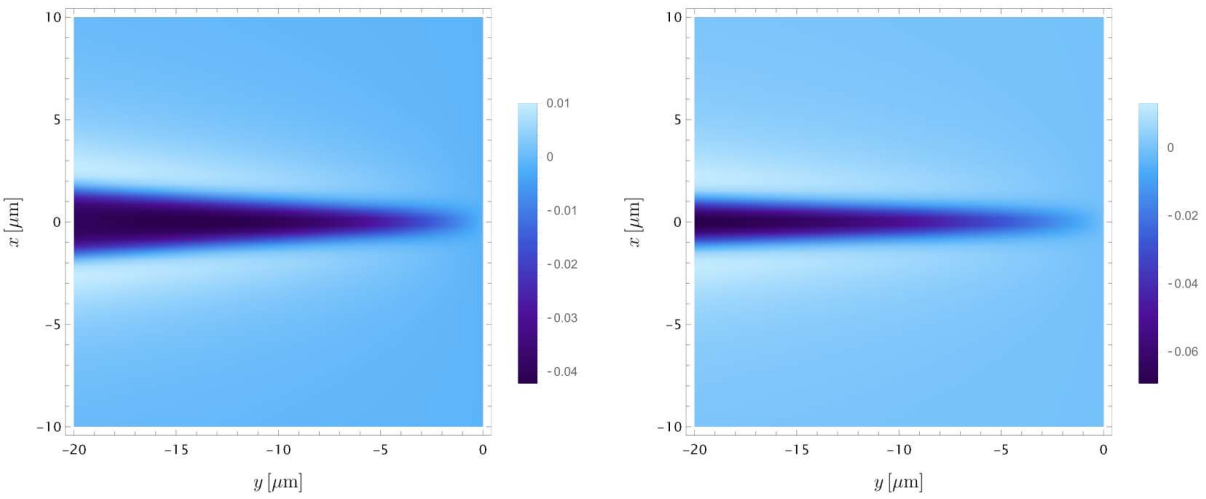

Figure 5.9: Wake pattern of the induced electrostatic potential, in units of Φ_0, given by equation (4.63) for different Froude numbers: $F_{pl} = 2.7$ (left) and $F_{pl} = 4.5$ (right), which corresponds to an external particle velocity ($z_0 = 1$ μm) of $v = 0.3c$ and $v = 0.5c$, respectively. Qualitatively it is possible to see a decrease in the wake angle for higher Froude numbers. The parameters are: Fermi energy of $E_F = 0.17$ eV, dielectric thickness of $d = 0.01$ μm in vacuum ($\epsilon_d = 1$). The chosen metal was titanium: $\omega_p = 2.80$ eV and $\epsilon_\infty = 2.2$.

Table 2: Apparent half wake angle θ_{app} (in degrees) of the cone produced by the moving plasmons in graphene induced by an external particle with parallel motion at a height $z_0 = 1$ μm. The Fermi energy of the electron gas is of $E_F = 0.17$ eV and the dielectric thickness of $d = 0.01$ μm for vacuum ($\epsilon_d = 1$). The last line of the table gives the Froude number for this problem obtained to the expression $F_{pl} = \sqrt{v^2/z_0 a}$.

v/c	0.04	0.055	0.07	0.08	0.09	0.1	0.2	0.3	0.4	0.5	0.6	0.7	0.8	0.9
θ_{app}	37.3	27.1	21.8	19.4	17.5	16.0	9.2	7.2	6.6	6.1	5.8	5.6	5.5	5.4
F_{pl}	0.36	0.49	0.63	0.72	0.81	0.89	1.8	2.7	3.6	4.5	5.4	6.3	7.2	8.1

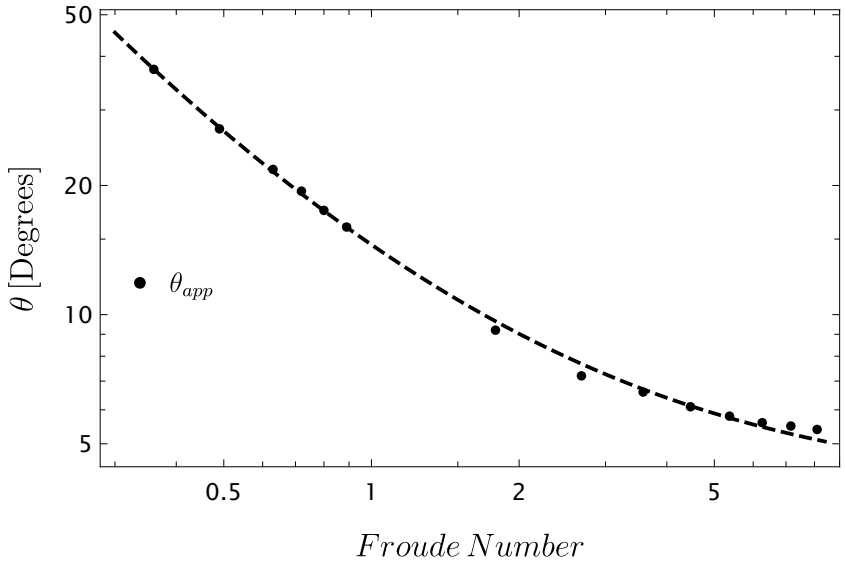

Figure 5.10: Graphical representation for the apparent angle θ_{app}, given by table 2, of the plasmonic cone for graphene in the vicinity of a local metal for $z_0 = 1$ μm. In this case, there is no Kelvin or Mach region in the whole domain. The angles follow a quadratic law given by $1/\delta_0 + 1/\delta_1 F_{pl} + 1/\delta_2 F_{pl}^2$, with $\delta_0 = 0.26$, $\delta_1 = 0.10$ and $\delta_2 = 1.30$. The parameters considered are: $E_F = 0.17$ eV, $d = 0.01$ μm and $\epsilon_d = 1$. For titanium: $\omega_p = 2.80$eV and $\epsilon_\infty = 2.20$.

Table 3: Apparent half wake angle θ_{app} (in degrees) of the cone produced by the moving plasmons in graphene induced by an external particle with parallel motion at a height $z_0 = 0.1$ μm. The Fermi energy of the electron gas is of $e_F = 0.17$ eV and the dielectric thickness of $d = 0.01$ μm for vacuum ($\epsilon_d = 1$). The last line of the table gives the Froude number for this problem obtained to the expression $F_{pl} = \sqrt{v^2/z_0 a}$.

v/c	0.03	0.05	0.07	0.09	0.1	0.15	0.2	0.3	0.4	0.5	0.6	0.7	0.8
θ_{app}	44.8	26.6	19.1	14.5	13.0	8.6	6.4	4.3	3.2	2.6	2.0	1.8	1.6
F_{pl}	0.84	1.4	2.0	2.5	2.8	4.2	5.6	8.4	11.3	14.0	16.9	19.7	22.5

5.3 Classical Wakes and Plasmonic Wakes

To finalize the study of the plasmonic wakes in graphene it is necessary to analyze the V-shape pattern and compare it to the wakes produced in water. Even more, we proceed to see the major similarities and differences between the classical and plasmonic wakes. This will allow us to understand the influence of

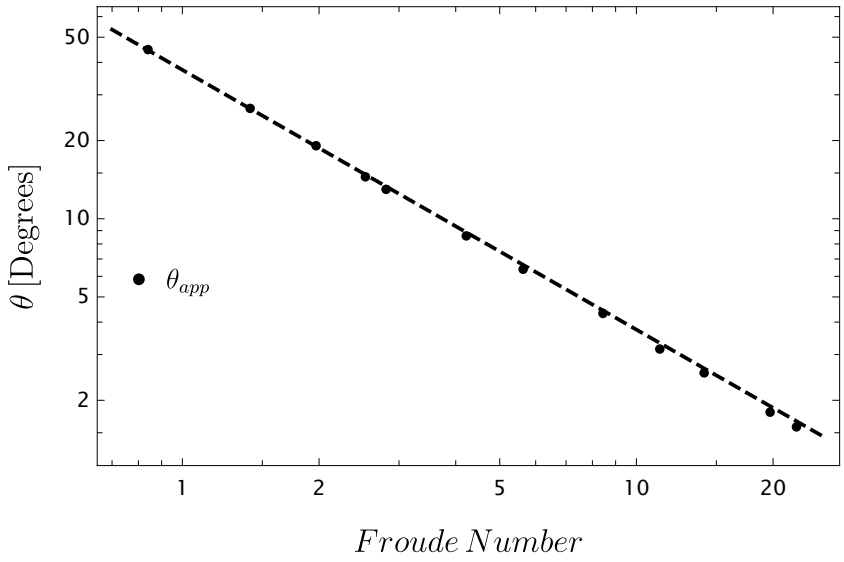

Figure 5.11: Graphical representation for the apparent angle θ_{app}, given by table 3, of the plasmonic cone for graphene in the vicinity of a local metal for $z_0 = 0.1$ μm. In this case, the only theory that describes the angle behavior is the Mach theory, $\theta = 1/(\delta F_{pl})$, where $\delta = 0.027$. The parameters considered are: $E_F = 0.17$ eV, $d = 0.01$ μm and $\epsilon_d = 1$. For titanium: $\omega_p = 2.80$ eV and $\epsilon_\infty = 2.20$.

the dispersion relation and the problem parameters in the shape of this type of wakes. In figure 5.12, it is shown a 3D representation for the problems we want to compare. The first one is the classical wakes that originated on the surface of the water by a moving source traveling in the y-direction. For water waves, the parameters in question are the gravity acceleration, g, the height of the water, h, and the velocity of the source producing the waves. The plasmonic configurations are the same as the ones studied in chapter 4. For graphene in the vicinity of a semi-infinite dielectric (configuration (b)), we have the acceleration of the electron gas $a = \frac{4\alpha_{FS}E_F\hbar c}{(1+\epsilon_d)\hbar^2}$, in graphene. The moving charge is placed at a height z_0 and moves with velocity v_y. When graphene is in the vicinity of a local metal (configuration (c)) we add an extra parameter to the problem, which is the dielectric thickness d.

In section 5.1.1 we study the dispersion relation of water waves, where it was shown that the phase velocity is related to the angular frequency as $v_p \propto \omega^\kappa$. For pure gravity waves in deep water the dispersion is proportional to $\sqrt{k}$ [equation 5.4], which means that the phase velocity is proportional to the inverse of the angular frequency, $v_p \propto \omega^{-1}$, which means that $\kappa = -1$. This provides an analogy with the electrostatic problem of graphene in the vicinity of a dielectric, where the dispersion relation is given by equation (4.24) and like pure gravity waves the dispersion is proportional to $\sqrt{k}$ and the phase velocity is proportional to the inverse of ω. As such, we can think of the plasmonic wake pattern as being similar to the wake pattern of pure gravity waves in deep water. Let us consider figure 5.13, where the calculated wakes for pure gravity waves and the plasmonic wakes for graphene in the vicinity of a dielectric are calculated. Both waves have the similarity of having $\kappa = -1$, which in other words, means that both wakes follow the law $v_p \propto \omega^{-1}$. The left 3D density plots show us the wakes created by an external particle moving parallel

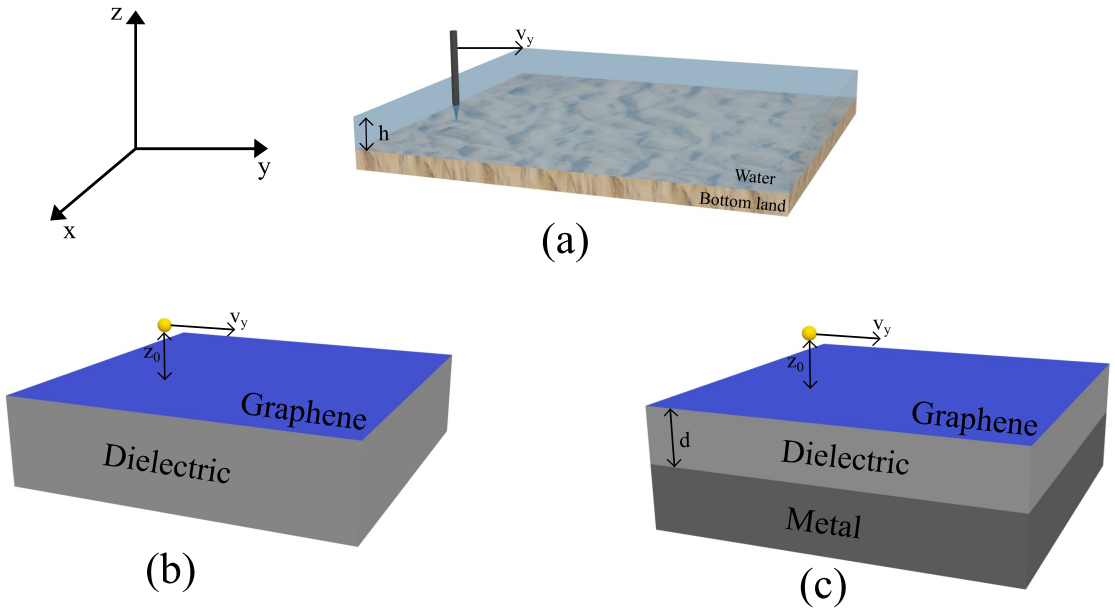

Figure 5.12: Representation of the configurations in the classical and plasmonic problems. In (a) the figure shows a perturbation moving in the y-direction in the water, which has a height h regarding the bottom land. The plasmonic configuration (b) represents graphene in the vicinity of a dielectric, with an external particle moving with velocity v_y at a height z_0 from the graphene sheet. Configuration (c) is characterized by graphene in the vicinity of a local metal with a dielectric separation of thickness d. Once again, we have an external charge moving with velocity v_y at a height z_0 from graphene.

to graphene at a height $z_0 = 0.1\ \mu$m, and the right density plots are the calculated pattern for pure gravity waves in deep water [25]. In the top panel, the wakes are generated by disturbances moving slower than those from the bottom panels. The clear similarities are given by the decrease of the V-shape pattern angle as the velocity increases and there are present transverse and divergent waves in both cases. This indicates that once we have graphene in the vicinity of a dielectric, an analogy can be made with pure gravity waves in shallow water. Here the semi-infinite dielectric plays the part of the deep water, where $h \longrightarrow \infty$.

Let us now take a look at when graphene is in the vicinity of a local metal. In this case, the dispersion is linear in the wavenumber k, which means that the phase velocity is constant and equal to the group velocity of the waves. The same happens for gravity waves in shallow water [equation (5.6)], that is, for gravity waves with wavelengths greater than the water depth. So when the dispersion of the waves is linear in k, then this limiting case is characterized by having $\kappa = 0$, for both problems. In figure 5.14, the classical wake pattern for κ close to zero and the analogous problem for the plasmonic wakes are shown. The classical wakes were computed with $\kappa = -0.1$. This choice is due to the impossibility of having $\kappa = 0$. These type of waves always show features for $\kappa > 0$, because very short capillary waves cannot be avoided even when reducing the surface tension σ to low values. However, this value of κ is very close to

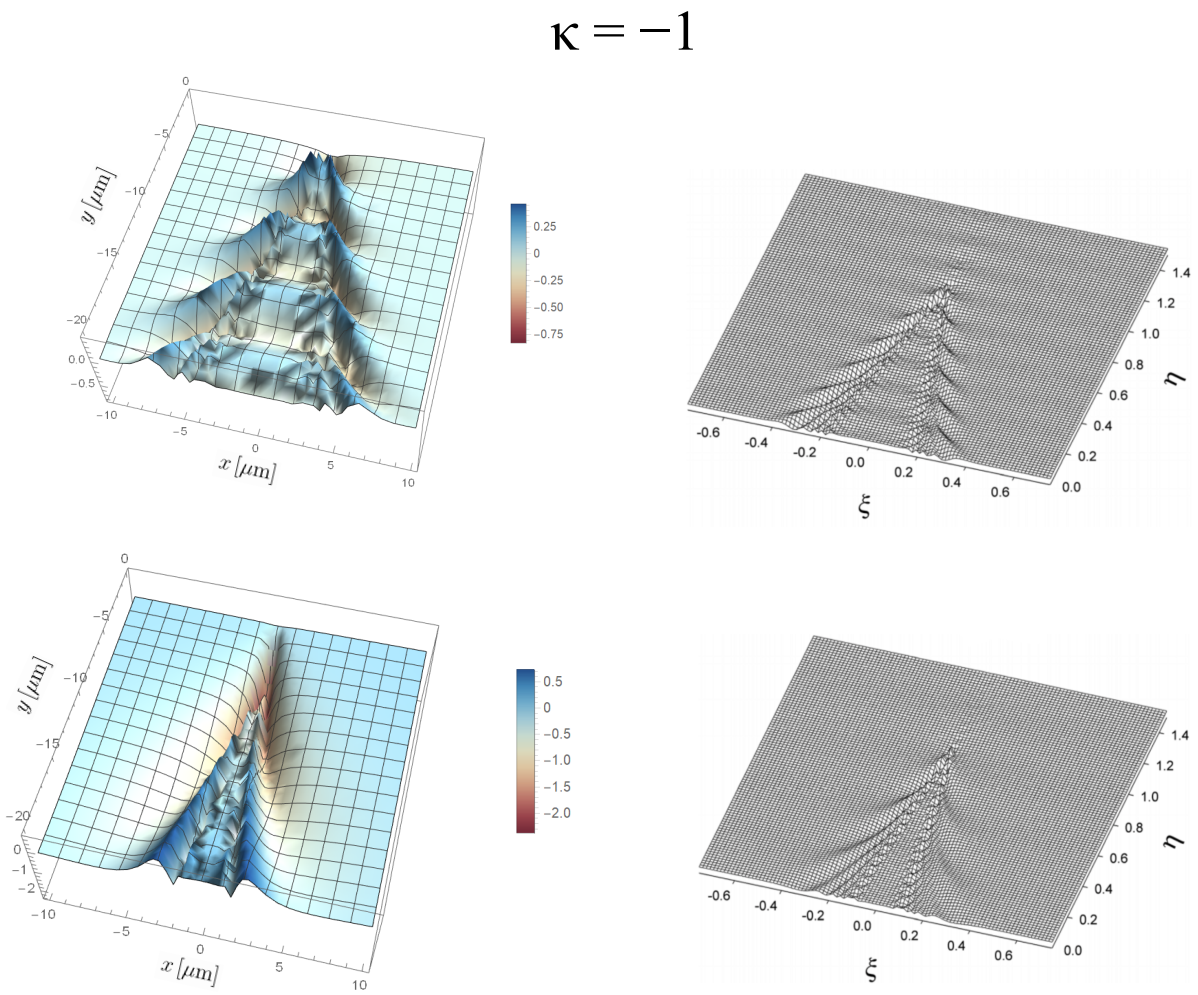

Figure 5.13: Wake pattern for the plasmonic (left) and classical (right) cases. Both patterns show similar structures, typical of the limiting case $\kappa = -1$, which are the oscillatory behavior and the presence of transverse and divergent waves. The bottom figures show disturbances speeds higher than the top ones, which bring a decrease on the wake angle. The case of graphene in the vicinity of a dielectric is similar to water wakes in deep water. For the plasmonic case the parameters are: $E_F = 0.17$ eV and $z_0 = 0.1$ μm. Right figures retrieved from [25].

zero and will allow us to study the wakes in this regime. This means that we have a parameter $0 < \delta \ll 1$ which changes the dispersion relation to $\omega \propto k^{1-\delta}$ and, consequently the phase velocity takes the form $v_p = \omega/k \propto k^{-\delta}$. In this case $\delta = -\kappa = 0.1$. For the plasmonic case, we are expecting the same to happen. However, let us study two different regimes: the first regime for $d \ll z_0$ corresponds to the case of shallow water, while the second regime $d \gg z_0$ corresponds to the deep water case. This is the same as saying that when the dielectric separation between metal and graphene increases then the influence of the metal in the system begins to decrease and we recover the oscillatory behavior of the potential and consequently the limiting case of $\kappa = -1$, which is analogous to the case of pure gravity waves in deep water. The similarities between the two wake patterns are visible in the continuous wake that the perturbations create on the surface of the water and on the surface of graphene, which means that when

graphene is in the vicinity of a local metal and $d \ll z_0$ the dispersion is linear in the wavenumber and the plasmonic configuration can be seen as waves in shallow water. In the classical case the depth is controlled by the height, h of the water, while for the plasmonic case what controls the shallow nature is the dielectric thickness, d, and the distance of the external particle and graphene, z_0. For the regime of $d \gg z_0$ we retrieve the oscillatory plasmonic shape in graphene, which implies the same behavior as pure gravity waves in deep water, as seen in figure 5.15 where we compare the two different regimes.

$$\kappa = -0.1$$

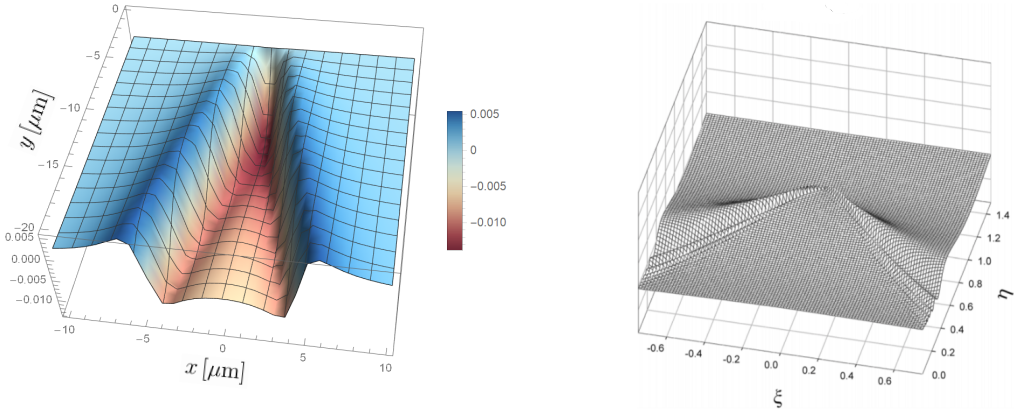

Figure 5.14: Graphical representation of the wake pattern in graphene near a metal (left) and the water wake pattern (right) for the limiting case $\kappa = -0.1$. This corresponds to water wakes in shallow water. Both shapes show us a continuous behavior in the central cone. In the water wake there are waves forming in the outer region of the pattern which is analogous to the bluest region in the plasmonic wake. For the plasmonic wake the parameters are: $v = 0.1c$, $E_F = 0.17$ eV, $d = 0.01$ μm and $z_0 = 1$ μm. The chosen metal was titanium. The right figure retrieved from [25].

From this chapter, a connection between the shape pattern of classical water waves and the plasmonic wakes propagating in graphene and created by an external charge moving parallel to it is visible. This reinforces the argument that the dispersion of the water waves and the surface plasmon-polaritons in graphene play an essential role in the shape of the wake pattern produced on the surface of the mediums. In such manner, the hydrodynamic model can be seen as a way to understand not only the nonlocal effects in materials at the nanoscale but also provide a connection between the classical and plasmonic world, which can lead to very interesting results, such as the ones obtained in this thesis. Finally, these results can lead to a more profound understanding of the optical and electromagnetic proprieties of plasmonic nanostructures, specifically how nonlocal graphene behave in the presence of external potentials and how we can use these results to boost the search for faster and more compact nanotechnology.

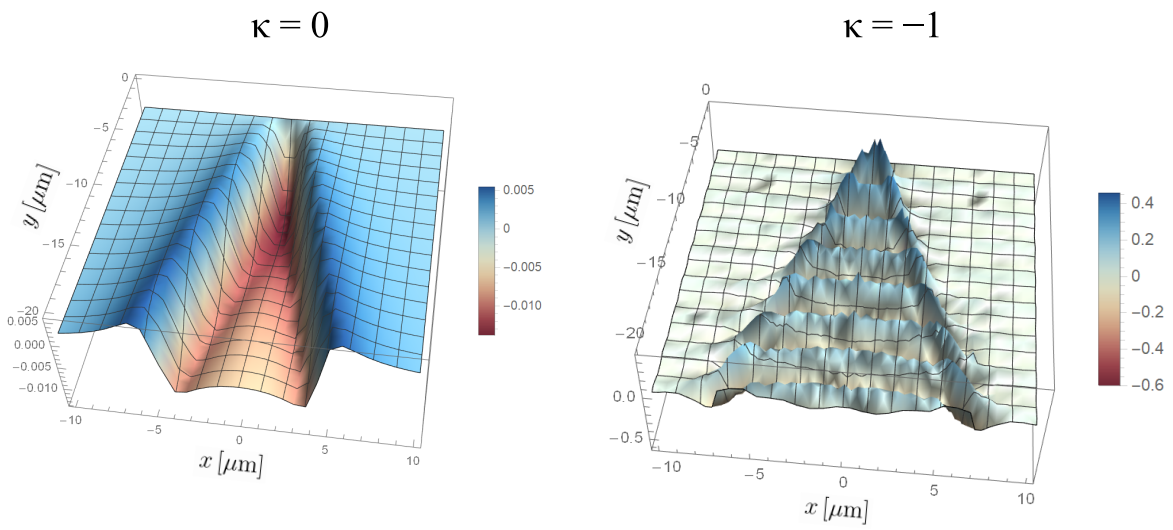

Figure 5.15: Graphical representation of the wake pattern in graphene near a metal for $d \ll z_0$ (left) and $d \gg z_0$ (right). For the limiting case $\kappa = 0$ we are in the shallow water regime, where $d = 0.01$ μm and $z_0 = 1$ μm. When we increase the dielectric thickness, there is a regime inversion and the oscillatory behavior is recovered, because we now have $d = 1$ μm and $z_0 = 0.1$ μm and this case is analogous to water wakes in deep water. The parameters are: $v = 0.1c$ and $E_F = 0.17$ eV. The chosen metal was titanium.

Chapter 6

Conclusion

The hydrodynamic model is a nonlocal theory that couples the Euler equation with Maxwell's equations of electromagnetism, and it is constituted by the following equations: Euler's equation, Poisson equation, and the continuity equation. This model is generalized for an electron gas (regarding the spatial dimension). However, it is possible to consider various geometries composed of metals, semiconductors, and dielectric materials where the model remains valid if supported by specific boundary conditions for each geometry. The main goal of this thesis was to make use the hydrodynamic model to analyze the plasmonic nonlocal effect in graphene, considering an electrostatic approximation for the electron gas. Various planar geometries in the form of slabs oriented perpendicular to the z-axis and infinite in all the other directions were studied. Through a first approach, the nonlocal effects in the spectrum of the surface plasmon-polaritons and on the electrostatic potentials in some problems, such as a semi-infinite and finite metal slab embedded in vacuum were analyzed. For a graphene sheet in vacuum and a 2D electron gas, it was recovered the known dispersion of the SPPs, which are proportional to the square root of the wavenumber k. Literature was already aware of these problems. The additional problems came with graphene in the vicinity of a nonlocal metal. When graphene is in the vicinity of a semi-infinite metal, the dispersion of the SPPs presents a linear nature, rather than a $\omega \propto \sqrt{k}$ behavior like graphene in vacuum. As graphene is moved away from the metal, that is, the dielectric separation increases, it was verified that the SPPs show higher energies from a higher dielectric thickness. Therefore, the further graphene is from the metal, the greater the growth in terms of surface plasmon energy. However, when increasing the dielectric separation, the nonlocal metal will start to behave more like a local metal. For graphene near a finite metal with thickness a, it was seen a linear dispersion for different values of the thickness a. Moreover, the energy of the plasmons decrease with the decrease of the metal slab thickness, which is a counter intuitive result, because as the metal thickness decrease the spectrum of the SPPs should be the one obtained for graphene near a semi-infinite metal. However, when we take the limit of the background permittivity

to infinity it is retrieved the case of a semi-infinite local metal. Also, taking the limit of the dielectric and metal thicknesses going to zero and consider the dielectrics as vacuum, it was recovered the expression for graphene in vacuum, as it was expected. These studies were made for the metals gold and titanium and it was uncovered that the nonlocality in metals depends on some parameters, such as the dielectric separation d, the background permittivity ϵ_∞, the plasmon frequency ω_p and the relaxation frequencies Γ. Due to its intrinsic proprieties, titanium shows an enhanced nonlocal behavior when compared to gold.

Furthermore, it was study the effect of an external charge moving parallel to a graphene sheet (in the y-direction) at a height z_0 for two configurations: graphene in the vicinity of a dielectric and graphene in the vicinity of a local metal. The goal of the external charge was to see the induced potential created in the graphene sheet and study the pattern of the wakes produced in it so as to compare it to the classical pattern created by water waves. When graphene is near a dielectric, an oscillatory pattern in graphene was created. This means that in this structure the plasmonic wakes demonstrate a V-shaped pattern format, just like a disturbance perturbing the water at linear flow. The wake was shown for charge velocities of $z_0 = 1$ μm and $z_0 = 0.1$ μm. In both cases, it was possible to recognize two types of waves: the divergent waves at the outer region of the wake and the transverse waves at the center region of the pattern. To study the dependence of the wake angle on the velocity of the external particle, an adimensional parameter, known as the Froude number, which is proportional to the charge velocity was used. By considering graphene in vacuum, the half-wake angle of the potential cone, induced in the graphene sheet, is constant for lower Froude numbers with a value of $21°$. However, this behavior changes for a Froude number of 2.2. This constant angle behavior is indicative of the Kelvin region, which happens in water wake patterns. According to Kelvin's theory, the half angle of the wake created on the surface of the water is constant and equal to $19.47°$. For Froude numbers greater than 2.2 the angle of the cone decreases with $1/v$, which corresponds to a Mach wave typical behavior. Moreover, when increasing the dielectric value constant, the wake angle decreases for the same Froude numbers. When the charge is closer to graphene, the angle of the wake also decreases due to the greater approximation. It is when graphene is near a local metal that interesting results occur. In this case, the potential does not show an oscillatory behavior but rather a V-shaped potential, which presents a potential peak that tends to a continuous behavior for graphene points further away from the charge. Regarding the angle of the cone and the pattern angle, for $z_0 = 1\mu m$, there is no Kelvin or Mach region, however the angles follow a polynomial law that is quadratic for all Froude numbers. The angle does not remain constant for lower velocities, but rather increases as the Froude number decreases. This could be due to the dispersion relation being different in each case, that is, for graphene near a dielectric, the dispersion of the plasmons is proportional to the square root of k, while in the case of the local metal the dispersion is linear in the wave vector. In such manner, the dispersion allows us to make an analogy between the classical wake and the plasmonic wake. That is, by studying the phase velocity of the waves, it was found for the limiting cases $\kappa = -1$ and $\kappa = 0$, that these correspond to pure gravity waves in deep water and gravity waves in shallow water, respectively. Just like water waves in deep water, when graphene is near a dielectric, the SPP dispersion is proportional to $\sqrt{k}$. This provides similarities between this type of wakes and the induced wakes in graphene. Both are

oscillatory and formed by transverse and divergent waves. There is also a transition between the Kelvin theory and the Mach theory for a specific Froude number. For graphene near a metal, the limiting case is at $\kappa = 0$ and for $d \ll z_0$, due to the linear dispersion, which makes this plasmonic problem analogous to gravity waves in shallow water. When the dielectric thickness is increased at a value $d \gg z_0$ the influence of the metal decreases and the behavior of the potential starts to be oscillatory once again. The dispersion becomes proportional to $\sqrt{k}$ and the regime changes to $\kappa = -1$, just like pure gravity waves in deep water. In conclusion, it was verified that within the hydrodynamic model it is possible to retrieve the nonlocal effects in nanostructures of metals and graphene, which are strongly influenced by some material parameters. Specifically, this work permitted the study of acoustic graphene plasmons, which disperse linearly in the wavenumber, by introducing the metal to a graphene configuration. Further research will still be necessary in order to understand the full applications of the nonlocal character of metals and graphene in nanoplasmonics. It still is necessary to understand why the problem of graphene near a finite nonlocal metal is giving counter intuitive results. Furthermore, it should be interesting to provide the same methods in this thesis, but for different hetero-structures geometries, such as cylindrical and spherical configurations, rather than just planar slabs. However, before that, the study must be completed by figuring out the plasmonic physics and the consequences of a charge moving perpendicular to graphene in the vicinity of a metal. Also, for the external charge configuration, a local metal has always been used, nonetheless it would be interesting to analyze the effects that a nonlocal metal can provide to the wake pattern. On a more practical basis, the next step should be the development of an experimental setup so as to test the results obtained in this thesis. At last, this research has allowed us to infer the optical and electromagnetic proprieties of graphene and metallic nanostructures close to each other, which is a way to enhance the nonlocal effects.

Bibliography

[1] A. Bylinkin et al. “Tight-binding terahertz plasmons in chemical-vapor-deposited graphene”. In: *Physical Review Applied* 11.5 (2019), p. 054017.

[2] B. Hermann et al. “Inverse-Designed Narrowband THz Radiator for Ultrarelativistic Electrons”. In: *ACS photonics* 9.4 (2022), pp. 1143–1149.

[3] V. J. Sorger et al. “Toward integrated plasmonic circuits”. In: *MRS bulletin* 37.8 (2012), pp. 728–738.

[4] A. Wiener. “Nonlocal Effects in Plasmonic Nanostructures”. In: *Faculty of Natural Sciences, the Blackett Laboratory - Imperial College London* (2014).

[5] R. W. Wood. “XLII. On a remarkable case of uneven distribution of light in a diffraction grating spectrum”. In: *The London, Edinburgh, and Dublin Philosophical Magazine and Journal of Science* 4.21 (1902), pp. 396–402.

[6] S. Enoch and N. Bonod. *Plasmonics: from basics to advanced topics*. Vol. 167. Springer, 2012.

[7] P. A. D. Gonçalves and N. M. Peres. *An introduction to graphene plasmonics*. World Scientific, 2016.

[8] A. Karch. “Surface plasmons and topological insulators”. In: *Physical Review B* 83.24 (2011), p. 245432.

[9] J. F. O’Hara, R. D. Averitt, and A. J. Taylor. “Prism coupling to terahertz surface plasmon polaritons”. In: *Optics Express* 13.16 (2005), pp. 6117–6126.

[10] J. Homola, I. Koudela, and S. S. Yee. “Surface plasmon resonance sensors based on diffraction gratings and prism couplers: sensitivity comparison”. In: *Sensors and Actuators B: Chemical* 54.1-2 (1999), pp. 16–24.

[11] L. Ju et al. “Graphene plasmonics for tunable terahertz metamaterials”. In: *Nature nanotechnology* 6.10 (2011), pp. 630–634.

[12] Y. Hancock. “The 2010 Nobel Prize in physics—ground-breaking experiments on graphene”. In: *Journal of Physics D: Applied Physics* 44.47 (2011), p. 473001.

[13] N. M. Peres. “Colloquium: The transport properties of graphene: An introduction”. In: *Reviews of modern physics* 82.3 (2010), p. 2673.

[14] A. N. Grigorenko, M. Polini, and K. Novoselov. “Graphene plasmonics”. In: *Nature photonics* 6.11 (2012), pp. 749–758.

[15] E. J. Dias et al. “Probing nonlocal effects in metals with graphene plasmons”. In: *Physical Review B* 97.24 (2018), p. 245405.

[16] M. G. Silveirinha. *Lecture note of nano-eletromagnetics: plasmonics and metamaterials*. 2019.

[17] A. Chaves et al. “Hydrodynamic model approach to the formation of plasmonic wakes in graphene”. In: *Physical Review B* 96.19 (2017), p. 195438.

[18] A. Aldea and V. Bârsan. *Trends in nanophysics*. Springer, 2010.

[19] A. Moreau, C. Ciraci, and D. R. Smith. “Impact of nonlocal response on metallodielectric multilayers and optical patch antennas”. In: *Physical Review B* 87.4 (2013), p. 045401.

[20] A. Moradi. *Canonical problems in the theory of plasmonics*. Springer, 2020.

[21] H. A. Baquero. “Plasmonic waves in two-dimensional electron gas”. In: *Journal of Physics: Conference Series*. Vol. 1141. 1. IOP Publishing. 2018, p. 012006.

[22] A. Chaves et al. “Scattering of graphene plasmons at abrupt interfaces: An analytic and numeric study”. In: *Physical Review B* 97.3 (2018), p. 035434.

[23] A. L. Fetter. “Electrodynamics of a layered electron gas. I. Single layer”. In: *Annals of Physics* 81.2 (1973), pp. 367–393.

[24] G. B. Arfken, H. J. Weber, and F. E. Harris. *Mathematical methods for physicists: a comprehensive guide*. Elsevier, 2013.

[25] A. Likar and N. Razpet. “Towards the Kelvin wake and beyond”. In: *American Journal of Physics* 81.4 (2013), pp. 245–252.

[26] R. Pethiyagoda, S. W. McCue, and T. J. Moroney. “What is the apparent angle of a Kelvin ship wave pattern?” In: *Journal of fluid mechanics* 758 (2014), pp. 468–485.

[27] M. Rabaud and F. Moisy. “Ship wakes: Kelvin or Mach angle?” In: *Physical review letters* 110.21 (2013), p. 214503.

[28] A. Darmon, M. Benzaquen, and E. Raphaël. “Kelvin wake pattern at large Froude numbers”. In: *Journal of Fluid Mechanics* 738 (2014).

[29] E. Raphaël and P.-G. De Gennes. “Capillary gravity waves caused by a moving disturbance: wave resistance”. In: *Physical Review E* 53.4 (1996), p. 3448.

[30] E. Raphael and P.-G. De Gennes. “Effective mass of a charged particle travelling above a dielectric fluid surface”. In: *EPL (Europhysics Letters)* 31.5-6 (1995), p. 293.

[31] L. Birk. *Fundamentals of ship hydrodynamics: Fluid mechanics, ship resistance and propulsion*. John Wiley & Sons, 2019.

[32] G. Kuwabara, T. Hasegawa, and K. Kono. “Water waves in a ripple tank”. In: *American Journal of Physics* 54.11 (1986), pp. 1002–1007.

[33] N. Pallas and B. Pethica. “The surface tension of water”. In: *Colloids and Surfaces* 6.3 (1983), pp. 221–227.

[34] A. S. Peters. “A new treatment of the ship wave problem”. In: *Communications on pure and applied mathematics* 2.2-3 (1949), pp. 123–148.

[35] F. Moisy and M. Rabaud. “Scaling of far-field wake angle of nonaxisymmetric pressure disturbance”. In: *Physical Review E* 89.6 (2014), p. 063004.

Appendix A

Plasmonic Electrostatic Calculations

In this appendix, we show the explicit calculations of the boundary conditions and electrostatic coefficients, necessary to obtain the dispersion relation of the surface plasmon-polaritons for the two electrostatic problems studied in chapter 3.2: graphene in the vicinity of semi-infinite metal and graphene in the vicinity of a finite metal. The electrostatic configurations for these problems are given by figures 3.8 and 3.13. Following the same line of though of chapter 3.2 regrading the application of the boundary conditions we get

$$\phi_1^{metal}(-d) = \phi_1^{dielectric}(-d) \tag{A.1}$$

$$\epsilon_\infty \frac{\partial \phi_1^{metal}(-d)}{\partial z} = \epsilon_d \frac{\partial \phi_1^{dielectric}(-d)}{\partial z} \tag{A.2}$$

$$\phi_1^{dielectric}(0) = \phi_1^{graphene}(0) \tag{A.3}$$

$$\frac{\partial \phi_1^{graphene}(0)}{\partial z} - \epsilon_d \frac{\partial \phi_1^{dielectric}(0)}{\partial z} = \frac{e}{\epsilon_0} n_1(\mathbf{k}, \omega) \tag{A.4}$$

where ϵ_∞ and ϵ_d are the background permittivity and the dielectric constant, respectively. To the latter equations we apply the potential coefficients given in equations (3.42), (3.43) and (3.44), that correspond to metal, dielectric and graphene, respectively. This will lead to

$$Be^{-\alpha d} + Ce^{-kd} = De^{kd} + Fe^{-kd} \tag{A.5}$$

$$\epsilon_\infty \left[\alpha Be^{-\alpha d} + kCe^{-kd}\right] = \epsilon_d \left[-kDe^{kd} + kFe^{-kd}\right] \tag{A.6}$$

$$D + F = G \tag{A.7}$$

$$-kG - \epsilon_d \left[-kD + kF\right] = \frac{e}{\epsilon_0} n_{2D,1}(\mathbf{k}, \omega) \tag{A.8}$$

Recall that α is a nonlocal parameter given by equation (3.6). The hydrodynamic model provides an extra boundary conditions, that states the null current of the electron gas at the normal direction of the interface. In mathematical terms this means

$$\frac{\epsilon_0 \omega_p^2}{e n_0} \frac{\partial \phi_1^{(metal)}}{\partial z} = \frac{\beta^2}{n_0} \frac{\partial n_1^{(metal)}}{\partial z} \tag{A.9}$$

where ω_p is the plasma frequency, n_0 the homogeneous electronic density and β the nonlocal parameter. The first order electronic density n_1 is given by equation (3.41). This boundary condition give rise to the expression

$$\omega_p^2 \left[\alpha B e^{-\alpha d} + kC e^{-kd}\right] + (\omega^2 - \omega_p^2)\alpha B e^{-\alpha d} = 0 \tag{A.10}$$

Dividing this last equation by ω_p^2 we obtain

$$C = -\frac{\omega^2}{\omega_p^2} \frac{\alpha}{k} e^{(k-\alpha)d} B \tag{A.11}$$

At last, we derived the expressions that allow us to construct the coefficient matrix M presented in chapter 3.2. The solution for all coefficients is then given by

$$B(k,\omega) = \frac{2\epsilon_d \omega_p^2 e^{d(k+\alpha)}}{\epsilon_d(1 - \epsilon_d + e^{2dk}(1+\epsilon_d))(\alpha\omega^2 - k\omega_p^2) + \alpha(\epsilon_d - 1 + e^{2dk}(1+\epsilon_d))(\omega^2 - \omega_p^2)\epsilon_\infty} \tag{A.12}$$

$$C(k,\omega) = -\frac{2\epsilon_d \alpha e^{2dk} \omega^2}{k[\epsilon_d(1 - \epsilon_d + e^{2dk}(1+\epsilon_d))(\alpha\omega^2 - k\omega_p^2) + \alpha(\epsilon_d - 1 + e^{2dk}(1+\epsilon_d))(\omega^2 - \omega_p^2)\epsilon_\infty]} \tag{A.13}$$

$$D(k,\omega) = -\frac{\epsilon_d(\alpha\omega^2 - k\omega_p^2) + \alpha(\omega_p^2 - \omega^2)\epsilon_\infty}{k[\epsilon_d(1 - \epsilon_d + e^{2dk}(1+\epsilon_d))(\alpha\omega^2 - k\omega_p^2) + \alpha(\epsilon_d - 1 + e^{2dk}(1+\epsilon_d))(\omega^2 - \omega_p^2)\epsilon_\infty]} \tag{A.14}$$

$$F(k,\omega) = -\frac{e^{2dk}(\epsilon_d(\alpha\omega^2 - k\omega_p^2) + \alpha(\omega^2 - \omega_p^2)\epsilon_\infty)}{k[\epsilon_d(1 - \epsilon_d + e^{2dk}(1+\epsilon_d))(\alpha\omega^2 - k\omega_p^2) + \alpha(\epsilon_d - 1 + e^{2dk}(1+\epsilon_d))(\omega^2 - \omega_p^2)\epsilon_\infty]} \tag{A.15}$$

$$G(k,\omega) = -\frac{(1+e^{2dk})(\alpha\omega^2 - k\omega_p^2)\epsilon_d + \alpha(-1+e^{2dk})(\omega^2-\omega_p^2)\epsilon_\infty}{k[\epsilon_d(1-\epsilon_d+e^{2dk}(1+\epsilon_d))(\alpha\omega^2-k\omega_p^2)+\alpha(\epsilon_d-1+e^{2dk}(1+\epsilon_d))(\omega^2-\omega_p^2)\epsilon_\infty]} \tag{A.16}$$

Then the potentials in the momentum space take the form

$$\phi_1(\mathbf{k},z,\omega) = \begin{cases} \frac{e}{\epsilon_0} n_1(\mathbf{k},\omega)[B(k,\omega)e^{\alpha z} + C(k,\omega)e^{kz}] & \text{if } z < -d \\ \frac{e}{\epsilon_0} n_1(\mathbf{k},\omega)[D(k,\omega)e^{-kz} + F(k,\omega)e^{kz}] & \text{if } -d < z < 0 \\ \frac{e}{\epsilon_0} n_1(\mathbf{k},\omega)[D(k,\omega) + F(k,\omega)]e^{-kz} & \text{if } z > 0 \end{cases} \tag{A.17}$$

Now let us take a look at the problem of graphene in the vicinity of a finite metal of thickness a, which is given by configuration 3.13. In this case, the boundary condition to apply take the form

$$\phi_1^{metal}(-d-a) = \phi_1^{dielectric\ 1}(-d-a) \tag{A.18}$$

$$\epsilon_\infty \frac{\partial \phi_1^{metal}(-d-a)}{\partial z} = \epsilon_{d_1} \frac{\partial \phi_1^{dielectric\ 1}(-d-a)}{\partial z} \tag{A.19}$$

$$\phi_1^{metal}(-d) = \phi_1^{dielectric\ 2}(-d) \tag{A.20}$$

$$\epsilon_\infty \frac{\partial \phi_1^{metal}(-d)}{\partial z} = \epsilon_{d_2} \frac{\partial \phi_1^{dielectric\ 2}(-d)}{\partial z} \tag{A.21}$$

$$\phi_1^{dielectric\ 2}(0) = \phi_1^{graphene}(0) \tag{A.22}$$

$$\frac{\partial \phi_1^{graphene}(0)}{\partial z} - \epsilon_{d_2} \frac{\partial \phi_1^{dielectric\ 2}(0)}{\partial z} = \frac{e}{\epsilon_0} n_1(\mathbf{k},\omega) \tag{A.23}$$

The hydrodynamic model provides the boundary condition described in equation (A.9), but in this case it has to be solves in the boundaries at $z = -(d+a)$ and $z = -d$. By using the potentials expressed in equations (3.52), (3.53), (3.54) and (3.55) in these boundary conditions it is found the coefficient expressions

$$B_1\cosh(\alpha(d+a)) + C_1\cosh(k(d+a)) - B_2\sinh(\alpha(d+a)) - C_2\sinh(k(d+a)) = De^{-k(d+a)} \tag{A.24}$$

$$\epsilon_\infty\left[-B_1\alpha\sinh(\alpha(d+a)) - C_1 k\sinh(k(d+a)) + B_2\alpha\cosh(\alpha(d+a)) + C_2 k\cosh(k(d+a))\right] = \epsilon_{d_1} kDe^{-k(d+a)} \tag{A.25}$$

$$B_1\cosh(\alpha d)+C_1\cosh(kd)-B_2\sinh(\alpha d)-C_2\sinh(kd)=F\cosh(kd)-E\sinh(kd) \tag{A.26}$$

$$\begin{aligned}&\epsilon_\infty\left[-B_1\alpha\sinh(\alpha d)-C_1k\sinh(kd)+B_2\alpha\cosh(\alpha d)+C_2k\cosh(kd)\right]\\&=\epsilon_{d_2}(-Fk\sinh(kd)+Ek\cosh(kd))\end{aligned} \tag{A.27}$$

$$F=G \tag{A.28}$$

$$-Gk-\epsilon_{d_2}Ek=\frac{e}{\epsilon_0}n_{2D,1}(\mathbf{k},\omega) \tag{A.29}$$

$$\begin{aligned}&\frac{\omega^2}{\omega_p^2}\alpha\left[B_2\cosh(\alpha(d+a))-B_1\sinh(\alpha(d+a))\right]\\&+k\left[C_2\cosh(k(d+a))-C_1\sinh(k(d+a))\right]=0\end{aligned} \tag{A.30}$$

$$\frac{\omega^2}{\omega_p^2}\alpha\left[B_2\cosh(\alpha d)-B_1\sinh(\alpha d)\right]+k\left[C_2\cosh(kd)-C_1\sinh(kd)\right]=0 \tag{A.31}$$

In a similar way as graphene in the vicinity of a semi-infinite metal, due to the complexity of the latter linear equation, it is necessary to solve the linear system of equations through matricial methods. In that order, we solve equation $M\cdot V=N$ to obtain the coefficient matrix $V=[B_1,B_2,C_1,C_2,D,E,F,G]$, with N the matrix of the free-coefficient terms $N=[0,0,0,0,0,(e/\epsilon_0)n_1(\mathbf{k},\omega),0,0]$. The matrix M is given by

$$M=\begin{bmatrix}\cosh(\alpha(d+a)) & -\sinh(\alpha(d+a)) & \cosh(k(d+a)) & \cdots\\ -\epsilon_\infty\alpha\sinh(\alpha(d+a)) & \epsilon_\infty\alpha\cosh(\alpha(d+a)) & -\epsilon_\infty k\sinh(k(d+a)) & \\ \cosh(\alpha d) & -\sinh(\alpha d) & \cosh(kd) & \\ -\epsilon_\infty\alpha\sinh(\alpha d) & \epsilon_\infty\alpha\cosh(\alpha d) & -\epsilon_\infty k\sinh(kd) & \\ 0 & 0 & 0 & \\ 0 & 0 & 0 & \\ -\frac{\omega^2}{\omega_p^2}\alpha\sinh(\alpha(d+a)) & \frac{\omega^2}{\omega_p^2}\alpha\cosh(\alpha(d+a)) & -k\sinh(k(d+a)) & \\ -\frac{\omega^2}{\omega_p^2}\alpha\sinh(\alpha d) & \frac{\omega^2}{\omega_p^2}\alpha\cosh(\alpha d) & -k\sinh(kd) &\end{bmatrix}$$

$$
\cdots \begin{bmatrix}
-\sinh(k(d+a)) & -e^{-k(d+a)} & 0 & 0 & 0 \\
\epsilon_\infty k\cosh(k(d+a)) & -\epsilon_{d_1} k e^{-k(d+a)} & 0 & 0 & 0 \\
-\sinh(kd) & 0 & \sinh(kd) & -\cosh(kd) & 0 \\
\epsilon_\infty k\cosh(kd) & 0 & -\epsilon_{d_2} k\cosh(kd) & \epsilon_{d_2} k\sinh(kd) & 0 \\
0 & 0 & 0 & 1 & -1 \\
0 & 0 & -\epsilon_{d_2} k & 0 & -k \\
k\cosh(k(d+a)) & 0 & 0 & 0 & 0 \\
k\cosh(kd) & 0 & 0 & 0 & 0
\end{bmatrix}
$$

By solving the linear system of equation with matrix M and matrix N, the solution for all the coefficients follow from matrix V. The potential in graphene (at $z = 0$) is in this way given by equation (3.56), with the auxiliary functions given by

$$
\begin{aligned}
G_1(k,\omega) = \epsilon_{d_1}\epsilon_{d_2}\cosh(kd)[&-2k\alpha\omega^2\omega_p^2(-1+\cosh(ka)\cosh(\alpha a)) \\
&+\left(\alpha^2\omega^4 + k^2\omega_p^4\right)\sinh(ka)\sinh(\alpha a)\Big]
\end{aligned} \tag{A.32}
$$

$$
\begin{aligned}
G_2(k,\omega) = \alpha\epsilon_\infty(\omega^2-\omega_p^2)\Big[&\left(\epsilon_{d_2}\cosh(kd)+\epsilon_{d_1}\sinh(kd)\right)\left(-k\omega_p^2\cosh(\alpha a)\sinh(ka)\right. \\
&\left.+\alpha\omega^2\cosh(ka)\sinh(\alpha a)\right)+\alpha\epsilon_\infty(\omega^2-\omega_p^2)\sinh(ka)\sinh(kd)\sinh(\alpha a)\Big]
\end{aligned} \tag{A.33}
$$

$$
\begin{aligned}
&T_1(k,\omega) = \epsilon_{d_1}\epsilon_{d_2}k(\cosh(kd)+\epsilon_{d_2}\sinh(kd)) \\
&\left(-2k\alpha\omega^2\omega_p^2\left(-1+\cosh(ka)\cosh(\alpha a)\right)+\left(\alpha^2\omega^4+k^2\omega_p^4\right)\sinh(ka)\sinh(\alpha a)\right)
\end{aligned} \tag{A.34}
$$

$$
\begin{aligned}
&T_2(k,\omega) = \\
&\alpha\epsilon_\infty k(\omega^2-\omega_p^2)\Big[-((1+\epsilon_{d_1})\epsilon_{d_2}\cosh(kd)+(\epsilon_{d_1}+\epsilon_{d_2}^2)\sinh(kd))\left(k\omega_p^2\cosh(\alpha a)\sinh(ka)\right. \\
&\left.-\alpha\omega^2\cosh(ka)\sinh(\alpha a)\right)+\alpha\epsilon_\infty(\omega^2-\omega_p^2)\sinh(ka)\sinh(\alpha a)(\epsilon_{d_2}\cosh(kd)+\sinh(kd))\Big]
\end{aligned} \tag{A.35}
$$

By this way, the matricial method provides the solution for the coefficients in the electrostatic potential, necessary to determine the spectrum of the surface plasmon-polaritons in graphene, like is done explicitly in chapter 3.2.

Appendix B

Green's Functions

The Green's function method is a simpler mathematical way to solve differential equations that contains an inhomogeneous term or in other words a source term, just like Poisson equation. In this thesis, we made use of the Green's functions to solve the differential equation (4.6b), where the left-hand side of this equation is the source term that has a contribution from the external charges and the electrostatic charges intrinsic to the materials. In this appendix we will show the equations and the boundary conditions that give rise the solution provided by equations (4.10), (4.18) and (4.40), that correspond to the Green's functions for graphene in vacuum, graphene near a dielectric and graphene near a local metal.

Graphene in the vicinity of a dielectric

To start let us see the case of graphene in a dielectric, with constant permittivity ϵ_d and the dielectric present at $z < 0$ as seen in figure 4.1. To find the solution of equation (4.6b) we need to impose boundary conditions to the Green's function based on the geometry of the problem. The boundary conditions are given by

$$g_I(z', z') = g_{II}(z', z') \tag{B.1}$$

$$\frac{\partial g_I(z', z')}{\partial z} - \frac{\partial g_{II}(z', z')}{\partial z} = -1 \tag{B.2}$$

$$g_{II}(0, z') = g_{III}(0, z') \tag{B.3}$$

$$\frac{\partial g_{II}(0, z')}{\partial z} = \epsilon_d \frac{\partial g_{III}(0, z')}{\partial z} \tag{B.4}$$

The oscillatory form of the Green's functions is shown in equation (4.17), by substitution in these last boundary conditions we obtain the following explicit set of equations

$$A(z')e^{-kz'} = C_1(z')e^{-kz'} + C_2(z')e^{kz'} \tag{B.5}$$

$$kA(z')e^{-kz'} - kC_1(z')e^{-kz'} + kC_2(z')e^{kz'} = 1 \tag{B.6}$$

$$C_1(z') + C_2(z') = B(z') \tag{B.7}$$

$$-kC_1(z') + kC_2(z') = \frac{1}{\epsilon_d}kB(z') \tag{B.8}$$

Solving this linear system of equation, we obtain the following coefficients

$$A(z') = \frac{e^{kz'}}{2k} + \left(\frac{1-\epsilon_d}{1+\epsilon_d}\right)\frac{e^{-kz'}}{2k} \tag{B.9}$$

$$B(z') = \frac{1}{(1+\epsilon_d)k}e^{-kz'} \tag{B.10}$$

$$C_1(z') = \left(\frac{1-\epsilon_d}{1+\epsilon_d}\right)\frac{1}{2k}e^{-kz'} \tag{B.11}$$

$$C_2(z') = \frac{1}{2k}e^{-kz'} \tag{B.12}$$

This lead to the solution for the Green's function, when graphene is in the vicinity of a dielectric as seen in equation (4.18). To obtain the expression for a graphene sheet in vacuum, we simply compute $\epsilon_d = 1$ in the last expressions. This will lead to $g_{II}(z,z') = g_{III}(z,z')$, and the Green function in this case can be expressed like equation (4.10). Where the modulus assures the different solution for the two distinct regions ($z > z'$ and $z < z'$)

Graphene in the vicinity of a local metal

Now for the graphene near a local metal the procedure is similar, but in this case we will have a new boundary conditions at the interface metal/dielectric, that correspond to the regions IV and III, respectively. Just like the configuration in figure 4.4. For this geometry the boundary conditions are

$$g_I(z',z') = g_{II}(z',z') \tag{B.13}$$

$$\frac{\partial g_I(z',z')}{\partial z} - \frac{\partial g_{II}(z',z')}{\partial z} = -1 \tag{B.14}$$

$$g_{II}(0,z') = g_{III}(0,z') \tag{B.15}$$

$$\frac{\partial g_{II}(0,z')}{\partial z} = \epsilon_d \frac{\partial g_{III}(0,z')}{\partial z} \tag{B.16}$$

$$g_{III}(-d,z') = g_{IV}(-d,z') \tag{B.17}$$

$$\epsilon_d \frac{\partial g_{III}(-d,z')}{\partial z} = \epsilon(\omega) \frac{\partial g_{IV}(-d,z')}{\partial z} \tag{B.18}$$

where $\epsilon(\omega)$ is the Drude dielectric function given by equation (2.40). Solving the boundary conditions with the Green functions presented in equation (4.39), we have

$$A(z')e^{-kz'} = C_1(z')e^{-kz'} + C_2(z')e^{kz'} \tag{B.19}$$

$$kA(z')e^{-kz'} - kC_1(z')e^{-kz'} + kC_2(z')e^{kz'} = 1 \tag{B.20}$$

$$C_1(z') + C_2(z') = B_1(z') + B_2(z') \tag{B.21}$$

$$-C_1(z') + C_2(z') = \epsilon_d \left(-B_1(z') + B_2(z')\right) \tag{B.22}$$

$$B_1(z')e^{kd} + B_2(z')e^{-kd} = D(z')e^{-kd} \tag{B.23}$$

$$\epsilon_d \left(-B_1(z')e^{kd} + B_2(z')e^{-kd}\right) = \epsilon(\omega)D(z')e^{-kd} \tag{B.24}$$

The coefficients in the last equations are obtained by solving the linear system through matricial methods in a similar way that was solved in chapter 3 and in appendix A, for the electrostatic problems of graphene near a semi-infinite and finite nonlocal metal, respectively. This leads to

$$A(z') = \frac{e^{-kz'}}{2k}\left(\frac{r_D + r_d e^{2kd}}{r_d r_D + e^{2kd}} + e^{2kz'}\right) \tag{B.25}$$

$$B_1(z') = \frac{e^{-kz'}}{2k}\left(\frac{t_d r_D}{r_d r_D + e^{2kd}}\right) \tag{B.26}$$

$$B_2(z') = \frac{e^{-kz'}}{2k}\left(\frac{t_d e^{2kd}}{r_d r_D + e^{2kd}}\right) \tag{B.27}$$

$$C_1(z') = \frac{e^{-kz'}}{2k}\left(\frac{r_D + r_d e^{2kd}}{r_d r_D + e^{2kd}}\right) \tag{B.28}$$

$$C_2(z') = \frac{e^{-kz'}}{2k} \tag{B.29}$$

$$D(z') = \frac{e^{-kz'}}{2k}\left(\frac{t_d t_D e^{2kd}}{r_d r_D + e^{2kd}}\right) \tag{B.30}$$

These coefficients give rise to the Green's functions admitted in equation (4.40). The Green function method provides, in this way the solution for Poisson's equation. This leads to the determination of the external charge potential and the potential induced in graphene by that external charge, as is stated in chapter 4.

Appendix C

Graphene/Metal Induced Potential Integral

When graphene is in the vicinity of a local metal, the potential induced in the graphene sheet by an external charge moving with velocity v in the y-direction can be computationally burden, due to the numerical solution of the integral. The potential integral in equation (4.63) can be separated into the integrals I_1 and I_2, with

$$I_1 = v^2 t_d^2 \int_0^{2\pi} \frac{d\theta}{2\pi} \oint_0^{\infty} \frac{kdk}{2\pi} \frac{e^{-k\beta} e^{ik\gamma}}{(kv\cos\theta)^2 - \omega_{spp}^2} \left(\frac{r_D(kv\cos\theta) + e^{2kd}}{r r_D(kv\cos\theta) + e^{2kd}} \right) \tag{C.1}$$

$$I_2 = -iv^2 t_d^2 \int_0^{\infty} \frac{dk}{4\pi} \left(\frac{g(k,\theta_1)}{|v^2 k^2 \cos\theta_1 \sin\theta_1|} - \frac{g(k,\theta_2)}{|v^2 k^2 \cos\theta_2 \sin\theta_2|} \right) \tag{C.2}$$

Computing these integrals separately, show us that I_1 is more time consuming than I_2. Luckily, both potential have the same form, which means that present a peak of potential and then become continuous. Regarding their numerical value, it was seen that both integral are approximately equal to each other, this is $|I_1| = |I_2|$. Since their value is equal and I_2 is computationally faster than I_1 we can obtain the induced potential only by using the second integral, this is

$$\Phi_{in}(\mathbf{r}, z, t) = 2I_2 \tag{C.3}$$

To make our point clearer, in the following tables is computed the numerical values for the integrals I_1 and I_2, for different values of the external charge velocity v, for various values of the polar coordinate r, different dielectric thickness d and external charge height z_0. In table 7 it is also computed the integrals for different angles of θ'. To recall this variable is the polar angle of $\mathbf{r}$ (see chapter 4.2). The tables show us that equation (C.3) is a good approximation to the induced potential where the ratio between the two integrals show that the values for I_1 and I_2 are very close to each other and we can consider $I_1 + I_2 = 2I_2$ in a good approximation. In all cases the dielectric constant chosen was $\epsilon_d = 1$ (vacuum).

Table 4: Numerical Value for the integrals in equation (4.63), for different velocities. The parameters were: $d = 0.01$ μm and $z_0 = 1$ μm and $\theta' = \pi$. Note that for every velocity the potential can be seen as $\Phi_{in}(\mathbf{r}, z, t) = 2I_2$ approximately. For every r the values for I_1 and I_2 are very close to each other and we can consider $I_1 + I_2 = 2I_2$ in a good approximation.

v/c	r [μm]	$\lvert I_1\rvert$	$\lvert I_2\rvert$	$\frac{\lvert I_1\rvert}{\lvert I_2\rvert}$	$\frac{\lvert I_1\rvert+\lvert I_2\rvert}{2\lvert I_2\rvert}$
0.05	1	0.0019	0.0029	0.66	0.83
	3	0.0033	0.0038	0.87	0.93
	6	0.0023	0.0026	0.89	0.94
	10	0.0015	0.0017	0.88	0.94
	12	0.0013	0.0014	0.93	0.96
	15	0.0011	0.0012	0.93	0.96
0.1	1	0.0021	0.0031	0.68	0.84
	2	0.0047	0.0054	0.87	0.94
	5	0.0070	0.0073	0.96	0.98
	8	0.0061	0.0063	0.97	0.98
	10	0.0053	0.0055	0.96	0.98
	15	0.0039	0.0041	0.95	0.98
0.3	1	0.0022	0.0031	0.71	0.85
	2	0.0055	0.0062	0.88	0.94
	4	0.0112	0.0116	0.97	0.98
	8	0.0186	0.0188	0.99	0.99
	10	0.0204	0.0205	$\sim$1	$\sim$1
	15	0.0214	0.0215	$\sim$1	$\sim$1
0.5	4	0.0118	0.0122	0.97	0.98
	8	0.0222	0.0224	0.99	$\sim$1
	15	0.0328	0.0329	$\sim$1	$\sim$1
	20	0.0355	0.0356	$\sim$1	$\sim$1
	25	0.0356	0.0357	$\sim$1	$\sim$1
	30	0.0345	0.345	$\sim$1	$\sim$1
0.9	5	0.0151	0.0155	0.97	0.99
	10	0.0294	0.0296	0.99	$\sim$1
	20	0.0507	0.0508	$\sim$1	$\sim$1
	30	0.0614	0.0615	$\sim$1	$\sim$1
	40	0.0645	0.0645	$\sim$1	$\sim$1
	50	0.0632	0.0632	$\sim$1	$\sim$1

Table 5: Numerical Value for the integrals in equation (4.63), for different velocities. The parameters were: $d = 0.01$ μm and $z_0 = 0.1$ μm and $\theta' = \pi$. Note that for every velocity the potential can be seen as $\Phi_{in}(\mathbf{r}, z, t) = 2I_2$ approximately. For every r the values for I_1 and I_2 are very close to each other and we can consider $I_1 + I_2 = 2I_2$ in a good approximation.

v/c	r [μm]	$\lvert I_1\rvert$	$\lvert I_2\rvert$	$\frac{\lvert I_1\rvert}{\lvert I_2\rvert}$	$\frac{\lvert I_1\rvert+\lvert I_2\rvert}{2\lvert I_2\rvert}$
0.05	1	0.0154	0.0173	0.89	0.95
	3	0.0054	0.0060	0.90	0.95
	6	0.0027	0.0030	0.90	0.95
	10	0.0016	0.0018	0.89	0.94
	12	0.0014	0.0015	0.93	0.97
	15	0.0011	0.0012	0.92	0.96
0.1	1	0.0546	0.0563	0.97	0.99
	2	0.0309	0.0317	0.98	0.99
	5	0.0128	0.0131	0.98	0.99
	8	0.0080	0.0082	0.98	0.99
	10	0.0064	0.0066	0.97	0.99
	15	0.0043	0.0044	0.98	0.99
0.3	1	0.1945	0.1960	0.99	$\sim$1
	2	0.2040	0.2048	$\sim$1	$\sim$1
	4	0.1324	0.1328	$\sim$1	$\sim$1
	8	0.0709	0.0711	$\sim$1	$\sim$1
	10	0.0572	0.0574	$\sim$1	$\sim$1
	15	0.0384	0.0386	$\sim$1	$\sim$1
0.5	4	0.3146	0.3147	$\sim$1	$\sim$1
	8	0.1891	0.1893	$\sim$1	$\sim$1
	15	0.1056	0.1057	$\sim$1	$\sim$1
	20	0.0798	0.0799	$\sim$1	$\sim$1
	25	0.0641	0.0641	$\sim$1	$\sim$1
	30	0.0535	0.0536	$\sim$1	$\sim$1
0.9	5	0.6396	0.6402	$\sim$1	$\sim$1
	10	0.4582	0.4585	$\sim$1	$\sim$1
	20	0.2527	0.2528	$\sim$1	$\sim$1
	30	0.1716	0.1717	$\sim$1	$\sim$1
	40	0.1296	0.1296	$\sim$1	$\sim$1
	50	0.1040	0.1040	$\sim$1	$\sim$1

Table 6: Numerical Value for the integrals in equation (4.63), for different velocities. The parameters were: $d = 0.1$ μm and $z_0 = 1$ μm and $\theta' = \pi$. Note that for every velocity the potential can be seen as $\Phi_{in}(\mathbf{r}, z, t) = 2I_2$ approximately. For every r the values for $I_1 + I_2 = 2I_2$ are very close to each other and we can consider $I_1 = I_2$ in a good approximation.

v/c	r [μm]	$\lvert I_1\rvert$	$\lvert I_2\rvert$	$\frac{\lvert I_1\rvert}{\lvert I_2\rvert}$	$\frac{\lvert I_1\rvert+\lvert I_2\rvert}{2\lvert I_2\rvert}$
0.05	1	0.0077	0.0122	0.63	0.82
	3	0.0049	0.0053	0.93	0.96
	6	0.0027	0.0028	0.96	0.98
	10	0.0016	0.0017	0.94	0.97
	12	0.0014	0.0014	1	1
	15	0.0011	0.0011	1	1
0.1	1	0.0138	0.0267	0.52	0.76
	2	0.0196	0.0298	0.66	0.83
	5	0.0120	0.0169	0.71	0.86
	8	0.0079	0.0111	0.71	0.86
	10	0.0064	0.0089	0.72	0.86
	15	0.0043	0.0060	0.72	0.86
0.3	1	0.0174	0.0263	0.66	0.83
	2	0.0411	0.0479	0.86	0.93
	4	0.0649	0.0688	0.94	0.97
	8	0.0580	0.0600	0.97	0.98
	10	0.0504	0.0520	0.97	0.99
	15	0.0365	0.0376	0.97	0.99
0.5	4	0.0856	0.0894	0.96	0.98
	8	0.1129	0.1149	0.98	0.99
	15	0.0905	0.0916	0.99	0.99
	20	0.0735	0.0743	0.99	0.99
	25	0.0610	0.0616	0.99	0.99
	30	0.0519	0.0524	0.99	$\sim$1
0.9	5	0.1186	0.1217	0.97	0.99
	10	0.1893	0.1909	0.99	$\sim$1
	20	0.1913	0.1921	$\sim$1	$\sim$1
	30	0.1519	0.1524	$\sim$1	$\sim$1
	40	0.1214	0.1218	$\sim$1	$\sim$1
	50	0.1001	0.1004	$\sim$1	$\sim$1

Table 7: Numerical Value for the integrals in equation (4.63), for different velocities. The parameters were: $d = 0.01$ μm, $z_0 = 1$ μm, $\theta' = 3$ (for velocities of $0.05c$ and $0.1c$) and $\theta' = 3.1$ (for velocities of $0.3c$ and $0.8c$). Note that for every velocity the potential can be seen as $\Phi_{in}(\mathbf{r}, z, t) = 2I_2$ approximately. For every r the values for I_1 and I_2 are very close to each other and we can consider $I_1 + I_2 = 2I_2$ in a good approximation.

v/c	r $[\mu m]$	$\lvert I_1\rvert$	$\lvert I_2\rvert$	$\frac{\lvert I_1\rvert}{\lvert I_2\rvert}$	$\frac{\lvert I_1\rvert+\lvert I_2\rvert}{2\lvert I_2\rvert}$
0.05	1	0.0017	0.0028	0.61	0.80
	3	0.0032	0.0038	0.84	0.92
	6	0.0024	0.0028	0.86	0.93
	10	0.0017	0.0019	0.90	0.95
	12	0.0014	0.0016	0.89	0.94
	15	0.0012	0.0013	0.92	0.96
0.1	1	0.0019	0.0029	0.66	0.83
	2	0.0039	0.0046	0.85	0.92
	5	0.0053	0.0057	0.93	0.97
	8	0.0055	0.0057	0.97	0.98
	10	0.0054	0.0055	0.98	0.99
	15	0.0049	0.0050	0.98	0.99
0.3	1	0.0022	0.0031	0.71	0.85
	2	0.0054	0.0060	0.90	0.95
	4	0.0104	0.0108	0.96	0.98
	8	0.0157	0.0159	0.99	0.99
	10	0.0167	0.0169	0.99	0.99
	15	0.0176	0.0177	0.99	$\sim$1
0.8	5	0.0133	0.0136	0.98	0.99
	10	0.0187	0.0189	0.99	$\sim$1
	15	0.0170	0.0172	0.99	0.99
	20	0.0124	0.0124	1	1
	25	0.0071	0.0071	1	1
	30	0.0021	0.0022	0.95	0.98